Mechanisms of Erythroid Iron Sensing and Uptake: Roles for TfR2 in the Iron Deprivation Response and Mitochondrial Iron Delivery

Shadi Khalil

Department of Pathology

2017

ABSTRACT

Erythroid progenitors are the major consumers of iron in the human body. These cells must ultimately deliver iron to the mitochondrial matrix, where it is used in heme synthesis to support hemoglobinization. Iron homeostasis is tightly coupled with erythroid iron utilization: declining levels of circulating iron result in suppressed erythropoiesis, thus sparing the body's supply of iron when threatened by erythroid consumption. This response, termed the erythroid iron deprivation response, underlies the pathogenic mechanism of various human anemias. Such iron-restricted human anemias are associated with resistance to erythropoietin (Epo), the major cytokine regulating survival, proliferation, and differentiation of erythroid progenitors. The mechanism of the erythroid iron deprivation response has remained unknown, but aconitase enzymes and transferrin receptor 2 (TfR2) have been identified as erythroid iron-sensing components. The results described herein define a pathway of erythroid iron sensing that culminates with regulation of Epo receptor (EpoR) surface presentation and signaling. Briefly, TfR2 undergoes accelerated lysosomal trafficking and degradation upon iron deprivation, resulting in the co-catabolism of the essential TfR2 binding partner: Scribble. Scribble is a key orchestrator of receptor trafficking and signaling that is required for erythroid surface presentation of EpoR and normal Epo-dependent Stat signaling. We identify the coordination of a TfR2-driven nutrient-sensing pathway with altered receptor trafficking and cytokine responsiveness, thus limiting progenitor expansion while maintaining survival. Interestingly, under iron replete conditions, TfR2 was found to traffic to the lysosome and undergo degradation, although the rate of degradation was reduced. The

mechanism by which erythroid iron is ultimately trafficked from endosome to mitochondria has remained unclear, as cytosolic transit of iron is not observed. The existence of an alternative erythroid iron uptake pathway is suggested by the demonstration of residual erythropoiesis in mice lacking TfR1 and DMT1, proteins involved in canonical iron uptake. Further, mice with marrow-selective TfR2 deficiency have been found to exhibit microcytosis, suggesting that TfR2 may also contribute to erythroid hemoglobinization. Assessing whether TfR2 contributes to iron uptake identified an alternative pathway of iron uptake initiated by TfR2 lysosomal transferrin delivery. Imaging studies reveal an erythroid lineage-specific organelle arrangement consisting of a focal lysosomal cluster surrounded by a nest of mitochondria, with direct contacts between these two organelles. Erythroid TfR2 deficiency yields aberrant mitochondrial morphology and impaired heme synthesis, implicating TfR2-dependent transferrin trafficking in iron uptake and mitochondrial maintenance. Human *TFR2* shares a lineage- and stage- specific expression pattern with *MCOLN1*, encoding a lysosomal iron channel, and *MFN2*, encoding a mitochondrial protein mediating organelle contacts. Functional studies reveal these latter factors to be involved in mitochondrial regulation and erythroid differentiation: *Mcoln1 -/-* animals exhibit anemia and erythroid mitochondrial perturbation, while erythroid Mfn2 knockdown reduces the frequency of mitochondrial-lysosomal contacts and blocks erythropoiesis. These findings identify an alternative role for TfR2, driving lysosomal delivery of transferrin and mitochondrial iron uptake. Thus, TfR2 is identified as a driver of both erythroid iron sensing and iron uptake.

TABLE OF CONTENTS

1. CHAPTER 1: General Introduction……..…5
Overview of hematopoiesis……..……6
Erythropoiesis……9
Iron Metabolism……..……20
Iron Deprivation Response……..……..29
Scribble……..……35
CHAPTER 1 Figures……..……..……38

2. CHAPTER 2: The Human Erythroid Iron Deprivation Response Couples Iron Sensing with EpoR Trafficking through a Scribble-TfR2 Module…..…….. 39
Abstract……..……..…… 40
Introduction……..……41
Results……..……44
Discussion……..……..52
Materials and Methods……..……..……56
CHAPTER 2 Figures……..……68

3. CHAPTER 3: A Specialized Pathway for Erythroid Iron Delivery Through Lysosomal Trafficking of Transferrin Receptor 2 ..……..86
Abstract……..……...87
Introduction……..……89
Results……..……92
Discussion……100
Materials and Methods……..……104
CHAPTER 3 Figures……..…..……116

4. CHAPTER 4: General Discussion……..……137
TfR2: Balancing Iron Uptake with Sensing……..…..…..……138
Organelle Apparatus in Erythroid Iron Uptake……..…..……141
Mitochondria-Lysosomal Contacts……..…..……..……145
Mechanism of Isocitrate Rescue……..…..…..……..……149
Post-translational Modifications of Scribble……..……..……152
Compensation to TfR2 Knockdown……..……..……155
Iron Re-exposure……..……..……..……158
Hepatocyte Iron Sensing……..……..……..……160
Soluble TfR1 as an ERFE effector……..……..……162
miRNAs in Circulating Erythrocytes……..……..……164
CHAPTER 4 Figures……..……..……..……166

5. References……..……..……175

CHAPTER 1:

General Introduction

Overview of hematopoiesis

Hematopoiesis is the process by which undifferentiated hematopoietic progenitors give rise to blood cells. In humans, the process begins at embryonic week 3, when the embryonic yolk sac, in a transient process termed “Primitive Hematopoiesis”, gives rise to progenitors that seed tissues with long-lived tissue resident macrophages (Microglia of the brain, Kupffer cells of the liver, Langerhans cells of the dermis) (1, 2). These cells self-maintain for life in their respective tissues without repopulation, undergoing replacement under pathological circumstances. The stem cell pool that persists for life contributing to “Definitive Hematopoiesis” is generated beginning at embryonic week 4, when the embryonic mesoderm gives rise to hematopoietic stem cells (HSCs) in the intraembryonic aorta (3, 4). Lineage-tracing studies in mice have identified Cadherin5+ endothelial cells of the aorta that become the definitive HSCs (5, 6). At embryonic week 12, definitive HSCs migrate to the fetal liver, where they generate circulating blood cells. Finally, at week 16, the cells take residence in the bone marrow of the entire skeleton, where they generate blood throughout adolescence. By puberty, hematopoiesis is mostly confined to the axial skeleton, consisting of the pelvis, spine, shoulder, and skull (7).

Hematopoietic stem cells persist in the bone marrow, giving rise to the two major lineages of blood cells: lymphoid cells (T-cells, B-cells, and NK-cells) and myeloid cells (granulocytes, monocytes, eosinophils, basophils, erythrocytes, and megakaryocytes). HSCs undergo self-renewing divisions to maintain the niche in addition to generating all of the blood types. This homeostasis is maintained by the bone marrow, a finely adjusted

microenvironment that supports the maintenance of this niche. Studies have identified relative hypoxia of the marrow (8), extracellular matrix proteins (9), chemokines (10), non-hematopoietic cells (11), and adrenergic signaling by sympathetic nerves (12), as essential for proper function of the niche.

Histologically, the bone marrow consists of endothelia-lined sinusoids that show differential permeability to oxygen. HSCs associate with less permeable arterial blood vessels, establishing a hypoxic microenvironment that is critical in maintaining the reduced levels of ROS necessary for HSC maintenance and quiescence (13). These arterioles are found throughout the endosteam and contain rare NG2+ pericytes that contribute to HSC maintenance through an unknown mechanism (14). Leakier sinusoids tend to be sites of trafficking and progenitor expansion of the various hematopoietic lineages. Within the parenchyma, adipocytes are frequent, found at a 1:1 ratio with hematopoietic cells in the healthy adult, and are suggested to suppress hematopoiesis and HSC maintenance (15). Megakaryocytes, which contact sinusoids and release platelets into the plasma, closely associate with and promote HSCs quiescence through the release of chemokines (16).

As part of their pluripotent function, HSCs divide to yield lineage restricted progenitors which further proliferate and divide to generate mature blood cells. These cells, termed colony-forming-units (CFUs), demonstrate further lineage commitment and express receptors that respond to cytokines to regulate proliferation and differentiation.

This process allows for the fine-tuning of hematopoietic output of specific lineages according to the needs of the body, independent of HSC mobilization and expansion.

Under conditions of stress, HSCs themselves can rapidly expand to meet the demand of the body. IFN-alpha (17) and IFN-gamma (18), both released by the body in response to infectious pathogens, can directly activate and drive HSC cell cycle. In response to irradiation, HSC expansion can similarly be induced, in part due to liver-secreted chemokines (19). This expansion can result in the movement of HSCs and other progenitors to the spleen, in a process termed “extramedullary hematopoiesis”. Extramedullary hematopoiesis is observed in small mammals in response to increased demand for mature cells, but likely does not occur in humans, as human marrow is adipocyte rich, and expansion of progenitors can be accommodated for by the marrow space (20).

Erythropoiesis

Mature circulating red blood cells, or erythrocytes, have a lifespan of approximately 120 days in humans (21). Circulating erythrocytes are non-nucleated, functioning in the transport of metabolic gases, O2 and CO2, to sustain oxidative metabolism in the body periphery. With time, erythrocytes lose phospholipid asymmetry of their membranes and expose phosphatidylserine to the outer membrane leaflet, causing them to be engulfed by splenic red pulp macrophages (22).

This process is likely associated with oxidation of RBCs, as N-acetyl-L-Cysteine prolongs circulating erythroid life span (23). Also at play in the modulation of erythrocyte clearance are other surface molecules, such as CD47 (24), which inhibits engulfment in young erythrocytes and is both lost (25) and modified (26) with erythrocyte age, thus resulting in erythrocyte engulfment.

Human blood contains 5×10^6 erythrocytes per microliter of blood, amounting to 2×10^{11} erythrocytes that must be newly generated daily to maintain the loss of 1% of circulating erythrocytes. Deficiency or dysfunction in the generation of new erythrocytes results in the various types of human anemias, discussed further below.

Erythropoiesis describes the process by which progenitor cells expand and differentiate to generate mature erythrocytes. In primitive hematopoiesis of developing mammalian embryos, nucleated progenitor cells enter the circulation and expand in the

bloodstream (27, 28). In the adult, however, steady-state erythropoiesis takes place solely in the bone marrow, where mature, enucleated erythrocytes enter the bloodstream and circulate until removal. Under conditions of erythroid stress, the spleen can contribute to erythropoiesis as the site of erythroid progenitor expansion.

Beginning with multipotent hematopoietic stem cells, lineage-restriction occurs in multiple steps to generate erythroid-committed progenitors. First, concomitant CD38 expression on CD34+ HSCs defines the common myeloid progenitor (CMP), which is restricted to non-lymphocytic lineages. Further loss of surface IL-3R defines the Megakaryocyte/erythroid progenitor (MEP), a common progenitor that gives rise to megakaryocytes, the cells generating platelets, and erythrocytes. From this stage, surface expression of CD41 yields lineage-committed megakaryocytic CFUs, while surface expression of CD71 (TfR1) yields the erythroid-committed burst forming unit (BFU-E), a precursor to the erythroid CFU-E (29, 30). BFU-Es are motile (and appear in the circulation at very low frequency), and thus give rise to spatially-separated colonies containing thousands of cells, when plated on methylcellulose (31). CFU-Es, characterized by the loss of surface CD34 and increased abundance of CD71 (32), are found in the bone marrow at a frequency of approximately 5 per 1000 bone marrow cells, with each cell capable of giving rise to over 100 mature hemoglobinized erythrocytes. With differentiation and cell division, erythroid progenitors progressively reduce their soma size, ultimately generating 6μm diameter mature erythrocytes from larger, 16μm diameter, CFU-Es (33). Further differentiation and expansion of CFU-Es, termed terminal erythropoiesis, is characterized by the upregulation of glycophorin A (GPA) or Ter119 in

mouse, eventual loss of CD71, and progressive hemoglobinization as erythroid progenitors undergo maturation, successively generating: pro-erythroblasts, basophilic erythroblasts, polychromatic erythroblasts, orthochromatic erythroblasts, and then ultimately enucleated reticulocytes (34). These stages of erythropoiesis are named by appearance under H&E stain, and have recently been described to correlate with the surface expression of Band3, a surface ion transporter that is upregulated with terminal erythroid differentiation (35). Reticulocytes, so named because of their reticular appearance, are immature erythrocytes that contain ribosomes, mitochondria, and endosomes. These organelles are cleared before mature erythrocytes are released into the circulation. With increased erythropoietic output by the marrow, reticulocytes can be observed in the circulation. In mice, with some evidence supporting the observation in humans, terminal erythroid differentiation occurs in a histologic unit termed the “erythroblastic island” (36, 37). This bone marrow structure consists of a central macrophage projecting processes through nests of differentiating erythroblasts. Later-staged erythroblasts are positioned distal to the soma of the central macrophage, where ultimately extruded nuclei, termed pyrenocytes, are engulfed by terminal macrophage processes (38). Adhesion between erythroblasts and macrophages is mediated by erythroblasts-macrophage protein (EMP), which is expressed on both cell types, in addition to erythroid integrin-a4b1 and macrophage Vcam1 (39). EMP knockout mice have no observable islands, demonstrate impaired terminal erythroid differentiation, and are not viable, highlighting the importance of the erythroblastic island in erythropoiesis (40). Additionally, the interaction between erythroid cells and macrophages in vitro can be disrupted by anti-EMP antibody (41). Similarly antibody-mediated disruption of the

integrin-Vcam1 interaction also disrupts the formation of erythroblastic islands in vitro (39). The erythroblastic island is believed to support several aspects of erythroid differentiation, including paracrine cytokine stimulation, iron internalization by erythroid cells, and pyrenocyte clearance by macrophages (42).

Similar to its function as a phagocytic “eat-me” marker on apoptotic cells, surface phophatidylserine is expressed on extruded pyrenocytes and functions in the clearance of erythroid nuclear remnants. While differentiating erythroblasts show minimal levels of surface phosphatidylserine, extruded pyrenocytes demonstrate upregulation of surface phosphatidylserine and are readily engulfed by macrophages. This engulfment process is blocked upon molecular shielding of surface phosphatidylserine (43).

Erythroid contact is critical in the homeostatic maintenance of erythropoiesis. One such contact-dependent mechanism for controlling the number of generated erythroblasts occurs through CD95 (FAS) signaling. While less mature erythroblasts express high levels of FAS, terminally differentiated cells selectively gain the expression of FAS ligand, resulting in downstream signaling that impairs erythropoiesis and possibly induces apoptosis in FAS+ less differentiated progenitors (44). While FAS signaling in many cell types is strongly associated with caspase activation and apoptosis, erythroid caspase activation is non-apoptotic, largely affecting differentiation through the cleavage of essential erythroid transcription factors such as GATA-1 (45) and SCL/Tal-1 (46). Interestingly, activation of apoptosis-related pathways occurs during terminal erythropoiesis: transient activation of multiple caspases (-2, -3, -9), PARP cleavage, and

increased mitochondrial transmembrane potential are all observed with differentiation of erythroblasts. Caspase activation is required for terminal differentiation of human erythroid progenitors, as caspase inhibition potently blocks erythroid maturation at the basophilic stage (47). Caspase 3, in particular, may support terminal erythropoiesis (48) in part through facilitating chromatin condensation via release of histones through nuclear pores (49). Recent work describes Caspase 10 activation and Bid cleavage as necessary check-points in terminal erythropoiesis (unpublished data, Courtois lab, ASH:397).

In addition to apoptotic pathways, autophagic pathways are activated throughout erythropoiesis and contribute to red blood cell development. Proteins essential to autophagosome formation, including ATG7 and Nix, are required for normal erythropoiesis (50, 51). Prior to enucleation and erythrocyte release into the circulation, terminal erythropoiesis requires the consumption of mitochondria and other organelles, processes mediated by autophagosomes. However, while mitochondrial clearance occurs in terminally differentiated erythroblasts, autophagy genes are expressed in early erythropoiesis, suggesting that the activation of autophagy may play a role beyond the cellular debris cleanup (52). Supporting this concept, knockout of ATG7 in the hematopoietic compartment results in the accumulation of early-staged Ter119- progenitors, with trivial effect on terminal differentiation (52).

Immature erythroid progenitors are responsive to signaling by the cytokines TPO and SCF (53). With further differentiation, Epo, the principle cytokine regulating erythropoiesis, becomes relevant and critically essential for erythroid survival. Recent

work has described the exosome complex, a large multimeric complex regulating transcription, RNA maturation, and translation, as a regulator of the switch between SCF and Epo sensitivity. Specifically, the exosome complex, through occupancy at the *Kit* locus (which encodes c-Kit, the SCF receptor), allows for SCF-dependent proliferative signaling while suppressing Epo-dependent differentiation signaling. Erythroid progenitors with a disrupted exosome complex differentiate faster, with poorer expansion, due to hyperactivated Epo-dependent signaling in later-staged erythroid progenitors (54, 55).

The protein erythropoietin is the principle cytokine regulating erythropoiesis. Progenitors can respond as early as the BFU-E stage through the Epo Receptor (EpoR), a member of the cytokine receptor superfamily that is upregulated with further differentiation and highest at the proerythroblast stage (56). In response to hypoxia, Epo is synthesized and released by peritubular cells of the kidney, where it circulates back to the bone marrow and acts upon differentiating erythroid progenitors. The pathway of Epo release by the kidney involves HIF-1α stabilization under hypoxic conditions and consequent transcription, translation, and cellular export of the Epo protein. This allows for maintenance of adequate levels of RBCs, which in turn perfuse and oxygenate the kidney, lowering Epo levels in a multi-organ feedback system. HIF-1 signaling is additionally relevant in osteoblasts. In a process similar to that which occurs in kidney peritubular cells, osteoblasts monitor hypoxia of the trabecular bone and release Epo. While osteoblast-specific VHL deletion and consequent Epo upregulation result in enhanced erythropoiesis and polycythemia, osteoblast deletion of HIF-1 and HIF-2

minimally impair erythropoiesis, suggesting that osteoblast Epo functions as a supplementary pathway to renal Epo (57). Epo levels can vary several orders of magnitude in plasma between normal and pathologically elevated states (58), suggesting a dynamic physiologic range of receptor stimulation. Interestingly, Epo additionally affects non-hematopoietic tissues including the pancreas (59), immune system (60), and tumors (61). These findings have been limited, but suggest function of the Epo cytokine and expression of EpoR on other cell types.

Epo binding to EpoR activates signaling that drives proliferation, differentiation, and inhibition of apoptosis in erythroid progenitors. Upon binding to Epo, EpoR dimerization occurs, resulting in activation of cytoplasmic kinases. Activation of Jak2, bound to the cytoplasmic domain of EpoR, results in autophosphorylation of Jak2 and phosphorylation of tyrosine residues on the EpoR cytoplasmic tail. This functions in recruiting additional proteins and driving further signal transduction along several intracellular signaling pathways. The role of Epo was initially described as protecting erythroid progenitors from undergoing apoptosis (62). This is an incomplete picture of the multifaceted effects of Epo, which include support for proliferation and differentiation of progenitors as well. Interestingly, recent work describes Epo as affecting fate decisions of HSCs, which express low levels of the receptor. In mice subjected to exogenous Epo treatment, ex-vivo expansion of isolated Lin- Sca1+ cKit+ multipotent HSCs were found to be strongly biased towards the erythroid lineage, arguing that Epo can program cells that have yet to commit to the erythroid lineage (63).

A comprehensive picture of the effects of Epo on erythropoiesis remains incomplete, as Epo signaling activates multiple pathways and novel EpoR effectors continue to be discovered. Activation of Stat5 is the best understood and most recognized of these pathways. Phosphorylated Stat5 dimerizes and translocates to the nucleus, where it functions in activating the transcription of genes essential to erythropoiesis (64), including Myc (65), BCL-XL (66), and D-type Cyclins (67). A constitutively active Stat5 mutant was identified as completely capable of sustaining erythropoiesis in otherwise incompetent mouse progenitors subjected to EpoR and Jak2 deletion (64). Other important canonical signaling pathways activated by Epo include PI3K and ERK signaling, which also support the proliferation and differentiation of erythroid progenitors. In cells lacking EpoR, expression of an EpoR mutant with only one intracellular tyrosine residue responsible for recruiting PI3K (Y479) was sufficient to support erythropoiesis (68, 69). Epo-dependent upregulation of c-Myc is believed to occur through the activation of both PI3K and ERK pathways (70). Other more recently discovered pathways include Epo activation of NF-kB (60) and serpin-dependent inhibition of lysosomal activity (71).

EpoR contains intracellular tyrosines that allow it to transduce these various signals. Various EpoR mutants have been cloned and knocked into mice in assessing the contributions of the intracellular domains. One such mutant, denoted “EpoR-H”, was truncated to lack 7-of-8 intracellular tyrosine residues, maintaining only Y343 necessary for Stat5 phosphorylation. An alternative mutant, denoted “EpoR-HM”, was stripped of all eight tyrosine residues. In mice, the EpoR-HM knock-in mutant demonstrated anemia and impaired terminal erythropoiesis, while the EpoR-H mutant had elevated RBC values and

hematocrit (72, 73). The enhanced erythropoiesis observed in EpoR-H mutant animals implicates suppressive effects of much of the intracellular domain of EpoR, including domains required for EpoR internalization (74) and trafficking (75). EpoR trafficking and mobilization is finely tuned to allow progenitors to respond to widely different ranges of circulating Epo ligand. Upon Epo binding to EpoR and consequent Jak2 signaling, EpoR is internalized and degraded, first through proteasome-mediated clipping of the EpoR intracellular domain at the cell surface, then by lysosome mediated degradation of both Epo and EpoR (76, 77). Ubiquitylation and proteasome degradation is required for EpoR degradation not unlike other cytokine receptors (IL-2 IL-9) (78). EpoR is largely detected intracellularly with scare surface expression that is highly regulated by surface trafficking, recycling, and degradation. (76, 79). Recent experimental studies of Epo consumption and EpoR mobilization, however, has disputed the model of ligand-dependent internalization and argues for a model of EpoR turnover whereby large EpoR intracellular pools are constantly replenishing surface EpoR molecules, allowing for integration of signal across the dynamic range of circulating Epo levels. While ligand-binding and activation of EpoR results in the degradation of the receptor, the loss of the receptor is not felt by the vast pool of intracellular EpoR, which continues to provide surface EpoR for the additional sensing of ligand (76, 79). In conclusion, Epo-dependent signaling of EpoR is a carefully orchestrated process involving EpoR surface trafficking, signaling, and degradation that results in positive signals mediating erythropoiesis.

Human anemias, diseases in which there is a reduction in the total circulating red cell mass, can be the result of several different pathological mechanisms. Other than

anemia resulting from blood loss, human anemias can largely be divided into two groups: hemolytic anemias and anemias of ineffective erythropoiesis. Hemolytic anemias are characterized by reduced red cell life span, and include hereditary forms (G6PD deficiency, Sickle Cell, Thalassemia, Hereditary Spherocytosis) and acquired forms (Paroxysmal Nocturnal Hemoglobinuria, Immunohemolytic anemia, Red cell trauma). In these anemias, circulating Epo levels are elevated by the body's attempt to upregulate erythropoiesis. In cases of some hereditary forms of hemolytic anemias, the bone marrow can undergo ineffective erythropoiesis, the process in which erythropoiesis, although in overdrive, fails to generate normal levels of red blood cells due to apoptosis of progenitors (80, 81). Ineffective erythropoiesis, in addition to exacerbating the anemia, results in increased iron absorption and levels, due to physiologic mechanisms discussed below. Several anemias occur due to impaired erythropoiesis. Megaloblastic anemias result from deficiency in vitamins necessary for metabolism and proliferation. Aplastic anemias, characterized by global failure of the bone marrow, are mostly idiopathic, although many cases are associated with injury and infection. Pure red cell aplasias, in which the marrow demonstrates selective suppression of erythropoiesis, tend to be autoimmune or associated with infection. The largest categories of impaired erythropoiesis are iron deficiency anemia and anemia of chronic disease. Iron deficiency is the most common nutritional deficiency in the world. Erythropoiesis is exquisitely sensitive to changes in circulating iron, and this phenomenon underlies the pathogenic basis of these anemias (7).

While iron deficiency results in reduced iron circulation due to depleted iron stores, chronic disease results in impaired iron mobilization due to inflammatory mediators skewing iron metabolism, resulting in increased iron stores and reduced circulating iron. Details of the physiological mechanisms regulating iron absorption, storage, and circulation are discussed in the following section.

Iron metabolism

Iron is an essential metal, absorbed through the diet, that participates in oxidation-reduction (redox) metabolism and oxygen-binding of hemoglobin. It is most efficiently absorbed through the gut when bound to heme, with limited absorption of free iron (82). Although there is no iron excretion pathway, loss of iron through sloughing of the skin, sloughing of the mucosa, and blood-loss necessitates the reabsorption of milligrams of iron daily (83, 84). Free, soluble iron is toxic through its generation of reactive oxygen species (ROS) and must be constantly chaperoned by binding proteins to prevent iron-induced toxicity.

Dietary iron is mostly found in the oxidized (Fe^{3+}) Ferric state and consists of two forms: heme iron and non-heme iron. Heme iron is ingested from animal foods and is mainly myoglobin- and hemoglobin-associated. Through the acidicity and proteolytic activity of gut enzymes, heme from these proteins and transported across the apical brush border of the gut. Two heme transporters have been described in enterocytes: HCP1 (85) and FLVCR (86). Once heme is internalized by the enterocyte, it can undergo degradation intracellularly, where freed iron is believed to enter a common pathway of iron distribution. Non-heme iron is similarly freed by the environment of the gut, where it is absorbed by the duodenum of the small intestine (87). Ferric iron (Fe^{3+}) is first reduced to the Ferrous state (Fe^{2+}) via ferric reductases on the brush border (Duodenal cytochrome B (88) and Steap2 (89) have both been described), so that it can interact with duodenal transporters. The channel Divalent Metal Transporter (DMT1) has been characterized to be the apical

duodenal transporter of Fe^{2+}, as it is expressed on the apical surface of enterocytes and is required for iron uptake into the cells. Once iron is inside the enterocyte, it is stored as ferritin and exported. Iron export from ferritin stores is dependent upon lysosomal degradation of ferritin via the cargo receptor NCOA4 and release of iron into the bloodstream (90, 91). Ferroportin 1 is the only protein described in iron export, and is expressed on multiple types of cells involved in iron metabolism, including on the basolateral membrane of the enterocyte (92, 93). Mouse ferroportin 1 global or enterocyte-specific deletion results in iron deficiency and enterocyte accumulation of iron (94). Once Fe^{2+} is exported from the enterocyte, the basolateral enzyme haphaestin reoxidizes the iron to Fe^{3+}, where it then binds circulating transferrin, a protein synthesized by the liver that functions as the primary chaperone of blood iron.

Total body iron content is normally 3 grams in women and 5 grams in men, and is divided into a functional pool and storage pool. The functional pool is associated proteins and enzymes, with the majority bound to hemoglobin. The storage pool, which comprises 20% of total body iron, is hemosiderin- and ferritin- bound and exists in the liver and in phagocytes. Physiological mechanisms exist to carefully balance the storage pool, functional pool, and dietary absorption.

Movement between the storage and functional iron compartments occurs through the plasma, via transferrin. A single transferrin molecule can exist unbound (apotransferrin), bound to a single ferric atom (monoferric transferrin), or bound to two ferric atoms (diferric-, or holo- transferrin). In a normal adult human, transferrin saturation

exists between 20-50%, meaning that 20-50% of the ferric binding sites are occupied by the sum of monoferric and diferric forms. Several studies have described monoferric transferrin as the predominant form over holotransferrin (95), although the precise nature of the circulating forms remains unclear.

Every cell in the body is iron-utilizing, accumulating iron from this circulating pool of transferrin. Transferrin enters the cell via receptor-mediated endocytosis. The transferrin receptor (TfR1), expressed on every cell type with the exception of circulating mature erythrocytes, is thought to be the sole receptor involved in transferrin uptake. TfR1 is localized to clathrin-coated pits and binds diferric transferrin with higher affinity than monoferric transferrin, and lowest affinity to apotransferrin. Once bound to transferrin, clathrin-mediated endocytosis occurs, generating a vesicle with transferrin bound to transferrin receptors (96). The vesicle undergoes trafficking through the recycling endosome pathway: first, Rab and Rab effector recruitment results in maturation of a vesicle into an early endosome (97, 98). Associated with this process is the acidification of the vesicle, which continues throughout the depth of the endo-lysosomal pathway, resulting in highly acidic lysosomes. With mild acidification, iron is displaced from the transferrin-TfR1 complex to become free in the endosome. This free ferric iron is reduced to ferrous iron via Steap3 reductase activity, followed by cytosolic transit to the cytosol via DMT1 to enter the cytosolic labile iron pool (99). Iron is then rapidly utilized or stored, as evidenced by the low volume of the cytosolic labile iron pool when measured biochemically (100). Without iron, the transferrin-TfR1 interaction is very stable in the endosome due to the acidic nature of the compartment. From the early endosome, the

transferrin-TfR1 complex enters the endosomal recycling compartment (ERC), where it is sorted into vesicles bound for return to the plasma membrane. Upon return to the cell surface, the more alkaline environment reduces the affinity of the transferrin-TfR1 interaction, and apotransferrin is shed from the cell to reenter circulation (101).

The importance of DMT1 is highlighted by *Slc11a2* -/- knockout animals, which lack DMT1 that mediates export of iron from endosomes and demonstrate anemia and iron deficiency erythropoiesis (102). The animals, however, are viable and demonstrate erythropoiesis, suggesting that while DMT1 contributes to iron homeostasis and the erythroid iron pool, there may be other pathways of relevance. Further suggesting the existence of an alternative pathway, in both a human patient with DMT1 deficiency and in *Slc11a2* -/- mice, erythropoietin treatment ameliorated anemia (103). The importance of TfR1 is highlighted by global knockout animals that demonstrate embryonic lethality (104), and conditional intestinal knockout animals that exhibit neonatal death (105). Although erythropoiesis is suppressed in both knockouts, some level of erythropoiesis is maintained, suggesting the existence of alternative pathways of erythroid iron uptake.

The above-described processes of canonical transferrin uptake and trafficking are believed to occur in all iron-accumulating cells, including erythroid progenitors. However, some findings have questioned the role of the cytosolic iron pool in erythroid iron accumulation. In erythroid cells, a large amount of iron must ultimately be delivered to the mitochondrial matrix, where it is inserted into protoporphyrin IX in the synthesis of heme (106). In a study examining at the uptake of transferrin-bound iron by reticulocytes, large amounts of radiolabeled iron were recovered from heme in reticulocytes, supporting the

concept that transferrin-bound endosomal iron is ultimately delivered to the mitochondria. Interestingly, when a chelator of the labile iron pool was introduced to the cytosol, delivery of iron to heme was unimpaired, suggesting that endosomal iron bypasses the cytosol in the direct delivery to the mitochondria. Immunofluorescent and electron microscopy confirmed the proximity of endosomes to mitochondria in what is described the “Kiss-and-Run” hypothesis of iron uptake. Kiss-and-Run has recently been described in non-erythroid cells, suggesting the existence of a general pathway of mitochondrial iron delivery (107).

Circulating iron levels must be critically maintained to balance absorption, loss, storage, and redistribution. The principle hormone regulating iron metabolism through modulation of absorption, storage, and circulation is hepcidin. Hepcidin, a protein synthesized by the liver in response to high iron, blocks iron release into the circulation and gut absorption of iron.

Although targets of hepcidin are well understood, the factors leading to its expression are less clear. Upon sensing of holotransferrin levels, hepcidin is synthesized and released into the circulation by hepatocytes in a manner that depends on several surface proteins. TfR1 is required for sensing of transferrin, as are two other proteins: HFE and the second transferrin receptor (TfR2). HFE is a membrane protein that contains a signaling domain and transferrin receptor binding domain (108). TfR2 is the second transferrin receptor, a paralog to TfR1 with expression limited to hepatocytes and erythroid cells (109). TfR2 has an affinity to holotransferrin that is 20-30 times lower than

that of TfR1, suggesting it has a limited role in iron uptake and a putative role in iron sensing (110-112). While the study of TfR2 in erythroid cells has been limited, several studies have highlighted the role of hepatocyte TfR2 in iron sensing, as hepatocytes lacking TfR2 fail to demonstrate a similar hepcidin response to transferrin. On hepatocytes, the currently accepted model is that the presence of holotransferrin displaces HFE from its normal binding partner, TfR1, to interact with TfR2 (113, 114). This then forms a signaling complex, resulting in the phosphorylation of SMADs and transcription of hepcidin (115).

The TfR2-HFE interaction results in further downstream BMP signaling dependent on another factor, hemojuvelin (HJV). HJV is a membrane BMP co-receptor that participates in a complex with TfR2 and HFE (116). Playing a molecular function similar to that of TfR2, HJV competes with TfR1 to bind HFE. HJV surface expression modulates the activity of downstream signaling and itself can be regulated surface protease activity of TMPRSS6 (117, 118).

Nearly all of the above-described factors involved in hepcidin release have been found to be associated with hereditary hemochromatosis. Type I,II,III,IV hereditary hemochromatosis are associated with mutations in the genes encoding HFE, hepcidin, TfR2, and ferroportin, respectively (119). The first three mutations are associated with loss of function of HFE, hepcidin, or TfR2, such that hepcidin levels are diminished and no negative regulation of iron absorption and circulation can occur. The pathogenic basis of type IV hemochromatosis is associated with hepcidin inability to bind ferroportin and

block iron absorption and release into circulation (an effector function of hepcidin further discussed below). With hemochromatosis, the body is overloaded with iron, resulting in high transferrin saturations and total body iron stores that ultimately cause damage to the heart, liver, pancreas, and other organs (120). These pathogenic outcomes highlight the toxicity associated with free iron beyond the body's capacity to chaperone, and underscore the necessity of such a fine-tuned system regulating the absorption and circulation of iron.

Hepcidin release by hepatocytes can additionally be modulated by inflammation and infection. Iron is an essential nutrient for several types of bacteria, especially gram negative and siderophilic bacteria, with levels closely associated with bacterial pathogenicity in certain strains. Given this threat, the body has developed a mechanism by which circulating cytokines can trigger the release of hepcidin to reduce the levels of circulating iron (121). This host adaptation is principally responsive to interleukin-6 (IL-6) (122), although TLR-4 (123) and IL-22 (124) are additionally implicated. IL-6-dependent activation of STAT3 is required for Hepcidin release by mouse hepatocytes (125). Importantly, some hepcidin release by macrophages has been documented following inflammation (126).

Hypoferremia due to elevated hepcidin levels is a driving factor in the pathogenesis of anemia of chronic disease (127). Hepcidin is additionally implicated in anemia of chronic kidney disease (CKD). Although the pathogenesis of CKD was initially assumed to be dependent upon impaired erythropoietin (Epo) release, clinical findings of patients

suggest alternative mechanisms driving the disease. Patients require high dose erythropoietin- stimulating agents, and efficacy is augmented by dosing simultaneously with iron (128). Further, levels of hepcidin anti-correlate with ferritin levels and renal function (129), and impaired renal function prevents the urinary excretion of hepcidin from the plasma (130). Hepcidin ultimately functions to reduce iron export and availability in circulation, through binding to its receptor ferroportin (131, 132). Ferroportin is expressed by enterocytes of the gut, macrophages, and hepatocytes. The channel functions to mobilize iron into the circulation through facilitating iron transport by enterocytes, recycling of iron from senescent RBCs phagocytosed by splenic macrophages, and release of body iron stores by hepatocytes (127). Iron in senescent red cells is taken up by phagocytes of the splenic red pulp and recycled into the bloodstream, generating the majority of iron required for erythropoiesis. Of the iron necessary for supporting daily erythropoiesis, 20-25mg is obtained from this recycled iron, while 1-2mg must be absorbed from the diet to make up for iron loss (127). Upon hepcidin finding to ferroportin, the complex is internalized and routed to the lysosome for degradation, thus impairing iron release from all three sources (132). In enterocytes, iron uptake from the gut is closely coupled with iron release: hepcidin-dependent ferroportin degradation results in intracellular iron accumulation, which degrades HIF-2α and inactivates iron regulatory proteins (protein iron sensors additionally discussed in the following section), ultimately reducing the synthesis of DMT1 and impairing iron absorption from the gut lumen (133-135) (Figure 1.1). Further, hepcidin binding to ferroportin results in the activation of ubiquitin ligases, which act upon DMT1 to result in the proteasomal degradation of the transporter (136). Type IV Hereditary hemochromatosis was identified to be caused be a

C326S mutation of the extracellular region of ferroportin that binds hepcidin. This mutation maintains iron export by ferroportin, but prevents hepcidin from binding the receptor to hinder iron export, resulting in iron overload (137).

One final factor that modulates iron metabolism is erythropoiesis itself. Patients with upregulated inefficient erythropoiesis (such as with sickle cell anemia) can display iron overload, suggesting a link between the marrow and the tissues involved in iron uptake (138). A physiological mechanism exists by which enhanced erythropoiesis suppresses hepcidin, resulting in enhanced iron circulation, ultimately allowing for matching of iron-demanding erythropoiesis with iron uptake to avoid iron deficiency. Erythroferrone (ERFE), a C1q/TNF-related protein, was recently described as a candidate hormone mediating this communication. Expression profiling of murine bone marrow following phlebotomy identified *Fam123*, the gene encoding ERFE, as an upregulated potential candidate (139). *Fam123* knockout mice fail to downregulate hepcidin in models of: beta-thallassemia (140), recovery following inflammation (141), and recovery following phlebotomy (139). Further, animals demonstrate worsened anemias in these models, underscoring the importance of enhanced iron absorption in enabling erythropoiesis. However, ERFE is difficult to detect in plasma at steady state, is not known to bind any receptor, and does not directly suppress hepatocyte hepcidin in vitro (139). This collection of findings highlights an emerging role for ERFE in erythropoietic hepcidin suppression, but emphasizes the gaps that remain in our scientific understanding of this physiological mechanism.

Iron Deprivation Response

The previous section discussed how changes in erythropoiesis can modulate iron metabolism. The relationship between both systems is strong and bidirectional: changes in iron metabolism have a strong effect on erythropoiesis. Erythroid progenitors are the major consumers of body iron: responsible for 80% of the body iron demand (142). When circulating iron levels drop below a critical threshold, erythropoiesis is paused, thus preserving the diminishing supply of body iron (143). This sensitive response of erythropoiesis to circulating transferrin saturation underlies the pathogenesis of Iron Deficiency Anemia, Anemia of Chronic Disease, and Anemia of Kidney Disease. Erythroid cells are uniquely sensitive to iron: when hematopoietic cells of different lineages are expanded in differential concentrations of iron-saturated transferrin, non-erythroid lineages are resilient to much lower iron saturations than required to demonstrate an erythroid iron deprivation response (143). The erythroid iron deprivation response occurs in a cell-autonomous fashion: erythroid progenitors themselves, without an interaction with other cell types, will fail to proliferate and differentiate when exposed to reduced circulating iron (144). Specifically, CFU-Es appear to be most affected, as they fail to mature to proerythroblasts when animals are subjected to iron deficiency (145). This iron deprivation response is non apoptotic (143, 146), resulting in a blockade of progenitors in ‘suspended animation’ which may have the potential to respond when iron levels are corrected. The extent to which iron-deprived progenitors can respond appropriately to a new bolus of iron has not been studied and is a potential area of interest. The erythroid iron deprivation response is associated with alterations in several signaling pathways:

ERK, PKC, TNF-alpha, and IFN-gamma signaling are found to be hyper-activated, while signaling through mTORC1 is downregulated (143, 147, 148).

Mechanisms exist by which any cell can sense and respond to fluctuations in intracellular iron levels. These iron response pathways are conserved in the erythroid lineage and contribute to erythroid iron homeostasis. Two proteins are involved in mediating the cell-autonomous iron response: Iron regulatory protein – 1 (IRP-1) and IRP-2. IRP-1 is an aconitase enzyme that switches between catalytic function and IRP-1 function depending on iron status (149). Aconitases enzymes catalyze the reversible conversion of citrate to isocitrate via iron-sulfur clusters, and thus are sensitive to fluctuations in intracellular iron (150). IRP-1, also known as cytosolic aconitase (c-aconitase), is encoded for by a gene separate than that encoding mitochondrial aconitase (m-aconitase), the TCA cycle enzyme. With reduced levels of iron, loss of iron-sulfur integrity results in conformational changes in c-aconitase, giving rise to non-catalytic IRP-1 function. IRP-2 shares sequence homology with IRP-1, but is exclusively understood as a responder to low iron, having no enzymatic function under iron replete conditions (151, 152). IRP-2, on the other hand, is ubiquitylated and degraded when iron is present, with resultant stabilization and function under conditions of iron deficiency (153, 154).

Both IRP-1 and IRP-2 function to respond to iron deprivation through binding to mRNA transcripts. Many mRNA transcripts associated with iron metabolism contain iron-responsive elements (IREs) that bind IRP-1 and IRP-2, resulting in selective stabilization or degradation of transcripts (155). Generally, IRP binding to 3’ IREs is associated with

stabilization of transcripts, while IRP binding to 5' IREs is associated with translational repression, although IRE sequences, the numbers of IREs per transcript, and differential affinities to IRP-1 versus IRP-2 may fine tune the regulation of specific transcripts (156, 157). IRP-regulated transcripts include the mRNAs encoding TfR1, DMT1, ferroportin, and ferritin. Under conditions of low iron, DMT1 and TfR1 are upregulated, while ferritin and ferroportin are downregulated, encouraging enhanced uptake by cells under conditions of iron deprivation. Conversely, iron-overloaded cells will lack IRP-1 and IRP-2 function, resulting in the upregulation of ferritin and proper handling of excess intracellular iron (158). The process by which IRPs can regulate DMT1 was discussed in the previous section and is the mechanism by which hepcidin inhibition of ferroportin-mediated iron export can ultimately impair DMT1-mediated iron uptake in enterocytes. IRP-1 and IRP-2 functions are largely redundant: *IRP-1 -/-* mice have no overt baseline phenotype, *IRP2 -/-* mice demonstrate minors perturbations in iron metabolism, while combined knockouts demonstrate embryonic lethality (159-161). *IRP-1 -/-* mice demonstrate transient polycythemia due increased Epo, as IRP1 represses HIF signaling by Epo-secreting cells (133, 162). This phenotype provides evidence that IRP1 does not mediate the iron deprivation response in erythroid cells and that a separate mechanism exists to suppress erythropoiesis.

Mitochondrial aconitase, because of its iron-sulfur utilization and expression in the erythroid lineage, was identified as a putative candidate in erythroid iron sensing. Through its interconversions of citrate and isocitrate, m-aconitase is an essential component of the TCA cycle. With iron deprivation, erythroid endogenous aconitase activity is reduced,

resulting in decreased intracellular isocitrate levels (143). Although IREs are observed on the transcript encoding aconitase, protein levels themselves are unaffected by iron deprivation, suggesting specific alterations in catalytic function dependent upon iron. Consistent with identifying a reduction in aconitase activity, erythroid cells subjected to iron deprivation demonstrated a three-fold reduction of intracellular isocitrate levels (143). In this setting, although TCA cycle activity is expected to be reduced, the largely glycolytic (163, 164) erythroid cells demonstrate no change in ATP, NADH, or NADPH levels. Thus, iron deprivation in erythroid cells is associated with altered metabolism, changes in the levels of isocitrate, but a nonetheless competent bioenergetic state.

Drug targeting of aconitase further confirms the enzyme as an effector of the iron deprivation response. Fluoroacetate is a specific inhibitor of aconitase, undergoing intracellular metabolism to fluorocitrate, which blocks aconitase enzymatic activity. Erythroid cells subjected to fluoroacetate treatment demonstrate impaired proliferation and maturation, recapitulating the effects of iron deprivation (165). Further conclusively demonstrating the role of aconitase activity in the erythroid iron deprivation response is the observation that isocitrate treatment can deceive iron-deprived erythroid progenitors into maturing and differentiating normally as they would in the presence of iron (143). This effect is specific to isocitrate: treatment with alpha-ketoglutarate (aKG), which is one enzymatic step downstream from isocitrate, does not rescue the iron deprivation response. In a rat model of arthritis that develops anemia of chronic disease, intraperitoneal isocitrate injections were found to rescue multiple blood parameters of anemia, including RBC, MCV, and MHC (147). Similar observations were made in a

separate model of anemia of chronic disease induced by bacterial toxin, affirming the ability of isocitrate to rescue iron-restricted erythropoiesis in vivo (166). In summary, aconitase senses iron through catalytic activity in erythroid cells, and functions as an effector of the iron deprivation response.

Recent findings have implicated TfR2, the receptor responsible for transferrin sensing by hepatocytes, in erythroid function and iron sensing. The studies are limited, but consist of human and mouse data suggesting TfR2 does play a role in erythropoiesis. In a landmark study, TfR2 was found to physically interact with EpoR, with suggestions that it is required for the surface presentation of EpoR (167). Erythroid cells subjected to TfR2 knockdown were impaired in their differentiation down the erythroid lineage as compared with control knockdown. With low iron, TfR2 was observed to traffic to the lysosome and undergo surface cleavage and removal, pointing to potential effector function by TfR2 in the iron deprivation response (168-171). The contribution of TfR2 to EpoR presentation, positive versus negative, remains unclear due to contradictory findings (146, 167). More recently, genome-wide association studies (GWAS) of human blood cell parameters demonstrate an association between TfR2 polymorphisms and both MCV and MCH, parameters affected by erythroid iron deprivation (172, 173). Finally, mice were studied following bone marrow transplant of TfR2-knockout marrow into wild type recipients, such that the erythroid lineage demonstrates specific deletion of TfR2 (erythroid cells are the only cells of the marrow that express TfR2). Through analysis of bone marrow and circulating erythrocytes, it was established that this model demonstrated accelerated erythropoiesis with reduced MCV (146). Interestingly, when

adolescent mice were subjected to an iron-deficient diet, those with hematopoietic TfR2 deletion failed to demonstrate an anemic response. TfR2, therefore, must function in iron sensing, but does not sense through the transduction of a positive iron signal as with aconitase.

Scribble

Scribble is a binding protein with many binding partners that has important roles in cell signaling, vesicle trafficking, and polarity. Initially characterized as a polarity protein and tumor suppressor in Drosophila (174), the mammalian homologue is also believed to be a tumor suppressor (175), regulating cell proliferation, cell polarity, and adhesion. In drosophila, scribble mutations in the eye disc are associated with aberrant growth due to expression of cyclin E, and a manner synergistic with Ras or notch mutations(176). Scribble levels are deficient in non small-cell lung cancer (177), and its absence contributes to aggressiveness in a lung cancer murine model (178). As a negative regulator of MAPK signaling, scribble suppresses the growth of prostate adenocarcinoma, and is frequently identified mutated in human prostate cancer (179). In a prostate cancer murine model driven by K-Ras, its loss promotes neoplasia and animal death. Scribble affects signaling in several different pathways, including the suppression of ERK signaling (178, 180), perturbation of TNF signaling (181), suppression of JNK (182, 183), and suppression of Akt (184). Interestingly, several of these pathways are associated with signaling responses of iron deprivation.

Scribble regulates the location and activity of the retromer complex, a master regulator of cargo sorting of the endosomal/golgi network. Retromer-dependent trafficking of endosomes is a requirement of polarity (185), and scribble thus defines cell polarity in one way through retromer regulation (186). In drosophila, a seminal study identified scribble at the apical-basal junction where it defined the apical milieu of membrane-bound

proteins through direct binding and localization of apical epithelial determinants by the basolateral PDZ protein scribble (174). An additional study has identified Scribble-dependent regulation of the apical-basal junction in mice through regulation of E-cadherin. E-cadherin association with beta catenin is critically dependent on Scrib, such that with Scribble knockdown E-cadherin is depleted from the surface and accumulates in the golgi (187). This regulation of E-cadherin may be associated with Scrib tumor suppressor function, as Scrib loss is associated with mesenchymal transformation (188, 189). Recent findings have implicated scribble in the maintenance of the immunological synapse, as it is required for T-cell asymmetry and synaptic contact with antigen-presenting cells (190).

Of great interest is the role of Scribble in modulating receptor trafficking. Scribble is associated with vesicle trafficking through its association with the retromer complex. Further, scribble regulates synaptic vesicles in the brain, directly binding beta catenin and regulating the localization of neurotransmitter-laden vesicles at the pre-synapse of developing neurons (191). Many cell surface receptors are dynamically regulated between the surface and intracellular vesicular pools through coordinated surface export, recycling, and degradation. Scribble, through its association with machinery responsible for regulating recycling and surface export, has been implicated in the surface presentation and proper signaling of several receptors. First, in studies of 3D epithelial organization of MDCK cells, responsivity to hepatocyte growth factor was critically dependent on scribble and its interaction with βPIX, an interaction that had previously been demonstrated to be involved in surface recruitment of Rac1 and Cdc42 (192). In

thyroid cell lines, the surface presentation of TSHR, the GPCR responding to Thyrotropin, was found to be dependent on scribble association with βPIX–GIT1, also known to be involved in vesicular trafficking (193). In the brain, Scribble is essential for recycling of Glun2a NMDA receptors throughout direct binding to AP2, thus coordinating their recycling (and not lysosome-mediated degradation) when internalized following ligand activation (194). In summary, the tumor suppressor scribble, through binding machinery involved in endocytic trafficking and recycling, has an increasingly understood role in the regulation of membrane trafficking and identity, although these contributions remain incompletely understood in the setting of hematopoiesis.

CHAPTER 1 Figures

Figure 1.1 Model for hepcidin regulation of plasma iron.

Current model of Hepcidin activity proposed by Ganz and colleagues. Hepcidin acts to block to ferroportin release of iron from enterocytes, splenic macrophages, and hepatocytes. (*Adapted from Ganz, Nemeth, 2012*) (127)

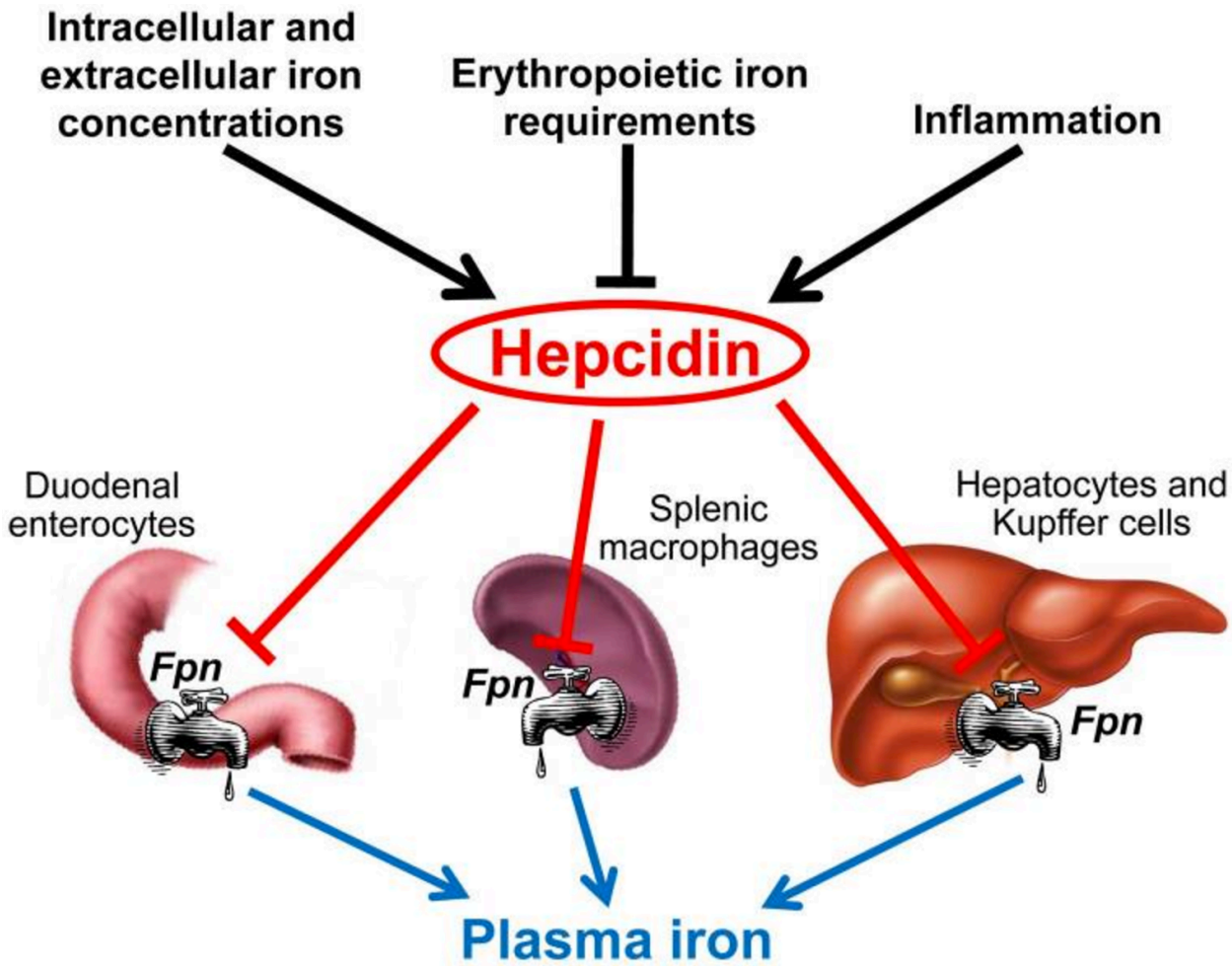

CHAPTER 2:

The Human Erythroid Iron Deprivation Response Couples Iron Sensing with EpoR Trafficking through a Scribble-TfR2 Module

Modified from the manuscript in preparation:

Shadi Khalil, Lorrie Delehanty, Stephen Grado, Maja Holy, Ryo Kurita, Yukio Nakamura, Grant Bullock, Adam Goldfarb. The Human Erythroid Iron Deprivation Response Couples Iron Sensing with EpoR Trafficking through a Scribble-TfR2 Module.

Abstract

Iron-restricted human anemias are associated with acquisition of marrow resistance to the hematopoietic cytokine erythropoietin. Regulation of erythropoietin responsiveness by iron availability serves as the basis for intravenous iron therapy in anemias of chronic disease. Erythropoietin engagement of its receptor normally promotes survival, proliferation, and differentiation of erythroid progenitors. However, erythropoietin resistance due to iron restriction selectively impairs proliferation and differentiation while preserving viability. Our results reveal that iron restriction limits surface display of erythropoietin receptor in primary progenitors and that mice with enforced surface retention of the receptor fail to develop anemia with iron deprivation. A mechanistic pathway is identified in which erythroid iron restriction downregulates a receptor control element, Scribble, through the mediation of the iron sensing transferrin receptor 2. Scribble deficiency reduces surface expression of erythropoietin receptor but selectively retains survival signaling via Akt. This mechanism integrates nutrient sensing with receptor function to permit modulation of progenitor expansion without compromising survival.

Introduction

Bone marrow erythroid progenitors, which give rise to circulating red blood cells, are the major consumers of iron in the human body. Heme synthesis during erythropoiesis utilizes approximately 80% of recycled and newly absorbed iron (195). When circulating iron levels are deficient, erythroid cells demonstrate a lineage-specific, non-apoptotic response in which they diminish proliferation and differentiation (143, 196). This nutrient deprivation response is a homeostatic mechanism in the metabolism of iron that protects iron stores in the face of depletion. This response also plays a pathogenic role by restricting erythropoiesis in iron deficiency anemia (IDA) and anemia of chronic disease and inflammation (ACDI). The molecular mechanisms mediating the iron deprivation response are incompletely understood but involve alterations in responsiveness to the primary erythroid cytokine erythropoietin (Epo). Notably, patients with IDA and ACDI demonstrate resistance to treatment with recombinant erythropoietin (128, 197), and intravenous iron therapy often restores Epo responsiveness (198-200).

Studies exploring erythroid iron sensing mechanisms have uncovered two upstream sensing elements: aconitase enzymatic activity and transferrin receptor 2 (TfR2). Aconitases are iron-sulfur cluster-dependent enzymes that convert citrate to isocitrate (150). With iron deprivation, endogenous aconitase activity declines in an erythroid lineage selective manner, decreasing intracellular isocitrate levels (143). Direct inhibition of aconitase activity recapitulates the iron deprivation response (165), while

isocitrate administration can rescue erythroblasts from the iron deprivation response in vitro and ameliorate anemia in animal models of IDA and ACDI (143, 147, 166).

TfR2 is a paralog of transferrin receptor 1 (TfR1), with expression limited mostly to hepatocytes and erythroblasts (109). TfR2 has a binding affinity for holo-transferrin thirty-fold lower than that of TfR1 (201) and thus has a proposed role in iron sensing rather than uptake (202, 203). In hepatocyte cultures, TfR2 recycling is impaired and levels are reduced with iron deprivation (169, 170). Further, TfR2 contributes to iron regulation of hepcidin levels, which act to regulate iron absorption and circulating iron levels (204). A role for TfR2 in erythropoiesis is suggested by GWAS linkages of the human locus to red cell number (RBC) and hematocrit (HCT) (205, 206). Further supporting this notion, mice lacking hematopoietic TfR2 show an abnormal erythroid response to iron deprivation including failure to downregulate RBC as well as expansion of immature progenitors in the marrow and spleen (146, 207). TfR2 regulation of iron responses occurs via signaling mechanisms that remain largely uncharacterized. Nevertheless, downstream features of the erythroid iron deprivation response include hyper-activation of multiple kinase pathways including PKCα and ERK (143), increased formation of endocytic vesicles (208), and sensitization of cells to inflammatory cytokines including IFNγ and TNFα (147). This cytokine sensitization contrasts with the Epo desensitization that also occurs with iron deprivation.

In this study, we describe a core erythroid iron deprivation circuit that links the iron sensors, aconitase and TfR2, with one another and with Scribble, a scaffolding protein

that integrates iron status with Epo receptor (EpoR) trafficking and signaling. A central feature of this circuit consists of cross-regulatory relationships in which iron availability and aconitase/isocitrate regulate lysosomal trafficking of TfR2. TfR2 physically interacts with and downregulates Scribble during iron deprivation by promoting lysosomal co-trafficking. Scribble downregulation has multiple consequences, including further loss of TfR2, impairment in EpoR surface delivery, and blockade in erythroid differentiation. The significance of impaired EpoR surface delivery in the erythroid iron deprivation response is highlighted by the finding that mutant mice with surface-trapped, endocytosis-defective EpoR fail to develop anemia in response to iron deficiency. Our results thus establish a tissue-specific nutrient-sensing pathway relevant to the pathogenesis of human anemias and their resistance to erythropoietin therapy.

Results

EpoR surface modulation is a critical component of the erythroid iron deprivation response

As Epo resistance is a critical feature of the erythroid iron deprivation response, we examined whether EpoR is affected by this pathway. To this end, primary human erythroid progenitors were subjected to overnight iron withdrawal or enzymatic aconitase inhibition followed by surface biotinylation, streptavidin pulldown, and immunoblot. We have previously shown in these progenitors that aconitase inhibition with 50 μM sodium fluoroacetate recapitulates the iron deprivation phenotype and does not impair viability (165). With the overnight treatments, total cellular EpoR levels remained unaffected (Figure 2.1). By contrast, surface EpoR levels underwent major decreases (~3-fold) with both treatments (Figure 2.2A). To determine whether this receptor modulation affected capacity for downstream signaling, iron replete and deprived progenitors underwent cytokine starvation followed by Epo stimulation for 0, 10, and 30 minutes. Consistent with their diminished surface EpoR levels, iron deprived progenitors showed a ~3-fold decrease in peak phosphorylation of STAT5 at 10 minutes (Figure 2.2B).

To assess whether alterations in EpoR surface expression contribute to the erythroid iron deprivation response, we analyzed mice with the *EpoR-H* knock-in mutation. This mutant allele causes truncation of the distal cytoplasmic domain containing motifs essential for receptor internalization (74) but retains the tyrosine 434 residue critical

for productive JAK2 signaling (209). Thus EpoR-H signals normally in response to Epo, but fails to execute the subsequent internalization and degradation characteristic of wild-type EpoR (79). For assessment of in vivo iron deprivation responses, wild type (WT) and *EpoR-H* mice were placed on an iron-deficient diet and monitored weekly for blood cell counts and indices. At the start of the study, the *EpoR-H* mice had elevated red cell numbers (RBCs) but normal size (MCV). After several weeks of iron deprivation WT animals manifested an RBC decline, which was highly significant at 42 days. By contrast, the iron deprived *EpoR-H* animals displayed no decline in RBC throughout the entire period (Figure 2.2C). Notably, both strains developed significant microcytosis over this period, with similar magnitudes and kinetics.

To compare ex vivo iron deprivation responses, we isolated Lin^- Kit^+ $Ter119^-$ erythroid stress progenitors from spleens of hemolytically-challenged WT and *EpoR-H* mice. These progenitors were then subjected to culture in a defined system adapted from iron deprivation studies in human progenitors (210). Specifically, this system used serum free medium with specified transferrin saturations and included an isocitrate treatment, which is known to reverse the erythroid iron deprivation response (210). With murine progenitors, these culture conditions permitted assessment of early erythroid differentiation, marked by CD71 upregulation, and provided an iron deprivation response reversible by isocitrate (Figure 2.2D). Notably, progenitors from the *EpoR-H* mice showed a complete loss of responsiveness to iron deprivation and isocitrate (Figure 2.2D-E), consistent with a cell-intrinsic role for surface EpoR modulation.

Scribble is regulated by the erythroid iron deprivation response and influences surface EpoR display

The alterations in surface EpoR seen with iron deprivation suggested potential involvement of Scribble, a large multidomain regulator of receptor trafficking and signaling (193, 194, 211). Notably, several features of the erythroid iron deprivation response phenocopy changes reported to occur with deficiency of Scribble: hyperactivation of multiple kinase pathways (143, 184, 188, 212, 213), enhanced formation of endocytic vesicles (208, 214), and sensitization of cells to TNFα (147, 214). Immunoblot analysis of human erythroblasts identified Scribble in cytosolic and membrane fractions as 3-4 species ranging from ~180 to 250 kD, with the largest form predominating in cytosolic and whole cell lysate preparations (Figure 2.3A). Assay specificity was confirmed using multiple independent antibodies and shRNA knockdown (Figure 2.4A-B). The basis for the multiple species appeared to arise, at least in part, from differential ubiquitylation, as treatment of cells with a deubiquitylase inhibitor induced a pattern shift to predominance of the largest form (Figure 2.4C). Importantly, Scribble levels in both fractions underwent robust downregulation with erythroid iron deprivation and showed restoration with isocitrate treatment (Figure 2.3A). Immunofluorescence on iron-replete erythroblasts revealed Scribble to be concentrated at the periphery of the cell, but also distributed throughout the cytoplasm in a vesicular pattern (Figure 2.3B). Scribble displayed a pan-cellular decrease with iron deprivation, and isocitrate treatment rescued expression particularly at the cell periphery (Figure 2.3B). In contrast to the protein changes, *SCRIB* transcripts did not decline with iron deprivation and did not respond to isocitrate (Figure

2.3C). To address the basis for Scribble downregulation at the protein level, iron deprived erythroblasts were screened with a series of protease inhibitors. As shown in Figure 2.3D, treatment of cells with a cell permeable cathepsin inhibitor CA074me prevented Scribble downregulation by iron deprivation (see also Figure 2.4D). In iron replete cells, cathepsin inhibition minimally affected cytosolic Scribble but did increase membrane levels.

To determine the consequences of Scribble downregulation on EpoR trafficking, primary progenitors underwent lentiviral shRNA-mediated knockdown. Scribble knockdown in these cells markedly diminished surface EpoR expression, but concomitant decrease in total EpoR levels complicated the interpretation of these findings (Figure 2.3E). To circumvent this limitation, we knocked down Scribble in additional human erythroid model systems. In K562 erythroleukemia cells, Scribble knockdown did not affect total levels of EpoR but dramatically reduced its surface levels (Figure 2.3F). Similarly, in HUDEP-2 cells, a non-transformed human erythroblast cell line (215), Scribble knockdown strongly decreased surface EpoR while minimally affecting total cellular levels (Figure 2.3G).

Scribble deficiency phenocopies characteristics of the erythroid iron deprivation response

Previous ultrastructural comparisons of erythroblasts from iron deficient and replete human marrow samples revealed a highly significant ($P < 0.001$) increase in

empty cytoplasmic vesicles associated with iron deficiency (208). This finding correlates with the erythrocyte vesicles specifically found in peripheral blood smears of iron deficient subjects (216). We therefore determined whether deficiency of Scribble, known to regulate vesicle formation in *Drosophila* (214), affected erythroid ultrastructure. In these studies, electron microscopy (EM) of erythroid progenitors demonstrated an association of Scribble deficiency with increases in peripheral, empty vesicles, resembling those Rozman et al. identified in patients with iron deficiency anemia (Figure 2.5A-B). Cells deficient in Scribble also displayed increases in larger vesicles with intraluminal vesicle formation.

Prior studies have determined that iron restriction of human progenitors cultured in unilineage erythroid medium for 3-5 days impairs their upregulation of surface glycophorin A (GPA) on flow cytometry (147, 210). Therefore, we employed this assay system to assess the consequences of Scribble deficiency under iron replete conditions. Strikingly, knockdown of Scribble blocked GPA upregulation in day 4 erythroid cultures, while fully maintaining cell viability (Figure 2.5C-D; and Figure 2.6A). As previously described for iron restriction (147), this blockade preferentially affected the later erythroid marker GPA, while permitting upregulation of the earlier marker CD36 (Figure 2.6B).

The capacity of iron deprived erythroid progenitors to maintain survival (143, 146, 217) despite EpoR downregulation suggested enhancement in Akt signaling, a pathway previously implicated in Epo-mediated survival (218). To examine this possibility, primary erythroblasts cultured overnight in iron-replete or free medium underwent cytokine

starvation followed by Epo stimulation. As previously observed (see Figure 2.2B), iron deprivation compromised Epo induction of STAT5 phosphorylation (Figure 2.5E). By contrast, Epo induction of Akt phosphorylation was unimpaired in iron deprived cells (Figure 2.5E). Similar studies in HUDEP-2 erythroblasts showed that iron deprivation actually enhanced Epo induction of Akt phosphorylation while blunting induction of STAT5 phosphorylation (Figure 2.5F). Prior studies have shown that Scribble, through recruitment of the phosphatases PHLPP1 and PTEN, acts as an inhibitor of Akt signaling (184, 219, 220). Consistent with this role, Scribble knockdown in erythroid progenitors induced Akt hyperphosphorylation, despite the concurrent downregulation of EpoR levels (Figure 2.5G).

Scribble and TfR2 are regulated by a shared pathway in erythroid iron deprivation

The cathepsin-dependent downregulation of Scribble in response to iron deprivation (see Figs. 2.3D and 2.4D) suggested involvement of lysosomal catabolism. Prior studies of TfR2 in hepatoma cells have shown that its destabilization in response to holotransferrin withdrawal occurs as a result of enhanced lysosomal trafficking (170). Our analysis of protein decay rates in cycloheximide-treated erythroblasts confirmed destabilization of TfR2, but not TfR1, by iron deprivation (Figure 2.7A). Notably, isocitrate treatment completely abrogated the destabilization caused by iron deprivation (Figure 2.7A-B). As expected for a factor regulated by lysosomal catabolism, treatment of cells with the cathepsin inhibitor CA074me robustly increased TfR2 levels under both iron replete and deficient conditions (Figs. 2.7C and 2.8A). This treatment also reversed the

block in GPA upregulation associated with iron deficiency, implicating lysosomal catabolism as an integral component of the erythroid iron deprivation response (Figure 2.7D).

The parallel regulation of TfR2 and Scribble by iron, isocitrate, and cathepsin (e.g. Figs 2.4D and 2.8A), raised the possibility of their participation in a protein complex. Supporting this notion, immunoprecipitation of endogenous TfR2 from K562 erythroleukemic cells efficiently co-precipitated Scribble, while immunoprecipitation of TfR1 did not (Figure 2.7E). This interaction was retained in the presence of iron chelation or aconitase inhibition. Due to a lack of antibodies suitable for endogenous Scribble immunoprecipitation, further studies were conducted with recombinant epitope-tagged factors. These studies used bi-directional immunoprecipations to confirm the interaction of Scribble with TfR2 but not with TfR1 (Figure 2.7F). Prior findings of TfR2 interacting with EpoR (167) raised the possibility of a Scribble-EpoR interaction, which was confirmed by immunoprecipitation of endogenous EpoR in K562 cells (Figure 2.8B-C). Through coexpression and immunoprecipitation of epitope-tagged components, Scribble was found to enhance interaction of TfR2 with EpoR-JAK2, and TfR2 was found to be critical for interaction of Scribble with EpoR-JAK2 (Figure 2.8D-E).

TfR2 regulates Scribble in the erythroid iron deprivation pathway

To dissect its role in regulation of the erythroid iron deprivation response, TfR2 underwent lentiviral shRNA-mediated knockdown in primary human progenitors. In iron-

replete erythroid cultures, its knockdown induced a major (~4-fold) increase in total cellular Scribble levels (Figure 2.9A-B). Because membrane-localized Scribble represents the active form (219, 220), we next focused on how this fraction was influenced by TfR2 during the erythroid iron deprivation response. In these experiments, TfR2 deficiency completely abrogated Scribble modulation by iron restriction and cathepsin inhibitor or isocitrate (Figure 2.9C-F). To determine the phenotypic consequences of these alterations, transduced progenitors were analyzed by flow cytometry, and TfR2 knockdown was found to eliminate GPA modulation by iron restriction and isocitrate (Figure 2.9 G-H). A model for erythroid coupling of iron availability with Epo responsiveness is shown in Figure 2.10. Key features of this model include the interaction of Scribble with TfR2 and their co-regulation by lysosomal catabolism in response to iron availability.

Discussion

Despite its clinical importance, the erythroid iron deprivation response has remained poorly characterized at the molecular level. Roles for TfR2 and aconitase enzymatic activity in this response have been supported by animal and ex vivo models (143, 146, 147, 165, 207). This study identifies unexpected crosstalk between these two disparate iron-sensing pathways: isocitrate, the product of aconitase, reverses the destabilization of TfR2 caused by iron deprivation. Although TfR2 has been implicated in erythroid iron sensing, little is known about critical aspects of this receptor including mechanisms of iron sensing, intracellular signaling pathways, key intracellular partner proteins, and the factors that influence its transport and catabolism. Our results address some of these gaps and provide evidence that TfR2 contributes to the erythroid iron deprivation response through functional and physical interaction with Scribble, a master regulator of receptor function.

A model depicting the relationships among TfR2, aconitase, Scribble, EpoR, and JAK2 is proposed in Figure 6. In this model, TfR2 in iron-replete erythroblasts undergoes both recycling and basal turnover through trafficking to the MVB-lysosome followed by cathepsin-mediated proteolysis. Adaptors involved in TfR2 endocytosis have not been ascertained, but the recently described interaction of Scribble with AP-2 (194) raises the possibility that this adaptor complex could participate. The surface delivery of recycling and newly synthesized TfR2 vesicles is proposed to depend on mitochondrial aconitase activity. In response to iron deprivation, TfR2 undergoes accelerated decay through enhanced lysosomal catabolism. Scribble physically interacts with TfR2 and responds to

iron deprivation with downregulation dependent on cathepsin activity and TfR2 expression. Thus, a critical feature of this iron-responsive circuit involves the regulation of Scribble by a TfR2 escort function. In the model, we postulate an early phase of iron deprivation in which increased catabolism is balanced by increased synthesis and a late phase characterized by net decline in TfR2 and Scribble levels. Scribble levels are proposed to function as a critical effector arm in this response, with downregulation affecting vesicular trafficking, EpoR surface expression, and EpoR-JAK2 signaling output.

With regard to vesicular trafficking, prior studies using electron microscopy on primary human marrow samples have shown increased “void ropheocytotic-like” cytoplasmic vesicles in erythroblasts of IDA patients as compared with healthy controls (208). In addition, prior comparisons of red cell morphology in blood smears from patients with IDA and thalassemia have identified a specific association of IDA with “prekeratocytes”, abnormal erythrocytes with submembranous vacuoles (216). Scribble deficiency in *Drosophila* imaginal disks strongly increased the numbers of Rab5-positive early endosomes (214). The identification of Scribble, known to regulate endosomal trafficking and sorting (191, 221), as a mediator of the erythroid iron deprivation response thus provides a molecular basis for the erythroid vesicular pathology seen in iron deficient patients. Notably, Scribble knockdown in human erythroid progenitors directly recapitulates the ultrastructural abnormalities of IDA, i.e. increased cytoplasmic void vesicles.

With regard to EpoR expression on the cell surface, prior cell line studies have shown the majority of this receptor to reside in intracellular pools that may not be destined for export, a property unique to this cytokine receptor (79, 222). The manner in which

EpoR cell surface density is regulated thus remains unclear, with proposed contributions coming from ligand-dependent and independent turnover (76, 79). Our results have identified Scribble levels as a major determinant of EpoR surface density, influencing both surface delivery and overall catabolism, analogous to the neuronal function of Scribble in synaptic vesicle delivery (191, 223). Previous studies have shown TfR2 to bind EpoR and promote its surface export (167). However, the role of TfR2 in erythropoiesis, positive versus negative, remains unresolved, as murine studies on TfR2 loss of function have provided conflicting results of increased and decreased erythroid Epo sensitivity (146, 167). Our knockdown studies in human progenitors suggest a more stringent requirement for Scribble than for TfR2 in surface EpoR delivery and erythropoiesis. Ultimately, our results support the existence of a multicomponent module containing Scribble, TfR2, EpoR, and JAK2, in which each component contributes to the integrity and trafficking of the whole. Thus, the complex interplay between iron regulation of TfR2 lysosomal trafficking and Epo regulation of lysosomal function could contribute to disparate functional results based on subtle differences in model systems.

Epo is the principal cytokine driving erythropoiesis, and one of its primary actions is to prevent apoptosis (62). A clinical hallmark of iron-restricted anemias (IDA and ACDI) consists of resistance to endogenous and exogenous Epo (128, 197). However, despite their Epo insensitivity, iron deprived erythroid progenitors do not undergo increased apoptosis (143, 146). Our work reconciles this paradox by demonstrating a reconfiguration of EpoR signaling associated with iron deprivation, in which decreased surface receptor expression is associated with diminished STAT5 phosphorylation but unchanged or enhanced Akt phosphorylation. This reconfiguration reflects Scribble's

opposing roles in positively regulating cell surface transport of receptors (193, 194, 211) while negatively affecting downstream survival signaling (184, 212, 213). Thus, the downregulation of Scribble associated with iron deprivation, aconitase inhibition, and mitochondrial perturbation may represent a novel nutrient/metabolic response that could concurrently desensitize growth signaling and sensitize survival signaling via a common cytokine receptor. Such a response would provide an adaptive advantage of maintaining a viable pool of erythroid progenitors poised to reconstitute erythropoiesis upon iron repletion.

Materials and Methods

Cell culture

Purified normal human donor CD34+ progenitors derived from G-CSF-mobilized peripheral blood mononuclear cells were purchased from Fred Hutchinson Cancer Research Center. After thawing, these cells were cultured 72 hours in pre-stimulation medium consisting of Iscove's modified Dulbecco's medium (IMDM, Gibco, Gaithersburg, MD) with BIT 9500 supplement (BITS, Stem Cell Technologies, Vancouver, Canada), and a cytokine mix comprising 100 ng/ml human SCF (PeproTech, Rocky Hill, NJ), 100 ng/ml human FMS-like tyrosine kinase 3 ligand (FLT3 ligand) (PeproTech), 100 ng/ml human thrombopoietin (TPO, PeproTech), and 20 ng/ml human IL-3 (PeproTech). Following pre-stimulation, the cells were moved to erythroid medium consisting of IMDM with 2 mM L-glutamine (ThermoFisher Scientific, Waltham, MS), Chelex-100-stripped (Sigma-Aldrich, St. Louis, MO) 0.05% bovine serum albumin (BSA, Sigma-Aldrich), Insulin-Transferrin-Selenium (ITS) supplement (Stem Cell Technologies), 0.0012% 1-thioglycerol (Sigma-Aldrich) recombinant human erythropoietin at 4.5 U/ml (Procrit, Beerse, Belgium), and 25 ng/ml human SCF. Where indicated, isocitrate (DL-trisodium salt isocitric acid, Sigma-Aldrich) was included at a concentration of 20 mM. Modulation of transferrin saturation was performed by combining holo-transferrin ITS-A (Stem Cell Technologies) and apo-transferrin ITS-B (Stem Cell Technologies) at the appropriate ratios. For most experiments, cells underwent analysis after three to five days of erythroid culture.

For analysis of TfR2 turnover rates, primary human CD34+ progenitors previously cultured three days in erythroid medium were treated with cycloheximide (Cell Signaling Technology, Danvers, MA) at 75 µg/ml for the indicated durations followed by immunoblot analysis. For treatment with cathepsin inhibitor, primary human progenitors underwent culture for the indicated durations in erythroid medium supplemented with 5 µM CA074me (#PI-126, Enzo Life Sciences, Farmingdale, NY) or DMSO-only as solvent control. For endogenous immunoprecipitation experiments, K562 cells were treated 16 hours with 50 µM fluoroacetate (FA, Sigma-Aldrich) or 50 µM desferrioxamine (DFO, Sigma-Aldrich). For analysis of the effects of iron deprivation on Epo signaling, primary human progenitors cultured three days in standard erythroid medium were moved into iron replete vs deficient (100% vs 0% TSAT) erythroid medium for 16 hours. HUDEP-2 cells were cultured in HUDEP-2 medium (described below) with doxycycline withdrawal for the last 24 hours of culture, -/+ iron deprivation for 16 hours. For Epo stimulation, both primary and HUDEP-2 cells underwent three hours of cytokine deprivation followed by Epo treatment at 4.5U/ml for the indicated durations and then immunoblot analysis of whole cell lysates.

K562 cells (ATCC, Manassas, VA) were grown in RPMI medium (ThermoFisher Scientific) with 10% fetal bovine serum (FBS, ThermoFisher Scientific), 2 mM L-glutamine, and Anti-Anti antibiotic supplement (ThermoFisher Scientific). HEK293T cells (ATCC) were grown in DMEM with 10% FBS, 2mM L-glutamine, and Anti-anti antibiotic supplement. HUDEP-2, a non-transformed, immortalized human umbilical cord blood erythroid progenitor cell line was derived as described (Kurita et al., 2013). HUDEP-2 cells were cultured in StemSpan SFEM (Stem Cell Technologies) with 50 ng/ml human

SCF, 3 U/ml Epo (Procrit), 1 μM dexamethasone (Sigma-Aldrich), and 1 μg/ml doxycycline (Sigma-Aldrich).

Flow cytometry

For flow cytometry, cells were centrifuged, washed, and re-suspended in PBS with 1% FBS and conjugated antibody cocktail mix. Antibodies were added at 2 μl per 100 μl of sample, which also contained a 1/100 dilution of Zombie Violet™ dye (BioLegend, San Diego, CA). After 30 minutes of staining on ice, the samples were washed with PBS with 1% FBS and run on a CyAn ADP Analyzer (Beckman Coulter, Brea, CA) or a FACSCalibur™ flow cytometer (BD, Franklin Lakes, NJ). Data analysis employed the FlowJo 8.8.7 software package, which was used for compensation and gating of live cells (based on FSC/SSC and Zombie exclusion). Fluorochrome-conjugated monoclonal antibodies to human markers (CD235a, CD36, CD13, and CD34) and murine markers (Ter119, CD71) were purchased from BD-Pharmingen (San Jose, CA).

Microscopy

For immunofluorescence, cells at a density of 10^6/ml were cytospun onto glass slides (10^5 per slide) and fixed with 4% paraformaldehyde (PFA) in PBS for 15 minutes at room temperature. Slides were washed in PBS, then permeabilized and blocked in staining buffer (0.06% Triton X-100, 2% BSA, 2% FBS in PBS) for one hour at room temperature. Staining was performed using rabbit anti-human Scribble (sc-28737, Santa Cruz

Biotechnology, Santa Cruz, CA) at a dilution of 1:100 in staining buffer overnight in a hybridization chamber at 4°C. Slides were washed three times with staining buffer, and Alexa Fluor® 488-conjugated secondary antibody (ThermoFisher Scientific) was applied at dilution of 1:500 in staining buffer for one hour at room temperature. Slides were washed three times in staining buffer, once in PBS, mounted with coverslip and medium (#H-1000, Vectashield, Burlingame, CA), and imaged on a Zeiss LSM-700 confocal microscope with 40X oil objective. Images were analyzed by Fiji ImageJ version 2.0.0. For transmission electron microscopy on primary erythroid progenitors -/+ knockdown of Scribble, cells were washed in PBS and fixed in PBS with 2% PFA and 2% glutaraldehyde for 20 minutes at room temperature. Samples were post-fixed in 1% osmium tetroxide for one hour at room temperature, and then embedded and polymerized at 65°C for 24 hours. 70 nM sections were placed on 200 mesh grids and stained with uranyl acetate and lead citrate. Grids were carbon coated to minimize conductance and imaged on a JEOL 1230 electron microscope at 80 kV. Images were assessed in a blinded manner to quantify small circular 50-100 nm vesicles and large intraluminal vesicle-containing multivesicular bodies.

Cell extraction, fractionation, immunoblot, and immunoprecipitation

To produce whole cell lysates for SDS-PAGE, cell pellets were combined with equivalent volumes of 2X Laemmli sample buffer (60 mM Tris HCl pH 6.8, 2% SDS, 100 µM DTT, 10% glycerol, 0.01% bromophenol blue) supplemented with cOmplete® Protease Inhibitors (#11836170001, Roche Diagnostics, Indianapolis, IN) and PhosSTOP®

Phosphatase Inhibitors (#04906845001, Roche Diagnostics) followed by shearing of DNA and boiling for five minutes. Isolation of cytosolic and membrane fractions employed the Abcam Cell Fractionation Kit (ab109719, Abcam, Cambridge, MA). Kit buffers and detergents were stored as frozen aliquots and supplemented with cOmplete® protease inhibitors and PhosSTOP® phosphatase inhibitors prior to cellular extraction. After electrophoresis and transfer to nitrocellulose or PVDF membranes, the blots were probed overnight at 4°C or one hour at room temperature with primary antibodies at a 1:1000 dilution in TBST with 1% non-fat dried milk. HRP-conjugated secondary antibodies (Bethyl Labs, Montgomery, TX) were applied for one hour at room temperature at a 1:5000 dilution. For global detection of biotinylated proteins, goat polyclonal anti-biotin HRP-conjugate (ab19221, Abcam) was used for one hour at room temperature at a 1:5000 dilution. HRP detection was performed using chemiluminescent SuperSignal West Pico substrate and West Femto Maximum Sensitivity Substrate (both from ThermoFisher Scientific).

Immunoblot primary antibodies consisted of the following: rabbit polyclonal anti-Scribble (#4475, Cell Signaling Technology), mouse monoclonal anti-human TfR2 (sc-32271, Santa Cruz Biotechnology), rabbit polyclonal anti-EpoR (sc-695, Santa Cruz Biotechnology), rabbit polyclonal anti-TfR1 (sc-9099, Santa Cruz Biotechnology), rabbit polyclonal anti-ATP1A1 (#3010, Cell Signaling Technology), rabbit polyclonal anti-STAT5 (#9363S, Cell Signaling Technology), rabbit monoclonal anti-phosphoSTAT5 (pY694, #4322P, Cell Signaling Technology), rabbit monoclonal anti-phosphoAkt (pS473, #4060S, Cell Signaling Technology), rabbit monoclonal anti-Akt (#4685S, Cell Signaling

Technology), mouse monoclonal anti-Tubulin (clone DM1A, #T9026, Sigma-Aldrich), rabbit polyclonal anti-LDH (#sc-33781, Santa Cruz Biotechnology).

For immunoprecipitations (IPs) on K562 cells -/+ DFO or FA treatment, cells were washed in PBS and resuspended in IP lysis buffer (150 mM NaCl, 2 mM $MgCl_2$, 10 mM HEPES (ThermoFisher Scientific), 0.5% NP40, cOmplete® protease inhibitor, and PhosSTOP® phosphatase inhibitor) at a density of 2 x 10^6 cells per 100 µl. For IPs on HEK293T transfectants, cells were washed and overlaid with 500 µl IP lysis buffer per semi-confluent 10 cm plate. Suspensions were incubated on ice for 15 minutes and centrifuged 10 minutes at 15,000 rpm at 4°C. Protein content in the supernatant was quantified by BCA. For all immunoprecipitations, 6 µg of antibody was added to 3 mg of protein extract in 1 ml lysis buffer. The following antibodies were used for immunoprecipitation of K562 endogenous proteins: goat polyclonal anti-human EpoR (ab10653, Abcam), goat IgG control (sc2028, Santa Cruz Biotechnology), mouse monoclonal anti-human TfR1 (sc-32272, Santa Cruz Biotechnology), mouse monoclonal anti-human TfR2 (sc-376278, Santa Cruz Biotechnology), and mouse IgG control (sc-2025 Santa Cruz Biotechnology). The following antibody conjugates were used for immunoprecipitation of epitope-tagged recombinant proteins: mouse monoclonal anti-Myc magnetic beads (#5698S, Cell Signaling Technology), mouse monoclonal anti-FLAG® magnetic beads (#M8823, Sigma-Aldrich), and control mouse IgG magnetic beads (#5873, Cell Signaling Technology). Immunoprecipitations with unconjugated antibodies were captured with a 1:1 mixture of magnetic beads conjugated to protein A (#88846, ThermoFisher Scientific) and to protein G (#88847, ThermoFisher Scientific), pre-washed three times in lysis buffer and added at a volume of 25 µl packed beads per

1 ml sample. Bead suspensions were rotated for two hours at 4°C, quickly washed twice in lysis buffer, slowly washed twice with 15 minutes of rotation in 4°C lysis buffer, again quickly washed twice in lysis buffer, resuspended in 50 µl Laemmli buffer, boiled, and analyzed by immunoblot as described above.

Immunoblot signals were quantified using a GS-800 calibrated densitometer (Bio-Rad, Hercules, CA). Signals were normalized using loading controls to derive relative band densities. Ponceau S stained membranes were imaged with an Alpha Innotech Fluorchem HD2 membrane imager, and total lane density was quantified by ImageJ. Immunoblots shown are representative of at least three independent experiments.

Cell surface biotinylation

Cells were washed with PBS and resuspended at a density of 10^7/ml in surface-impermeable biotinylation reagent: 1 mg/ml EZ-Link™ Sulfo-NHS-LC-Biotin (#21335, ThermoFisher Scientific) in PBS pH 8.0. The cell suspension was incubated on ice for 30 minutes and washed twice with PBS pH 8.0 supplemented with 100 mM glycine. The cells were resuspended at a density of 10^6 cells per 150 µl in biotin lysis buffer (150 mM NaCl, 5 mM EDTA, and 10 mM Tris HCl [pH 7.4] with 1% Triton X-100), incubated for 15 minutes on ice, and centrifuged at 17,000 rpm for ten minutes at 4°C. A portion of supernatant was directly analyzed by immunoblot as input, and the remainder was combined with pre-washed NeutrAvidin resin (ThermoFisher Scientific) at a ratio of 3:1 lysate:bead slurry. Slurry/lysate mixtures were rotated for one hour at 4°C, washed twice

in biotin lysis buffer, and resuspended in Laemmli buffer for immunoblot analysis of eluates.

Transfections and transduction

For cotransfections, HEK293T cells were grown in 10 cm plates to 60% confluency and transfected in normal culture medium with 20 µg plasmid using a CalPhos^{TM} kit (#631312, Clontech, Mountain View, CA). At 16 hours post transfection, the medium was exchanged with fresh growth medium for protein extraction or Opti-MEM^{TM} I (ThermoFisher Scientific) for lentiviral packaging. Protein extracts for immunoprecipitation were obtained 40 hours following initiation of transfection. For lentiviral vector packaging, supernatants were collected 40 hours following initiation of transfection.

Lentiviral packaging plasmids pCMV-dR8.74 (GAG POL TAT REV) and pMD2.G (VSV-G) were co-transfected with pLKO.1 shRNA vectors via calcium phosphate precipitation into HEK293T cells as above. A mass ratio of 3:1:4 for pCMV-dR8.74:pMD2.G:pLKO.1 was used for transfection. pLKO.1 vectors expressing shRNAs active against the following human targets were purchased (GE Dharmacon, Lafayette, CO): *SCRIB* (TRCN0000004457 and TRCN0000004458) and *TFR2* (TRCN0000063628 and TRCN0000063630). Viral supernatants were filtered with 0.45 µm syringe filters and stored at -80°C. K562 cells were incubated with viral supernatants for 24 hours, followed by puromycin selection at 2 µg/ml in growth medium for 48 hours. HUDEP-2 cells were incubated 24 hours in viral supernatants supplemented with 50 ng/ml human SCF, 3 U/ml

Epo, 1 μM dexamethasone, and 1 μg/ml doxycycline, followed by puromycin selection at 2 μg/ml in HUDEP-2 media for 72 hours. For human primary progenitors, cells were expanded in pre-stimulation medium for 48 hours and transferred to retronectin-coated 12-well plates containing viral supernatants supplemented with prestimulation cytokines. After 2 hours at 37°C, the plates were spun at 500 g for 90 minutes, then returned to 37°C. Following overnight culture, the cells were transferred to fresh viral supernatants with prestimulation cytokines, subjected to a second round of spinoculation and overnight culture followed by selection with 2 μg/ml puromycin in prestimulation medium. After 48 hours of puromycin selection, live cells were enriched by centrifugation on Ficoll-Paque PLUS^{TM} medium (#17-1440-02, GE Healthcare, Pittsburgh, PA) and washed in IMDM. Viable mononuclear cells were then subjected to erythroid cultures as described above.

The following expression constructs were used for cotransfection and coimmunoprecipitation: pcDNA6/myc-his human and mouse TfR1 and TfR2 from Dr. Paul Schmidt (Boston Children's Hospital); pcDNA3-FLAG human Scribble from Dr. Ian Macara (Vanderbilt University School of Medicine); pcDNA3-Human-EpoR and human-JAK2 from Dr. Frédérique Verdier (Institut Cochin, Université Paris Descartes, Centre National de la recherche Scientifique Paris, France) and Dr. Olivier Bernard (Universite´ Rene´ Descartes, Paris, France), respectively.

Murine models

All animal experiments were approved by the University of Virginia Institutional Animal Care and Use Committee (IACUC). The *EpoR-H* mouse strain was provided by Dr.

James Ihle (St. Jude Children's Research Hospital). For dietary induction of iron deficiency anemia, 3-week-old male weanlings were placed on iron-deficient chow (#TD.80396 custom diet, Envigo Teklad Diets, Cambridgeshire, UK) for the duration of the experiment. Weekly retro-orbital bleeds into EDTA-coated collection tubes were analyzed for complete blood counts (CBC) on a Hemavet 950 hematology system (Drew Scientific Group, Miami Lakes, FL).

For induction of erythroid stress progenitors, mice received phenylhydrazine hydrochloride (P6926, Sigma-Aldrich) at 60 mg/kg/day for two sequential days by intraperitoneal injection. Three days after the second injection, spleens were isolated, passed through a 70 μ filter mesh, incubated five minutes at room temperature in ammonium chloride lysis buffer (ACK lysis buffer, Thermo Fisher Scientific) to remove red blood cells, and washed in PBS. The cells were then incubated with a biotinylated anti-lineage cocktail (#130-090-858, Miltenyi Biotec, Bergisch Gladbach, Germany) and lineage-depleted on an AutoMACS Pro column (Miltenyi Biotec). The resulting cells were resuspended in 100 μl sterile PBS with 1% FBS plus 2μl APC-conjugated anti-c-Kit, and 2μl PE-conjugated anti-Ter119 (#341096, #555673, BD Pharmingen). Following a 30 minute incubation on ice, the stained cells were washed in PBS with 1% FBS, resuspended in IMDM, and subjected to sorting on a FACSVantage SE TurboSort DIVA (BD) in the University of Virginia flow cytometry core facility. The isolated Lin- Kit+ Ter119- progenitors were directly cultured in erythroid medium as described above, except that 100 ng/ml mouse SCF (Peprotech) was substituted for human SCF. Cells were analyzed by flow cytometry after 4 days of erythroid culture under the indicated conditions.

RNA analysis

RNA was isolated from human erythroid progenitors using the QIAGEN RNeasy Plus Mini Kit with DNAse treatment of columns prior to RNA elution. RNA yield and quality were determined on a Thermo NanoDrop spectrophotometer (Thermo Scientific). Reverse transcription was performed using the High-Capacity cDNA Reverse Transcription Kit (#4368814, Applied Biosystems). Quantitative PCR was performed using the iQ SYBR Green assay on a BioRad CFX Connect^{TM} Real-Time PCR Detection System (#1708880 Bio-Rad). For relative quantitation of transcript levels, we employed the comparative $\Delta\Delta C_t$ formula delineated in the ABI Prism 7700 Sequence Detection System user bulletin no. 2. All samples underwent triplicate analysis with normalization performed by subtraction of the C_t value for *GAPDH*. Primers were as follows: human *GAPDH* (F:5'AGCCACATCGCTCAGACA'3 R:5'GCCCAATACGACCAAATCC'3), human *SCRIB* (F:5'CTGACCCTCACCATCCTG'3 R:5'CAGAGCCACACCATTCAC'3).

Statistics

Individual results shown are representative of at least three independent experiments. All statistical analysis was performed with Prism 6 (GraphPad Software, La Jolla, CA). Graphs are displayed as mean of independent experiments +/- standard error of the mean. Data was analyzed either by two-tailed Student's *t* test, one-way ANOVA, or two-way ANOVA, on a minimum of three independent experiments. Post-hoc analysis of one-

way ANOVA studies was performed using Dunnett's multiple comparisons test. Post-hoc analysis of two-way ANOVA studies was performed using Sidak's multiple comparisons test.

CHAPTER 2 Figures

Figure 2.1. **Total EpoR levels do not change with iron and FA.**

Immunoblots of membrane fractions from erythroid progenitors untreated (Unt) or subjected to 16 hours of iron deprivation (-Iron) or fluoroacetate treatment (+FA).

Figure 2.2. **EpoR surface modulation is a critical component of the erythroid iron deprivation response.**

(A) Immunoblots (left and middle panels) of surface-biotinylated proteins from erythroid progenitors untreated (Unt) or subjected to 16 hours of iron deprivation (-Iron) or fluoroacetate treatment (+FA); densitometry (right panel) from multiple experiments for relative levels of surface EpoR associated with treatments, with normalization to total biotinylated protein levels (n = 4, one-way ANOVA, *, $P < 0.05$; **, $P < 0.01$). (B) Immunoblot analysis (left panel) of iron replete and deprived erythroid progenitors subjected to cytokine starvation and Epo stimulation for 0, 10 and 30 minutes; densitometry (right panel) from multiple experiments for fold change in STAT5a/b phosphorylation at 10 minutes associated with iron deprivation (n = 3, two-way ANOVA, *, $P < 0.05$; **, $P < 0.01$; ns: not significant). (C) Circulating red blood cell count (RBC) and red cell mean corpuscular volume (MCV) values in wild type and *EpoR-H* mutant mice subjected to dietary iron deprivation for the indicated number of days (n = 12/group, intra-group comparisons between day 7 and day 42 values, repeated measures two-way ANOVA, ***, $P < 0.001$). (D) Flow cytometry of splenic Lin^- Kit^+ progenitors from wild type and *EpoR-H* mutant mice cultured in erythroid medium with transferrin saturations of

100% or 10% -/+ isocitrate. (E) Summary of multiple flow cytometry studies as in (D) showing fold change in percentage of $CD71^+$ cells, normalized to wild type progenitors cultured in medium with 100% transferrin saturation (top panel); fold change in $CD71^+$ percentage associated with iron deprivation (middle); and fold increase in $CD71^+$ percentage associated with isocitrate treatment of iron deprived cells (bottom) (n = 3, top: two-way ANOVA, middle and bottom: Student's t test, *, $P < 0.05$; **, $P < 0.01$). Graphs depict mean ± standard error of the mean from the indicated number of independent experiments.

Figure 2.3. **Scribble is regulated by the erythroid iron deprivation response and controls surface EpoR display.**

(A) Immunoblot (left panel) of cytosolic (cy), membranous (me), and residual insoluble (in) fractions from progenitors cultured in erythroid medium at indicated transferrin saturations (%TSAT) -/+ isocitrate (IC); densitometry (middle and right panels) from multiple experiments for relative, normalized levels of membranous and cytosolic Scribble (n = 3 for each, one-way ANOVA, *, $P < 0.05$). (B) Immunofluorescent localization of Scribble in progenitors cultured in erythroid medium with the indicated transferrin saturations -/+ isocitrate (confocal microscopy with 40X oil objective). (C) qRT-PCR measurements of relative, normalized *SCRIB* transcripts in human progenitors cultured in erythroid medium with indicated transferrin saturations -/+ isocitrate (n = 3). (D) Immunoblots of cytosolic and membrane fractions from progenitors cultured in erythroid medium with the indicated transferrin saturations -/+ cathepsin inhibitor (CA074me). (E) Immunoblot of whole cell lysates (WCL, left panel) and surface-biotinylated proteins

(Streptavidin PD, middle panel) from primary progenitors transduced with lentiviral shRNA control (EV) or Scribble-targeting (shScrib) constructs; densitometry from multiple experiments (right panel) for relative levels of total EpoR, expressed as fold-change associated with Scribble knockdown, with normalization to tubulin (n = 3, t test, ***, P < 0.001). (F) Immunoblot of surface-biotinylated proteins (top left) and input lysates (top right) from K562 cells transduced with lentiviral shRNA control and Scribble-targeting constructs; densitometry (bottom) from multiple experiments as in top left panel for fold change in surface EpoR associated with Scribble knockdown, normalized to total surface-biotinylated protein (n = 3, t test, **, P < 0.01). (G) Immunoblot of surface-biotinylated proteins (top left) and input lysates (top right) from HUDEP-2 erythroblasts transduced with lentiviral shRNA control and Scribble-targeting constructs; densitometry (bottom) from multiple experiments as in top left panel for fold change in surface EpoR associated with Scribble knockdown, normalized to total surface-biotinylated proteins (n = 3, t test, ***, P < 0.001). Graphs depict mean ± standard error of the mean from the indicated number of independent experiments.

Figure 2.4. **Confirmation of three distinct protein species as Scribble and densitometry for Scribble modulation by iron deprivation and cathepsin inhibition.** (A) Immunoblot of membrane fractions from human progenitors cultured in erythroid medium. Identical samples run on three separate lanes were probed with three independent antibodies to Scribble: polyclonal rabbit from Santa Cruz Biotechnologies (SCT rab: sc-28737), monoclonal mouse from Santa Cruz Biotechnologies (SCT ms: sc-55543), and polyclonal rabbit from Cell Signaling Technologies (CST rab: 4475). (B)

Immunoblot of membrane fractions from progenitors transduced with control (EV) or Scribble-targeting (shScrib) lentiviral shRNA constructs and cultured in erythroid medium. (C) Immunoblot of membrane fractions from progenitors cultured in erythroid medium and treated with the deubiquitylase inhibitor PR-619 for 30 minutes, one hour, and three hours. (D) Densitometry from three independent experiments for Scribble levels in progenitors cultured in erythroid medium with indicated transferrin saturations -/+ cathepsin inhibitor CA074me (CA). Immunoblots on indicated subcellular fractions are normalized for loading, and values are expressed relative to Scrib levels with 100% TSAT and no cathepsin inhibitor.

Figure 2.5. **Scribble deficiency phenocopies characteristics of the erythroid iron deprivation response.**

(A) Electron microscopy of progenitors transduced with control or Scribble-targeting lentiviral shRNA constructs. Arrows denote large vesicles containing intraluminal vesicles (ILV). Arrowheads denote small peripheral vesicles. (B) Quantitation of small and large vesicles from electron micrographs of transduced progenitors as in (A), representing number of vesicles per cell-section (number of cells counted per group = 11, *t* test, **, $P < 0.01$). (C) Flow cytometry (left panel) of progenitors transduced as in (A) and cultured four days in erythroid medium; summary of multiple flow cytometry studies (right panel) of transduced progenitors ($n = 4$, *t* test, **, $P < 0.01$). (D) Summary of flow cytometry studies of transduced progenitors as in (C) depicting fold change in viability associated with Scribble knockdown ($n = 3$, *t* test, *, $p < 0.05$). (E) Immunoblot analysis (left panel)

of primary erythroid progenitors subjected to iron deprivation and Epo stimulation; densitometry (right panel) from multiple experiments for normalized differences in protein phosphorylation due to iron deprivation in cells treated with Epo for 10 minutes (*n* = 3, two-way ANOVA, *, P < 0.05; **, P < 0.01; ns: not significant). (F) Immunoblot analysis (left panel) of HUDEP-2 erythroblasts subjected to iron deprivation and Epo stimulation; densitometry (right panel) from multiple experiments for normalized differences in protein phosphorylation due to iron deprivation in cells treated with Epo for 10 minutes (*n* = 3, two-way ANOVA, **, P < 0.01; ***, P < 0.001). (G) Immunoblot of whole cell lysates from progenitors transduced with control or Scribble-targeting lentiviral shRNA constructs and cultured in iron-replete erythroid medium. Graphs depict mean ± standard error of the mean from the indicated number of independent experiments.

Figure 2.6. **Phenotypic consequences of Scribble knockdown on human erythropoiesis.**

(A) Flow cytometry assessment of viability in primary progenitors transduced with control (EV) or Scribble-tareting lentiviral shRNA constructs and cultured three days in erythroid medium, with gating on all cells. (B) Flow cytometry assessment of early and later erythroid markers, CD36 and GPA, in progenitors transduced with lentiviral shRNA constructs and cultured three days in erythroid medium, with gating on live cells.

Figure 2.7. **TfR2 stability is regulated by iron, isocitrate, and cathepsin activity.** (A) Immunoblot of whole cell lysates from human progenitors cultured in iron-replete (100% TSAT) or deficient (15% TSAT) erythroid medium -/+ isocitrate (IC) and treated with cycloheximide (CHX, 0-6 hours). (B) Densitometry for TfR2 fold decline over 3 hours of CHX, with normalization to TfR1 (*n* = 3, one-way ANOVA, *, P < 0.05; ***, P < 0.001). (C) Immunoblot of membrane fractions from progenitors cultured in erythroid medium with indicated transferrin saturations -/+ the cathepsin inhibitor CA074me. (D) Flow cytometry of progenitors cultured in erythroid medium with indicated transferrin saturations -/+ cathepsin inhibitor. Graph depicts percent decrease in GPA expression associated with iron deprivation -/+ cathepsin inhibition (*n* = 3, *t* test, *, P < 0.05). (E) Immunoprecipitation (IP) with indicated antibodies using extracts from K562 cells cultured untreated (Unt), with desferrioxamine (DFO), or with fluoroacetate (FA) followed by immunoblot detection (IB). Input immunoblot in right panel. (F) Immunoprecipitation (IP) of epitope-tagged recombinant proteins from extracts of HEK293T transfectants followed by immunoblot (IB). Graphs depict mean ± standard error of the mean from the indicated number of independent experiments.

Figure 2.8. **Densitometry for TfR2 modulation by iron deprivation and cathepsin inhibition; interactions between Scribble, TfR2, EpoR, and JAK2.**

(A) Densitometry for TfR2 levels from immunoblots of membrane fractions of human progenitors cultured in erythroid medium with indicated transferrin saturations -/+ cathepsin inhibitor (CA) (*n* = 3). (B) Immunoprecipitation (IP) with anti-EpoR antibody or control IgG on extracts from K562 cells, followed by immunoblot (IB) detection of Scribble

(Scrib). (C) IP with anti-EpoR antibody or control IgG on extracts from K562 cells cultured -/+ 50 μM fluoroacetate (FA), followed by IB detection of Scrib. (D) IP of epitope-tagged recombinant TfR2 from extracts of HEK293T transfectants followed by IB detection. Input IB is in right panel. (E) IP of epitope-tagged recombinant Scrib from extracts of HEK293T transfectants followed by IB detection. Input IB is in right panel.

Figure 2.9. **TfR2 regulates Scribble and the iron deprivation response.**

(A) Immunoblot of whole cell lysates from progenitors transduced with control (EV) or TfR2-targeting (shTfR2) lentiviral constructs and cultured in iron-replete erythroid medium. (B) Graph of densitometry from multiple experiments as in (A), reflecting fold change in levels of Scribble associated with TfR2 knockdown, with normalization to Tubulin (n = 3, one-way ANOVA, *, $P < 0.05$). (C) Immunoblot of membrane fractions from progenitors transduced with control (EV) or TfR2-targeting (shTfR2) lentiviral shRNA constructs and cultured in erythroid medium with indicated transferrin saturations -/+ cathepsin inhibitor (CA). (D) Graphs of densitometry from multiple experiments as in (C), comparing the impact of cathepsin inhibition on Scribble levels in progenitors -/+ TfR2 knockdown and iron deprivation as indicated, with normalization to total Ponceau signal (n = 3, t test, *, $P < 0.05$). (E) Immunoblot of membrane fractions from progenitors transduced with control (EV) or TfR2-targeting (shTfR2) lentiviral shRNA constructs and cultured in erythroid medium with indicated transferrin saturations -/+ isocitrate. (F) Graph of densitometry from multiple experiments as in (E) for relative Scribble levels, with normalization to total Ponceau signal (n = 3, two-way ANOVA, *, $P < 0.05$; ***, $P < 0.001$).

(G) Flow cytometry of progenitors transduced with control (EV) or TfR2-targeting (shTfR2) lentiviral shRNA constructs and cultured in erythroid medium with indicated transferrin saturations -/+ isocitrate. (H) Graphic summary of multiple flow cytometry studies as in (G) showing fold change in percentage of GPA+ cells, normalized to EV-transduced cells cultured in medium with 100% TSAT (left panel); fold decrease in GPA percentage associated with iron deprivation (top right); and fold increase in GPA percentage associated with isocitrate treatment of iron deprived cells (bottom right) (n = 4, two-way ANOVA for left panel and t test for right panels, **, P < 0.01; ***, P < 0.001; ns: not significant). Graphs depict mean ± standard error of the mean from the indicated number of independent experiments.

Figure 2.10. **A schematic model for erythroid coupling of iron availability and erythropoietin responsiveness.**

Under conditions of high iron (left panel), diferric transferrin engages TfR2 and promotes its recycling. Lysosomal catabolism of TfR2-Scribble complexes occurs at a basal rate, permitting maintenance of critical Scribble levels. At these levels, Scribble promotes EpoR surface presentation and supports STAT5 signaling while dampening Akt activation. Under conditions of low iron (right panel), TfR2-Scribble complexes undergo enhanced lysosomal catabolism. Scribble levels fall below a critical threshold, impairing surface delivery of EpoR and diminishing STAT5 activation in the face of rising serum Epo levels. The decline in Scribble also releases Akt from inhibition to enhance survival signaling from the residual surface EpoR pool.

Figure 2.1

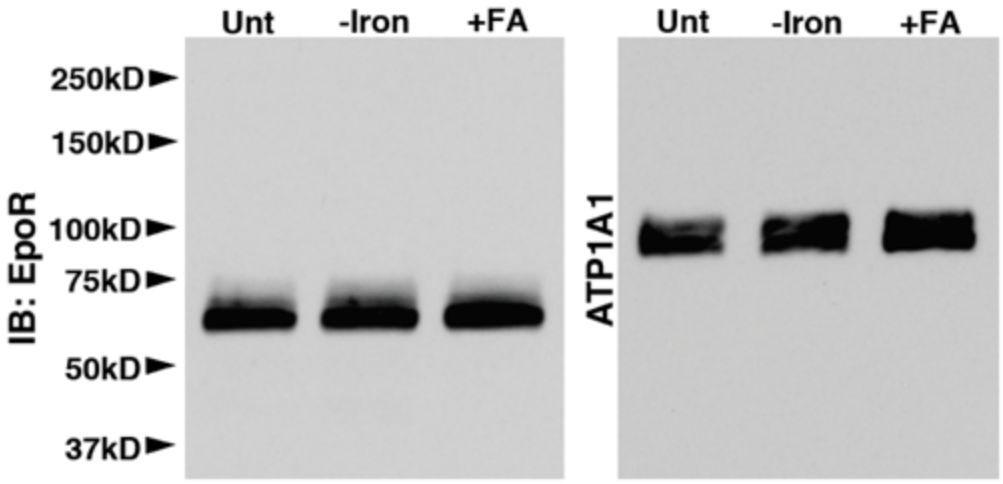
Unt
-Iron
+FA
Unt
-Iron
+FA
250kD
150kD
100kD
75kD
50kD
37kD
IB: EpoR
ATP1A1

Figure 2.2

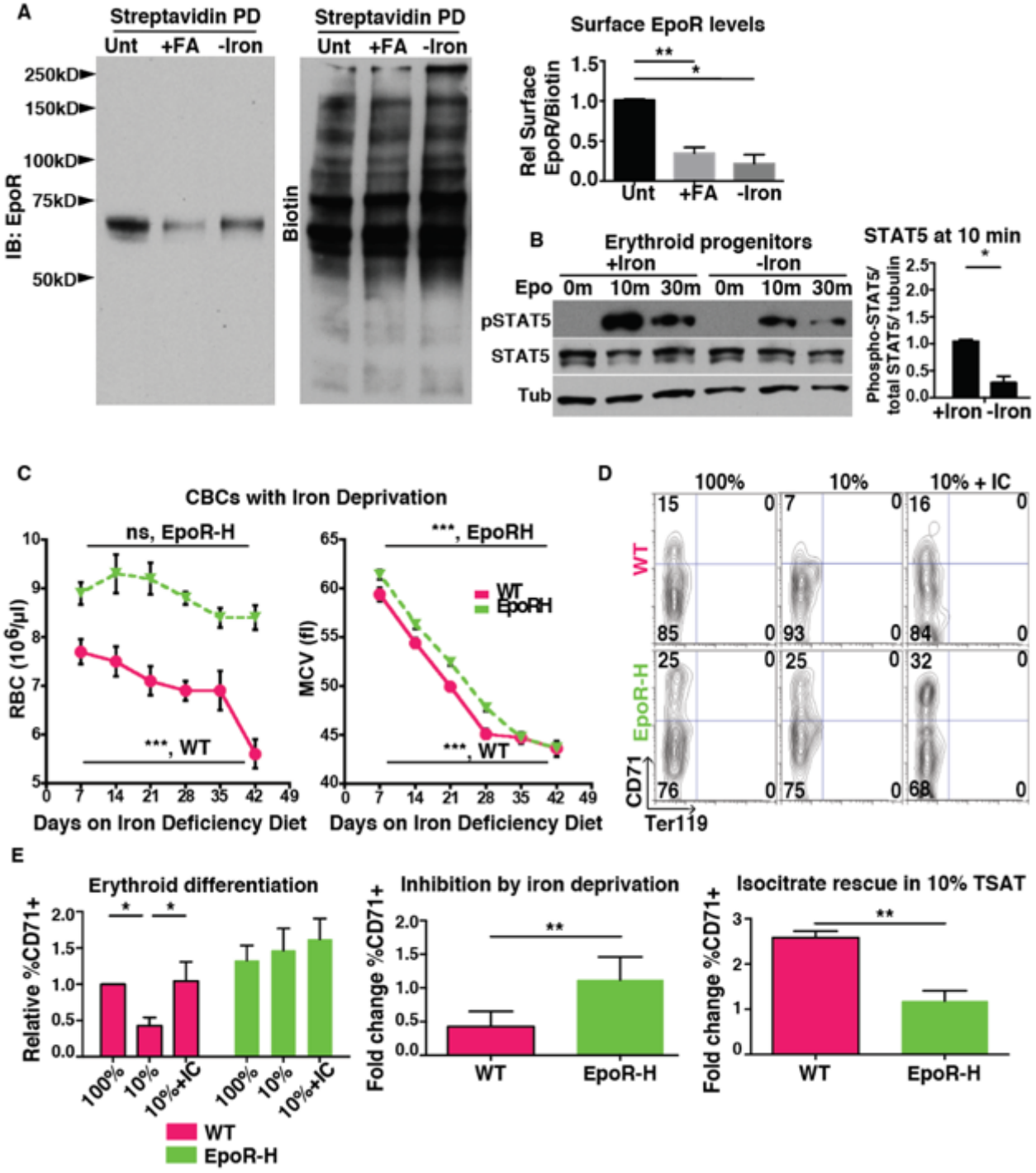
A
Streptavidin PD
Unt +FA -Iron
250kD
150kD
100kD
75kD
50kD
IB: EpoR
Streptavidin PD
Unt +FA -Iron
Biotin
Surface EpoR levels
Rel Surface EpoR/Biotin
Unt +FA -Iron
B
Erythroid progenitors
+Iron -Iron
Epo 0m 10m 30m 0m 10m 30m
pSTAT5
STAT5
Tub
STAT5 at 10 min
Phospho-STAT5/ total STAT5/ tubulin
+Iron -Iron
C
CBCs with Iron Deprivation
ns, EpoR-H
***, WT
RBC (10^6/µl)
Days on Iron Deficiency Diet
***, EpoRH
WT
EpoRH
***, WT
MCV (fl)
Days on Iron Deficiency Diet
D
100%
10%
10% + IC
WT
EpoR-H
CD71
Ter119
15 7 16
85 93 84
25 25 32
76 75 68
E
Erythroid differentiation
Relative %CD71+
100% 10% 10%+IC 100% 10% 10%+IC
WT
EpoR-H
Inhibition by iron deprivation
Fold change %CD71+
WT
EpoR-H
Isocitrate rescue in 10% TSAT
Fold change %CD71+
WT
EpoR-H

Figure 2.3

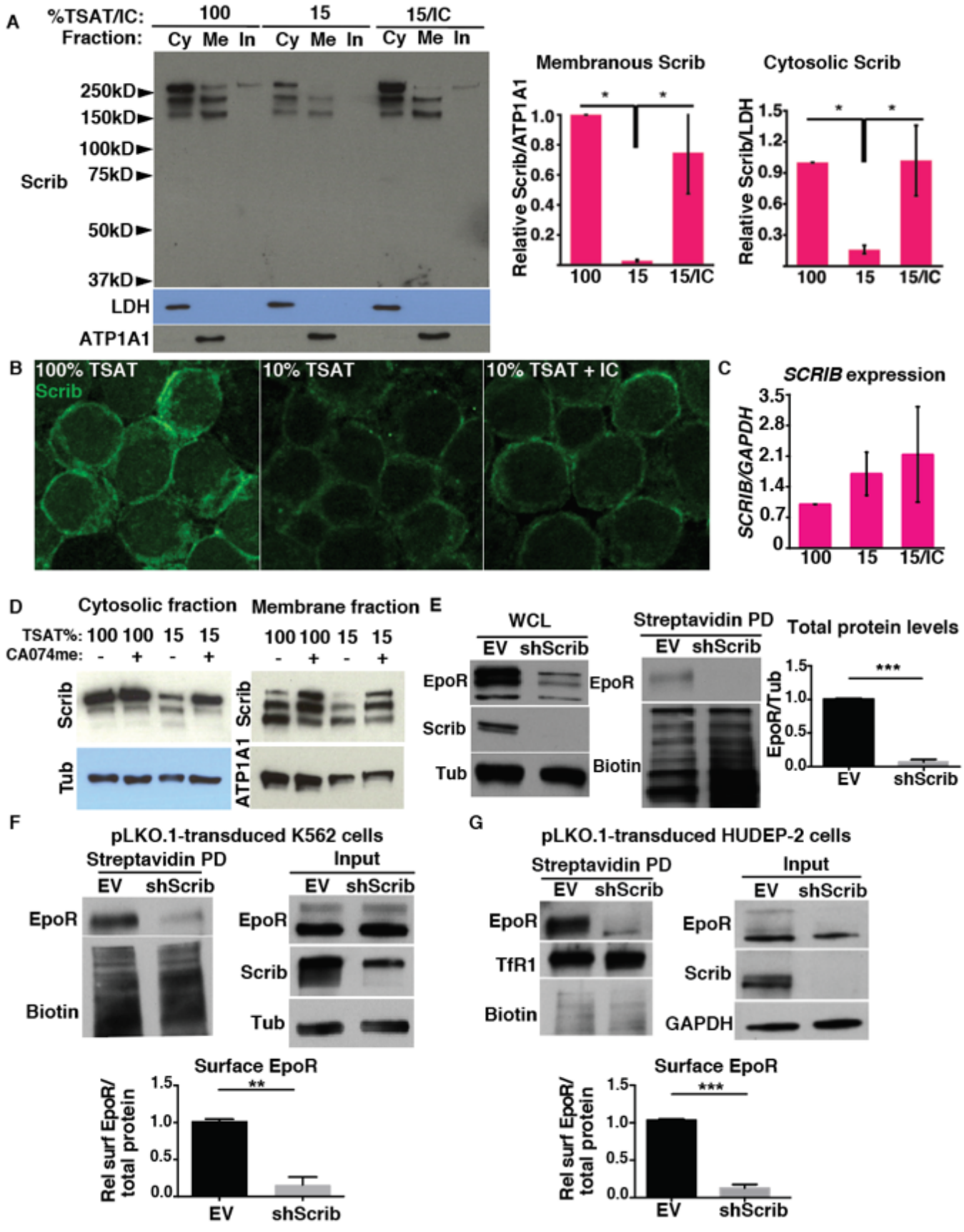
A
%TSAT/IC:
100
15
15/IC
Fraction:
Cy Me In Cy Me In Cy Me In
250kD
150kD
100kD
75kD
Scrib
50kD
37kD
LDH
ATP1A1
Membranous Scrib
Relative Scrib/ATP1A1
Cytosolic Scrib
Relative Scrib/LDH
B
100% TSAT
Scrib
10% TSAT
10% TSAT + IC
C
SCRIB expression
SCRIB/GAPDH
D
Cytosolic fraction
Membrane fraction
TSAT%: 100 100 15 15 100 100 15 15
CA074me: - + - + - + - +
Scrib
Tub
ATP1A1
E
WCL
Streptavidin PD
EV shScrib
EpoR
Scrib
Tub
Biotin
Total protein levels
EpoR/Tub
F
pLKO.1-transduced K562 cells
Streptavidin PD
Input
Surface EpoR
Rel surf EpoR/ total protein
G
pLKO.1-transduced HUDEP-2 cells
TfR1
GAPDH

Figure 2.4

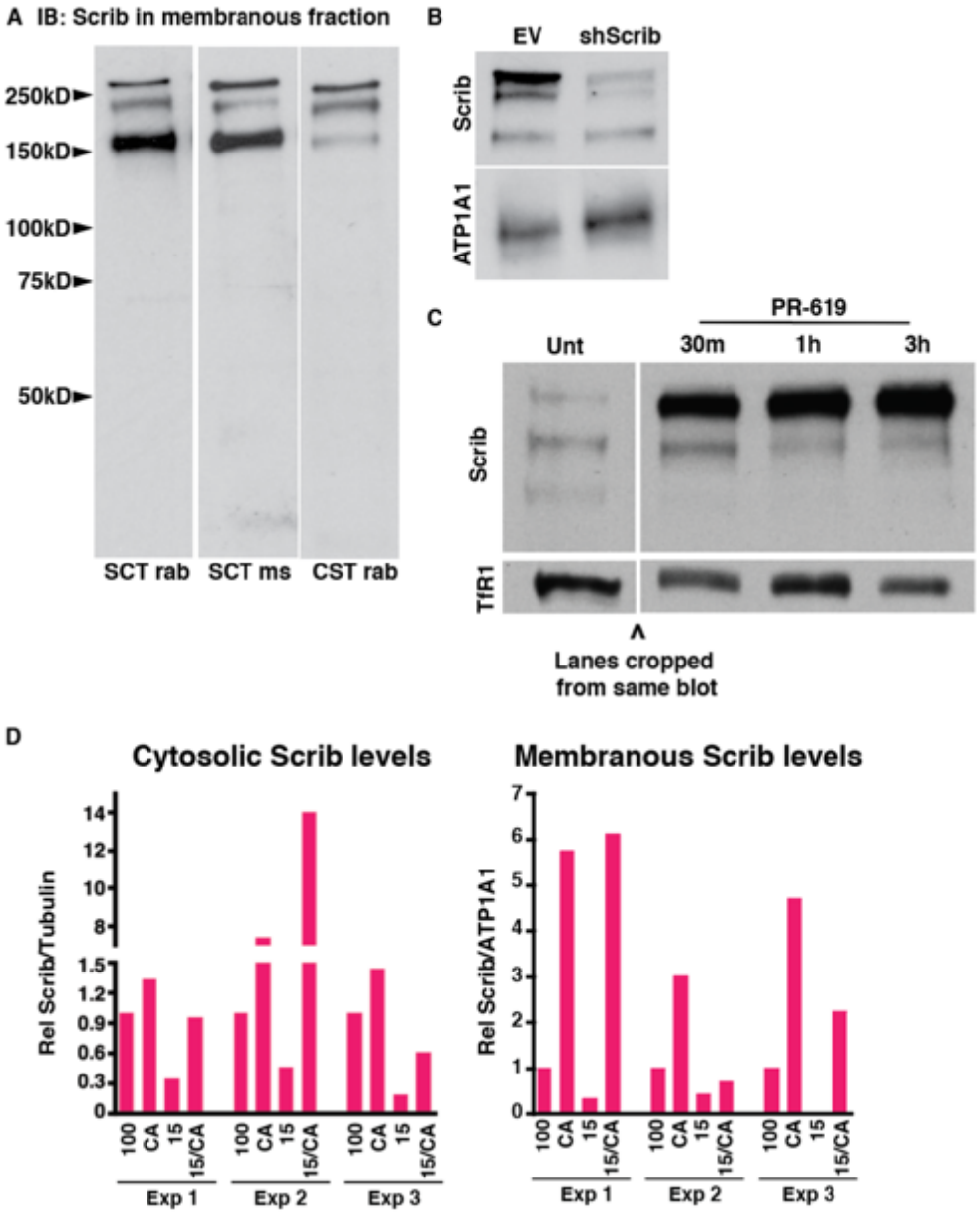
A IB: Scrib in membranous fraction
250kD
150kD
100kD
75kD
50kD
SCT rab
SCT ms
CST rab
B
EV
shScrib
Scrib
ATP1A1
C
PR-619
Unt
30m
1h
3h
Scrib
TfR1
Lanes cropped from same blot
D
Cytosolic Scrib levels
Membranous Scrib levels
Rel Scrib/Tubulin
Rel Scrib/ATP1A1
100
CA
15
15/CA
Exp 1
Exp 2
Exp 3

Figure 2.5

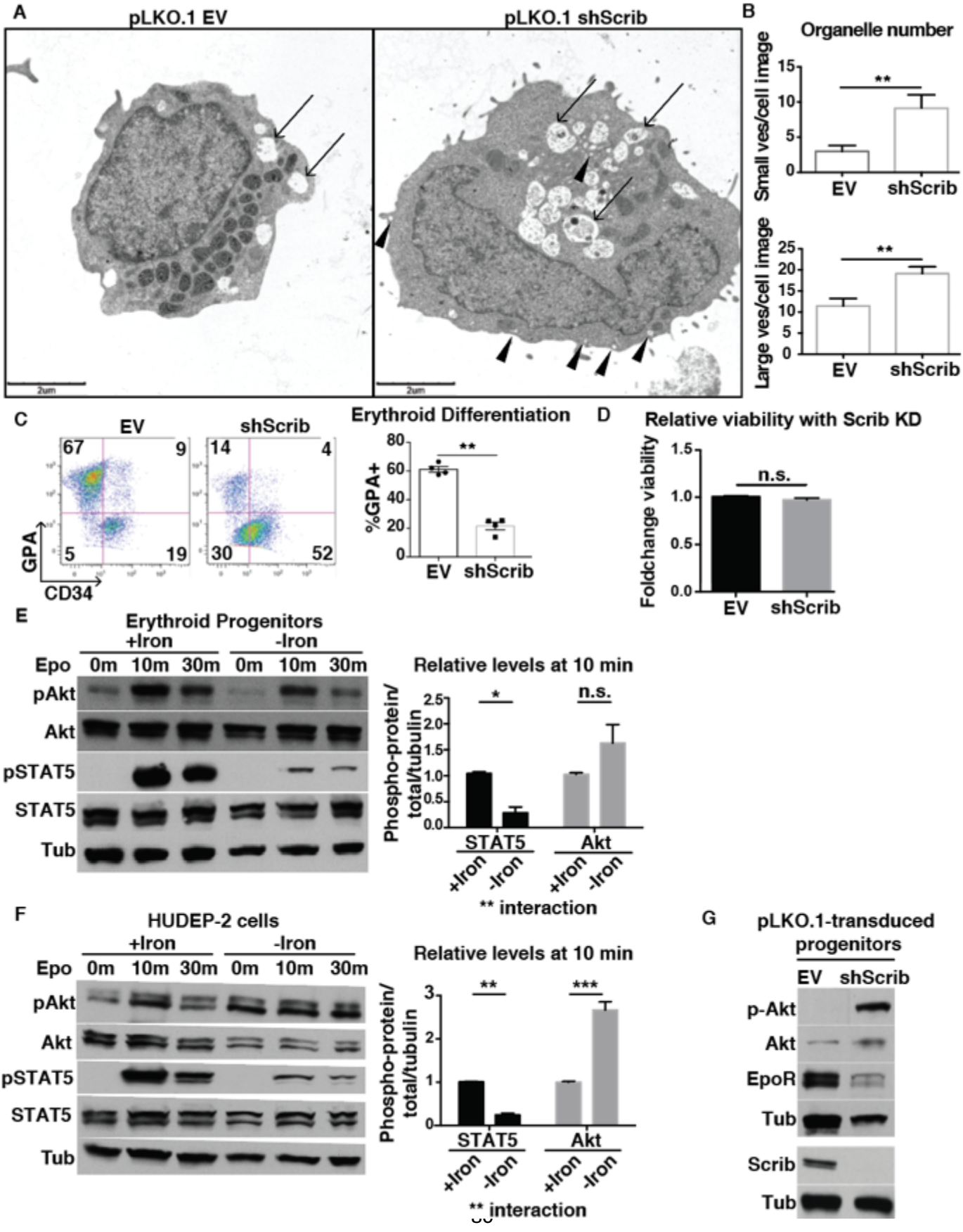
A
pLKO.1 EV
pLKO.1 shScrib
2um
2um
B
Organelle number
Small ves/cell image
15
10
5
0
**
EV
shScrib
Large ves/cell image
25
20
15
10
5
0
**
EV
shScrib
C
EV
shScrib
67
9
5
19
14
4
30
52
GPA
CD34
Erythroid Differentiation
%GPA+
80
60
40
20
0
**
EV
shScrib
D
Relative viability with Scrib KD
Foldchange viability
1.5
1.0
0.5
0.0
n.s.
EV
shScrib
E
Erythroid Progenitors
+Iron
-Iron
Epo
0m
10m
30m
0m
10m
30m
pAkt
Akt
pSTAT5
STAT5
Tub
Relative levels at 10 min
Phospho-protein/ total/tubulin
2.5
2.0
1.5
1.0
0.5
0.0
*
n.s.
STAT5
Akt
+Iron
-Iron
+Iron
-Iron
** interaction
F
HUDEP-2 cells
+Iron
-Iron
Epo
0m
10m
30m
0m
10m
30m
pAkt
Akt
pSTAT5
STAT5
Tub
Relative levels at 10 min
Phospho-protein/ total/tubulin
3
2
1
0
**
***
STAT5
Akt
+Iron
-Iron
+Iron
-Iron
** interaction
G
pLKO.1-transduced progenitors
EV
shScrib
p-Akt
Akt
EpoR
Tub
Scrib
Tub

Figure 2.6

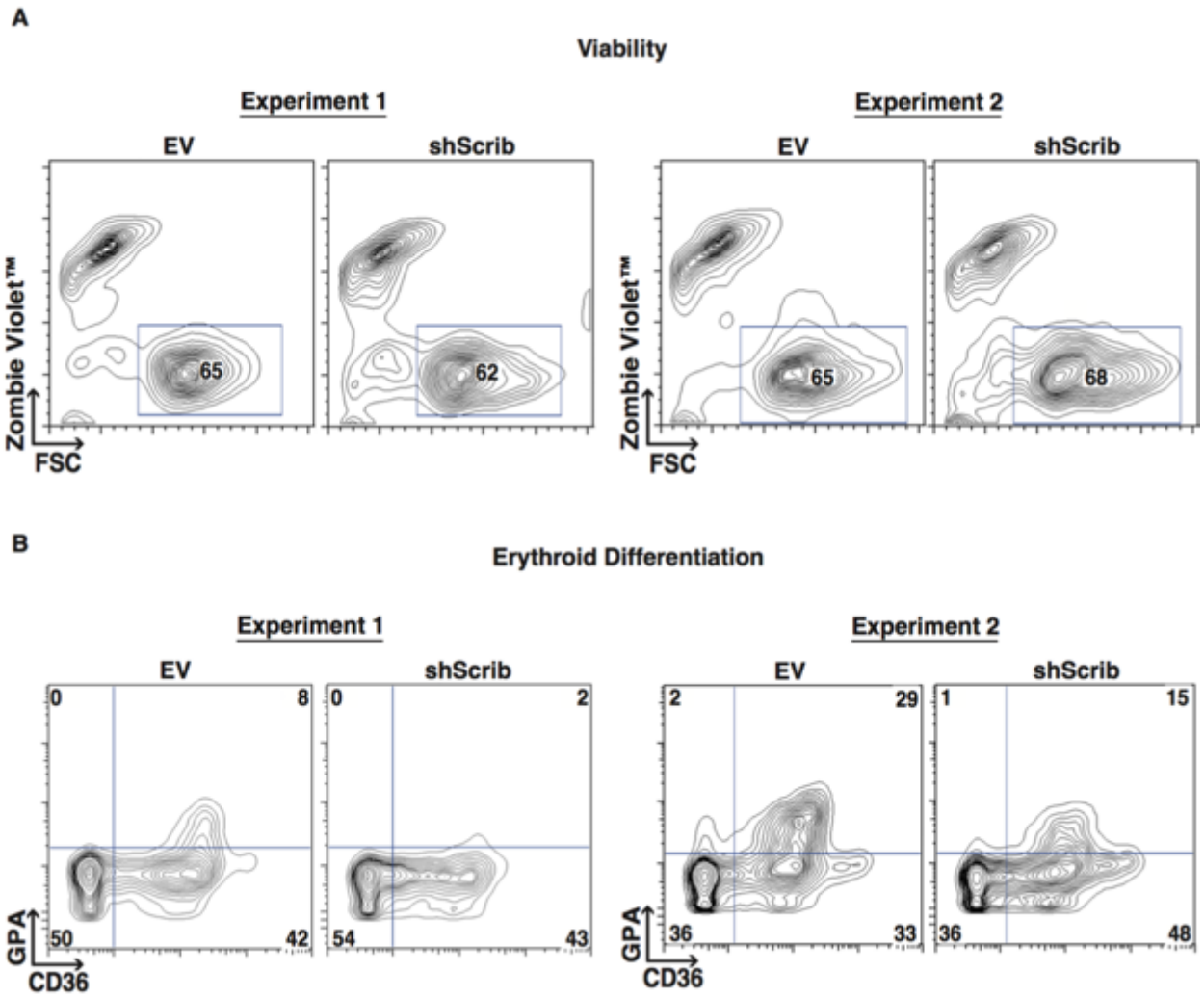
A
Viability
Experiment 1
EV
shScrib
Experiment 2
EV
shScrib
Zombie Violet™
FSC
65
62
65
68
B
Erythroid Differentiation
Experiment 1
EV
shScrib
Experiment 2
EV
shScrib
GPA
CD36
0
8
50
42
0
2
54
43
2
29
36
33
1
15
36
48

Figure 2.7

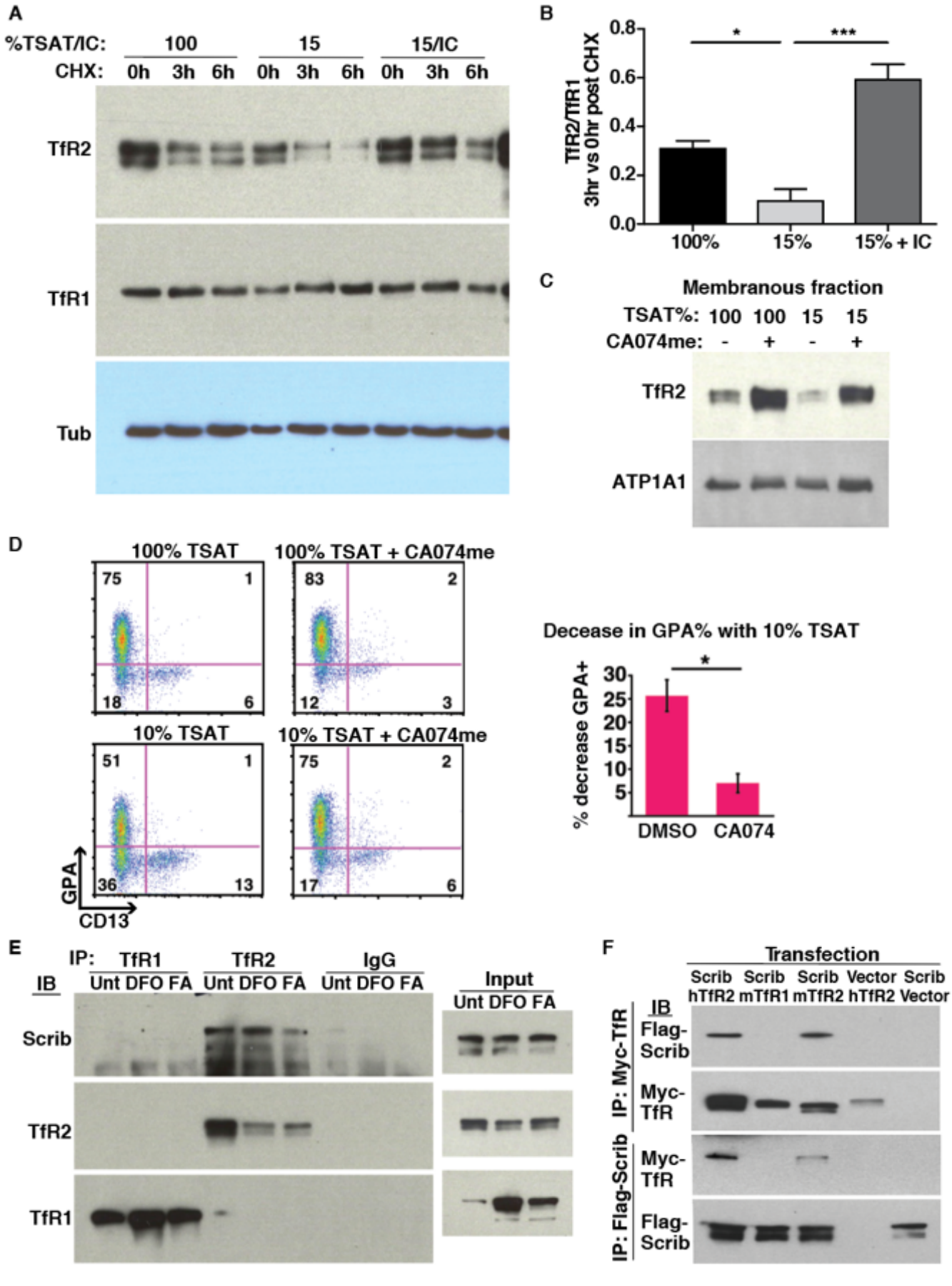
A
%TSAT/IC:
100
15
15/IC
CHX:
0h 3h 6h 0h 3h 6h 0h 3h 6h
TfR2
TfR1
Tub
B
TfR2/TfR1
3hr vs 0hr post CHX
0.8
0.6
0.4
0.2
0.0
*
***
100%
15%
15% + IC
C
Membranous fraction
TSAT%: 100 100 15 15
CA074me: - + - +
TfR2
ATP1A1
D
100% TSAT
100% TSAT + CA074me
10% TSAT
10% TSAT + CA074me
75
1
18
6
83
2
12
3
51
1
36
13
75
2
17
6
GPA
CD13
Decease in GPA% with 10% TSAT
% decrease GPA+
30
25
20
15
10
5
*
DMSO
CA074
E
IP:
TfR1
TfR2
IgG
IB
Unt DFO FA Unt DFO FA Unt DFO FA
Input
Unt DFO FA
Scrib
TfR2
TfR1
F
Transfection
Scrib hTfR2
Scrib mTfR1
Scrib mTfR2
Vector hTfR2
Scrib Vector
IB
IP: Myc-TfR
Flag-Scrib
Myc-TfR
IP: Flag-Scrib
Myc-TfR
Flag-Scrib

Figure 2.8

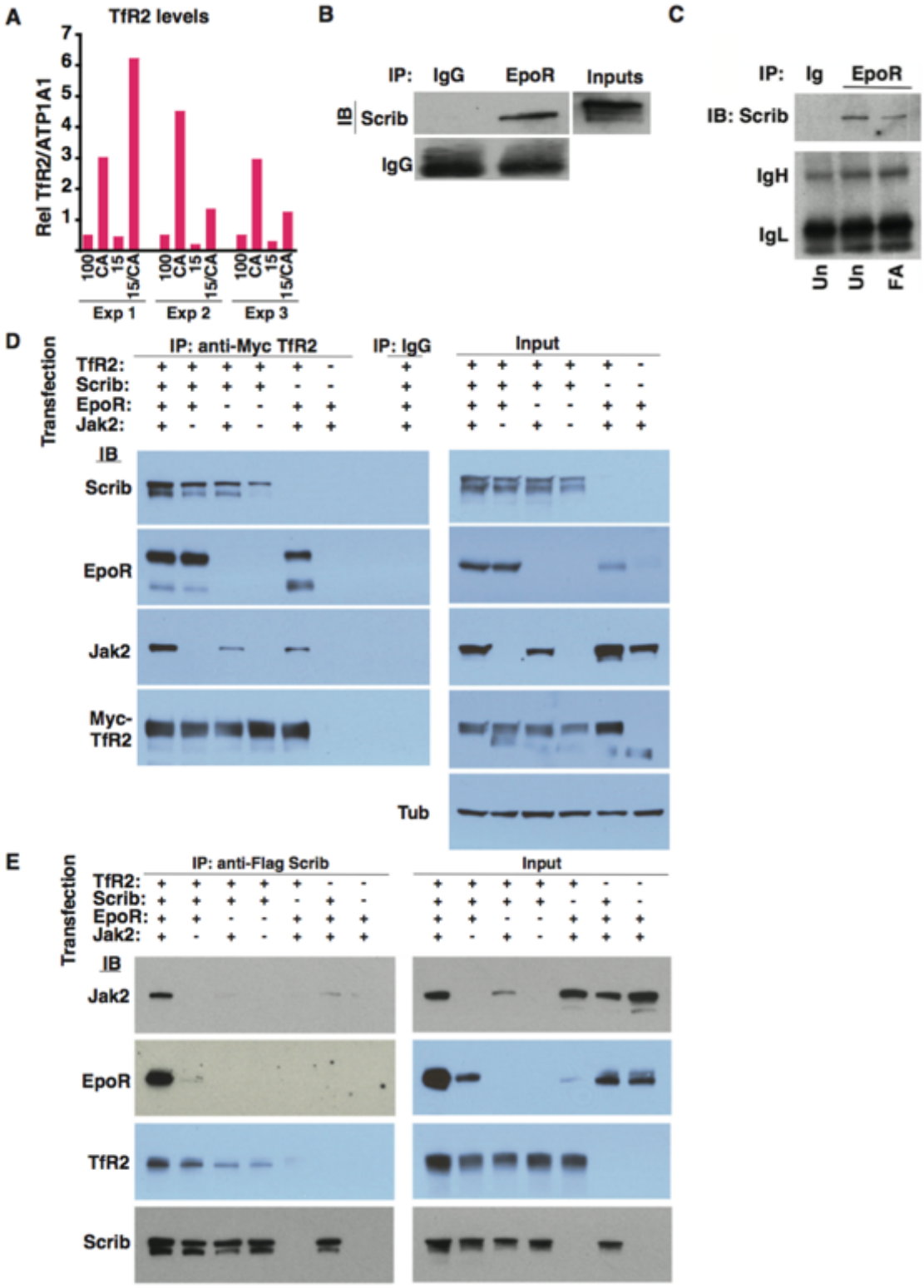
A
TfR2 levels
Rel TfR2/ATP1A1
100
CA
15
15/CA
Exp 1
Exp 2
Exp 3
B
IP: IgG EpoR Inputs
IB
Scrib
IgG
C
IP: Ig EpoR
IB: Scrib
IgH
IgL
Un
Un
FA
D
Transfection
IP: anti-Myc TfR2
IP: IgG
Input
TfR2:
Scrib:
EpoR:
Jak2:
IB
Scrib
EpoR
Jak2
Myc-TfR2
Tub
E
Transfection
IP: anti-Flag Scrib
Input
TfR2:
Scrib:
EpoR:
Jak2:
IB
Jak2
EpoR
TfR2
Scrib

Figure 2.9

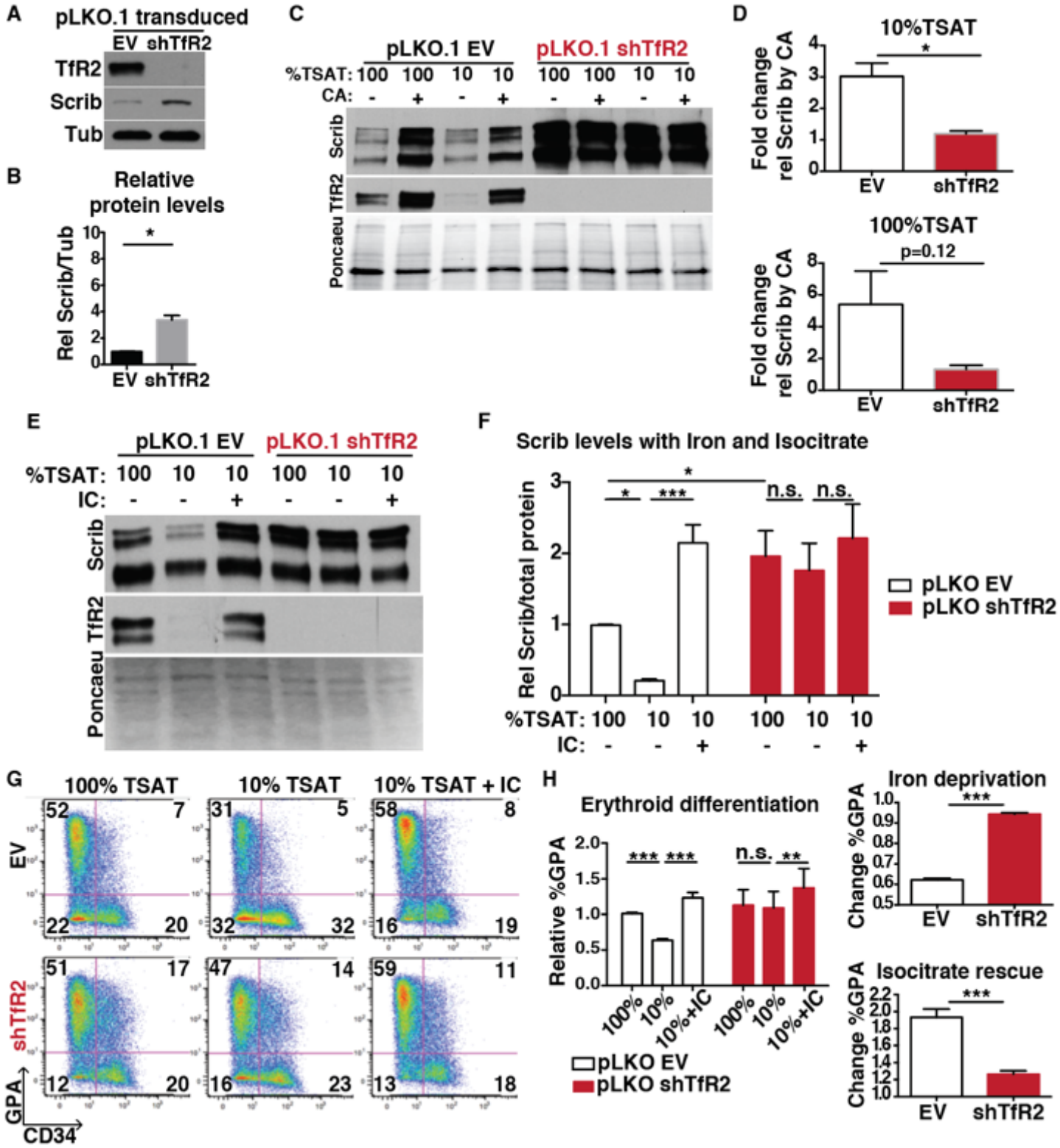
A
pLKO.1 transduced
EV shTfR2
TfR2
Scrib
Tub
B
Relative protein levels
Rel Scrib/Tub
EV shTfR2
C
pLKO.1 EV
pLKO.1 shTfR2
%TSAT: 100 100 10 10 100 100 10 10
CA: - + - + - + - +
Scrib
TfR2
Poncaeu
D
10%TSAT
Fold change rel Scrib by CA
EV shTfR2
100%TSAT
p=0.12
E
pLKO.1 EV
pLKO.1 shTfR2
%TSAT: 100 10 10 100 10 10
IC: - - + - - +
Scrib
TfR2
Poncaeu
F
Scrib levels with Iron and Isocitrate
Rel Scrib/total protein
n.s.
%TSAT: 100 10 10 100 10 10
IC: - - + - - +
pLKO EV
pLKO shTfR2
G
100% TSAT
10% TSAT
10% TSAT + IC
EV
shTfR2
GPA
CD34
H
Erythroid differentiation
Relative %GPA
100%
10%
10%+IC
pLKO EV
pLKO shTfR2
Iron deprivation
Change %GPA
EV shTfR2
Isocitrate rescue
Change %GPA
EV shTfR2

Figure 2.10

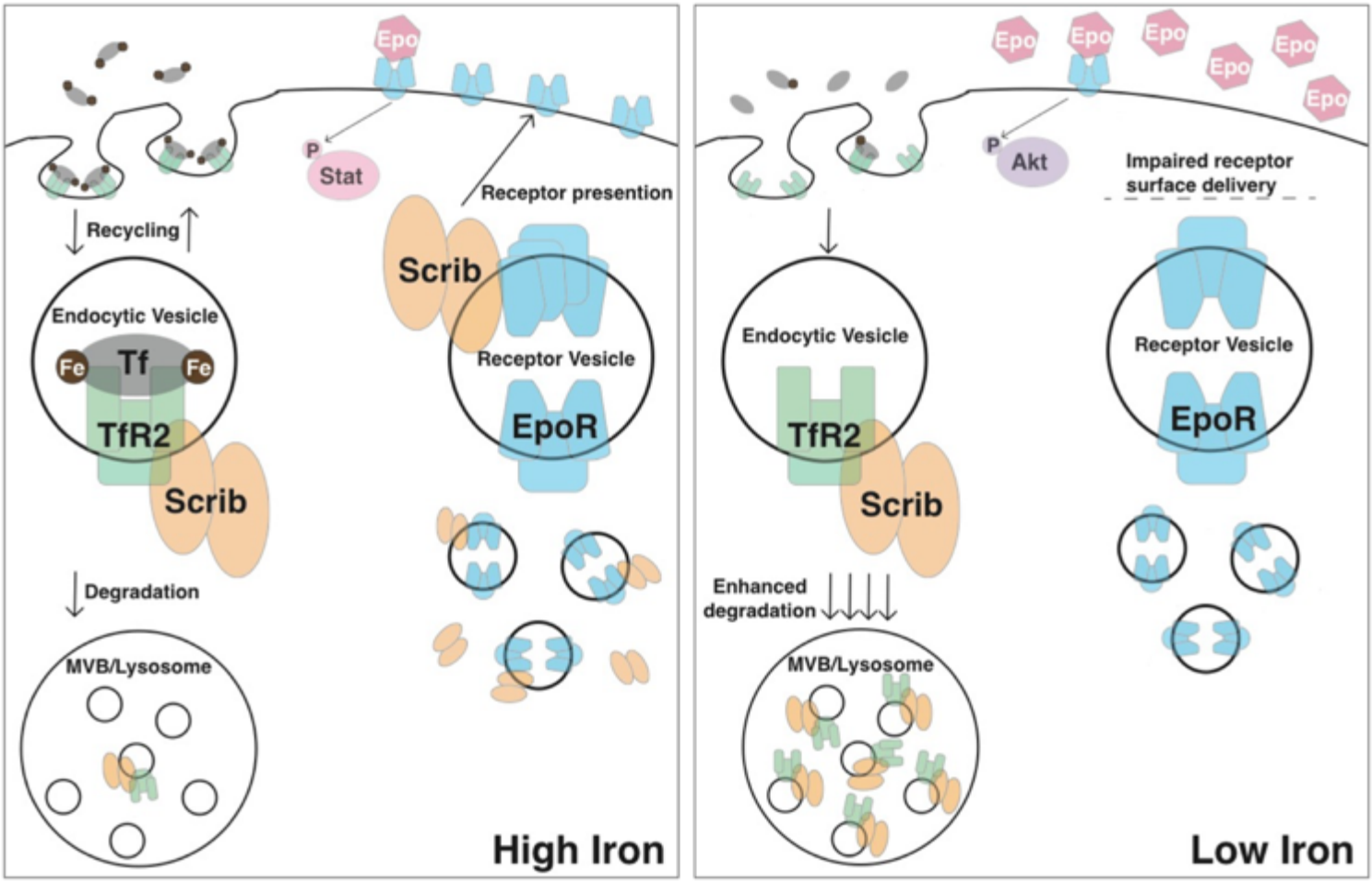
Epo
P
Stat
Receptor presention
Recycling
Scrib
Endocytic Vesicle
Fe
Tf
Fe
Receptor Vesicle
TfR2
EpoR
Scrib
Degradation
MVB/Lysosome
High Iron
Epo
Epo
Epo
Epo
Epo
Epo
P
Akt
Impaired receptor
surface delivery
Endocytic Vesicle
Receptor Vesicle
TfR2
EpoR
Scrib
Enhanced
degradation
MVB/Lysosome
Low Iron

CHAPTER 3:

A Specialized Pathway for Erythroid Iron Delivery Through Lysosomal Trafficking of Transferrin Receptor 2

Modified from the version in revision at Blood Advances:

Shadi Khalil, Maja Holy, Stephen Grado, Robert Fleming, Ryo Kurita, Yukio Nakamura, Adam Goldfarb. A Specialized Pathway for Erythroid Iron Delivery Through Lysosomal Trafficking of Transferrin Receptor 2. Blood Advances. 2017.

Abstract

Erythroid progenitors are the largest consumers of iron in the human body. In these cells, a high flux of iron must reach the mitochondrial matrix to form sufficient heme to support hemoglobinization. Canonical erythroid iron trafficking occurs via TfR1-mediated endocytosis of diferric-transferrin into recycling endosomes, where ferric iron is released, reduced and exported to the cytosol via DMT1. However, mice lacking TfR1 or DMT1 demonstrate residual erythropoiesis, suggesting additional pathways for iron utilization. How iron moves from endosomes to mitochondria is incompletely understood, with both cytosolic chaperoning and 'kiss-and-run' inter-organelle transfer implicated. TfR2, in contrast to its paralog TfR1, has established roles in iron sensing, but not iron uptake. Recently, mice with marrow-selective TfR2 deficiency were found to exhibit microcytosis, suggesting that TfR2 may also contribute to erythroid hemoglobinization. In this study, we identify alternative trafficking, in which TfR2 mediates lysosomal transferrin delivery. Imaging studies reveal an erythroid lineage-specific organelle arrangement consisting of a focal lysosomal cluster surrounded by a nest of mitochondria, with direct contacts between these two organelles. Erythroid TfR2 deficiency yields aberrant mitochondrial morphology, implicating TfR2-dependent transferrin trafficking in mitochondrial maintenance. Human *TFR2* shares a lineage- and stage-specific expression pattern with *MCOLN1*, encoding a lysosomal iron channel, and *MFN2*, encoding a protein mediating organelle contacts. Functional studies reveal these latter factors to be involved in mitochondrial regulation and erythroid differentiation, with Mfn2 required for mitochondrial-lysosomal contacts. These findings identify a new pathway for erythroid

iron trafficking involving TfR2-mediated lysosomal delivery followed by inter-organelle transfer to mitochondria.

Introduction

Erythroid cells utilize the major share of absorbed and recycling iron, approximately 25 mg daily, primarily in the synthesis of heme (224). For heme synthesis, iron must reach the mitochondrial matrix, where it is inserted into protoporphyrin IX (106). The major route of cellular iron uptake occurs through the internalization of diferric holo-transferrin via its interaction with the first transferrin receptor, TfR1. Iron is then released from transferrin-TfR1 complexes, and apo-transferrin is recycled to the cell surface. Although intracellular iron trafficking has been studied at length (225), specific mechanisms of iron delivery from endosome to mitochondrial matrix have remained incompletely understood (226). Current models include chaperone-guided cytosolic transit and direct inter-organellar transfer through transient interaction ("kiss and run") (227, 228).

Prior findings indicate additional, non-canonical iron trafficking mechanisms in erythropoiesis. For example, TfR1 null murine embryos exhibit circulating erythroid cells and are largely indistinguishable from wild type littermates during early embryogenesis. Yolk sac hematopoietic precursors from these animals can be expanded and stained for hemoglobin, indicating heme synthesis in the absence of TfR1 (104). In addition, *Slc11a2* -/- mice, which lack the Divalent Metal Transporter (DMT1) mediating export of iron from endosomes, are viable and demonstrate erythropoiesis (102). Finally, in a human patient and in mice with DMT1 deficiency, erythropoietin treatment ameliorated anemia (103). This erythropoietin responsiveness, usually lost under conditions of iron restriction, implies the existence of a DMT1-independent pathway of iron trafficking in erythroid cells.

An additional mediator of iron-transferrin uptake is the second transferrin receptor, TfR2, a paralog of TfR1 with expression restricted mainly to hepatocytes and erythroid progenitors (109). TfR2 can mediate iron uptake (229, 230), but its binding affinity for diferric transferrin is 25-30 times lower than that of TfR1 (110), leading to the notion that it functions in iron sensing rather than delivery. Consistent with its role as an iron sensor, hepatic TfR2 regulates production of hepcidin, the primary hormone regulating circulating iron levels (111, 112), and erythroid TfR2 mediates differentiation blockade in response to low iron, possibly through its interaction with the erythropoietin receptor (146, 207, 231). However, recent findings raise the possibility that TfR2 may also contribute to mitochondrial iron delivery. In a murine marrow transplant model, TfR2 null donor cells yield microcytic red cells, suggestive of defective hemoglobinization (146). This finding is further supported in humans by GWAS linkage of red cell mean corpuscular volume to the *TFR2* locus (173). Secondly, ectopic expression of TfR2 in HEK293 cells selectively increases uptake of radiolabeled iron in mitochondria as opposed to cytosol (232).

TfR2 endocytosis and intracellular trafficking employ pathways distinct from those of TfR1. Specifically, a significant fraction of TfR2 is routed to the lysosome through a TSG101-dependent ESCRT pathway, leading to its enhanced turnover as compared to TfR1. This lysosomal trafficking is further enhanced by deprivation of its ligand, holo-transferrin (168). The functional significance, mechanistic basis, and extent of ligand cotrafficking associated with TfR2 lysosomal transport remain unknown. However, emerging data support involvement of the lysosomal compartment in intracellular iron utilization. For example, mobilization of storage iron requires lysosomal catabolism of

ferritin through an autophagic pathway (90). In addition, a pathway for iron export from lysosomes has been identified, involving the cationic transporter Mucolipin-1 (233).

Our results using primary human progenitors reveal an erythroid-specific pathway of transferrin delivery to the lysosome dependent on TfR2. In addition, we identify specialized multi-organelle structures containing a core of aggregated lysosomes closely surrounded by a shell of mitochondria. At an ultrastructural level, these structures displayed frequent lysosomal-mitochondrial membrane contact sites (MCS), junctions previously implicated in transfer of ions (234-237) and metabolites (238-240). Finally, a cohort of factors is found that is developmentally coregulated with TfR2 and that participates in lysosomal biogenesis (cathepsin B), lysosomal iron transport (Mucolipin-1), and mitochondrial MCS assembly (Mitofusin-2). Loss of function studies for Mucolipin-1 and Mitofusin-2 uncovered critical roles in erythroid differentiation. The process by which erythroid cells deliver extracellular iron to heme is known to be extremely rapid and efficient (228), but evidence for a specific mitochondrial guidance system has hitherto proven elusive. These findings offer the first evidence for such a system and illustrate its participation in the erythroid differentiation program.

Results

Transferrin traffics to the lysosome in erythroid progenitors

The molecular mechanisms underlying erythroid iron delivery to mitochondria, and particularly whether lineage specific pathways exist for transferrin trafficking, remain unclear. To address these issues, initial experiments examined the uptake of transferrin in erythroid versus granulocytic progenitors. Using unilineage cultures of primary human CD34+ hematopoietic progenitors (143), cells of each lineage (Figure 3.1) were incubated with diferric transferrin conjugated with a pH-sensitive fluorochrome (pHrodo RED) to assess transferrin trafficking into acidic compartments. By fluorescence microscopy, erythroid progenitors demonstrated evidence of enhanced transferrin uptake, consistent with their increased intracellular iron demands (Figure 3.2A). Intracellular distribution in most erythroid progenitors was non-uniform and characterized by clustering of vesicles within a discrete perinuclear compartment (Figure 3.2A-B, arrows).

To determine the location of these clustered vesicles, erythroid progenitors were incubated with fluorophore-conjugated diferric transferrin and then co-stained for Lamp1, a marker of multivesicular bodies (MVB) and lysosomes. The transferrin-containing vesicles extensively co-localized with discrete perinuclear Lamp1+ aggregates (Figure 3.2C), consistent with transferrin trafficking to MVB/lysosomes. To further resolve the subcellular localization of transferrin in erythroblasts, cells were incubated with transferrin conjugated to 10 nm gold particles for uptake and subjected to electron microscopy. Transferrin was largely concentrated adjacent to intraluminal-vesicles (ILVs) inside

MVB/lysosomes, suggesting specificity of lysosomal entry via back-fusion of maturing endosomes (Figure 3.2D) (241). These findings were confirmed using transferrin conjugates with 30 nm gold particles, which can be visualized at lower magnifications (Figure 3.3A), as well as biotin-conjugated transferrin followed by streptavidin-gold staining (Figure 3.3B-C). One of the receptors for transferrin, TfR1, traffics predominantly in the recycling endosomal compartment with minimal localization in MVB/lysosomes (169). To further characterize erythroid patterns of transferrin distribution, progenitors were loaded with fluorochrome-conjugated transferrin followed by immunodetection of TfR1. Unexpectedly, transferrin showed minimal colocalization with TfR1 in erythroid cells, a finding confirmed with two independent antibodies (Figures 3.5A-B and 3.4). In stark contrast, granulocytic progenitors showed extensive colocalization of internalized transferrin with TfR1+ vesicles (Figures 3.5A-B). These findings reveal that the fundamental process of intracellular transferrin trafficking may vary dramatically based on cellular lineage.

TfR2 is required for the lysosomal trafficking of transferrin in erythroblasts

TfR2 is a paralog of TfR1, with strong extracellular homology and 30 times lower binding affinity for holotransferrin (110, 242). Clearly involved in iron sensing, a role for TfR2 in transferrin internalization has remained poorly understood. Studies in hepatocytes have shown that TfR2 undergoes lysosomal trafficking, which is enhanced by ligand deprivation (169). To compare the disposition of TfR2 and TfR1 in erythroid progenitors, we monitored the stability of a cohort of surface-labeled proteins in iron-replete culture

conditions. Consistent with its extensive recycling, TfR1 showed minimal decline at three hours following labeling. By contrast, surface-labeled TfR2 displayed a major decline at one hour and almost complete disappearance at three hours, consistent with extensive lysosomal trafficking even in the presence of holo-transferrin (Figure 3.5C).

To determine the contribution of TfR2 to lysosomal trafficking of transferrin, erythroid progenitors subjected to lentiviral shRNA knockdowns (Figure 3.6) were loaded with labeled transferrin and imaged by fluorescence microscopy and EM. In these experiments, knockdown of TfR2 dramatically changed the distribution of fluorochrome-tagged transferrin from peri-nuclear clustered vesicles to non-clustered vesicles distributed uniformly throughout the cell (Figure 3.5D). Ultrastructural characterization of gold-transferrin localization revealed a shift from MVB/lysosomes to the endosomal compartment in association with TfR2 knockdown (Figure 3.5E-F). To characterize this shift further, transduced cells loaded with fluorochrome-labeled transferrin underwent immunostaining for TfR1. In these experiments, TfR2 knockdown in erythroblasts induced the colocalization of transferrin vesicles with TfR1 (Figure 3.5G-H). Thus, TfR2 exerts an influence on the intracellular trafficking of transferrin and, in erythroid cells, promotes pathway redirection from the recycling endosome to MVB/lysosome.

Lysosomal interaction with mitochondria is a feature of the erythroid lineage

Based on the evidence for lysosomal iron transport in erythroid progenitors, we used multiple imaging techniques to examine the relationship of lysosomes with mitochondria, the principal site of iron delivery during erythropoiesis. AMNIS Imagestream

analysis of erythroid progenitors co-labeled for markers of surface lineage and internal organelles identified distinct nesting of mitochondria around a central lysosomal cluster (Figure 3.7A). These structures were not observed in similarly analyzed granulocytic progenitors (Figure 3.8A). Quantitative comparisons between the two lineages confirmed erythroid cells to have more tightly clustered lysosomes (decreased Lamp1 area), more asymmetry in mitochondrial and lysosomal distribution (increase in XY delta-centroid with respect to nucleus), and greater proximity of mitochondria to lysosomes (decrease in XY delta-centroid) (Figure 3.8B-D). Confocal fluorescence microscopy further highlighted the mitochondrial nesting around lysosomal clusters present in erythroid but not in granulocytic progenitors (Figure 3.7B). In addition, the images revealed signal overlap at the interface between the two organelle zones in erythroid cells, suggesting potential sites of inter-organellar contact.

Electron microscopy confirmed the specialized mitochondrial and lysosomal organization in erythroid progenitors (Figure 3.7C). Higher magnification images confirmed direct contacts between mitochondria and lysosomes, with evidence of mitochondrial distortion at sites of contact (Figure 3.7D, arrow). The frequency of these contacts, an average of 1.5 per 70 nm cell section, significantly exceeded that of mitochondrial-mitochondrial contacts, suggesting their specificity (Figure 3.7E). Analysis of cells loaded with gold-labeled transferrin as in Figure 3.5 further highlighted the direct contact of functional lysosomes with mitochondria (Figure 3.7F). Emphasizing the importance of lysosomal transport in the delivery of mitochondrial iron, total heme content was significantly reduced in erythroid progenitors treated with bafilomycin, an inhibitor of lysosomal transport and function (Figure 3.7G). Importantly, an ultrastructural comparison

of erythroid and granulocytic progenitors revealed the mitochondria-lysosomal contacts to be enriched in the erythroid lineage (Figure 3.7H-I).

TfR2 influences erythroid mitochondrial structure

Prior studies have shown impaired mitochondrial iron uptake to be associated with decreased organelle size (243). To examine the influence of TfR2 on mitochondria morphology, the erythroid cell line K562 underwent shRNA knockdown followed by AMNIS Imagestream quantitative analysis. In these studies, TfR2 knockdown clearly reduced mitotracker staining of cells, consistent with TfR2 regulation of mitochondrial mass (Figure 3.9A). Ultrastructural studies of marrow cells from wild type and *Tfr2*^{Y245X} murine strains further confirmed that TfR2 loss resulted in erythroid cells with reduced mitochondria size (Figure 3.9B-C). By contrast, granulocytes from *Tfr2*^{Y245X} mice were unaffected in mitochondrial size, suggesting that the erythroid defects are cell-intrinsic (Figure 3.9B-C).

An ultrastructural hallmark of intra-mitochondrial iron stored in mitoferritin consists of electron-dense foci within the mitochondrial matrix(244-250). In human hematopoietic progenitors, such foci were readily identified in erythroid mitochondria (Figure 4D). Notably, TfR2 knockdown in erythroblasts reduced the number of foci per mitochondria (Figure 3.9D-E). To assess the contribution of TfR2 and TfR1 to mitochondrial iron uptake, erythroid progenitors were subjected to either TfR2 or TfR1 knockdown (Fig 3.10A) and analyzed for total heme content. Transduced cells showed no significant difference in CD36 and GPA expression, markers of earlier and later erythroid

differentiation (Fig 3.10B). Both TfR2 and TfR1 knockdown significantly reduced total heme content (Fig 3.9F). Thus, TfR2 in erythroid cells showed an influence on multiple mitochondrial parameters including size, matrix deposits, and heme content.

Erythroid roles for lysosomal and mitochondrial factors co-regulated with TfR2

Our results have implicated the lysosomal compartment as an intermediate in erythroid iron flux, suggesting the existence of downstream pathway elements involved in lysosomal-mitochondrial iron transfer. Notably, the lysosomal divalent cation channel Mucolipin-1 has recently been demonstrated to mediate lysosomal iron efflux(233). To assess the role of Mucolipin-1 in erythropoiesis in vivo, heterozygous intercrosses were used to generate *Mcoln1*$^{-/-}$ mice. As compared with littermate controls, *Mcoln1*$^{-/-}$ mice displayed reductions in red blood cell counts, hemoglobin levels, and hematocrit (Figure 3.11A). Their anemia was associated with evidence of decreased marrow erythropoiesis, including gross pallor of the femur and increased proportion of marrow myeloid progenitors as assessed by H&E stain (Figure 3.11B-C). Flow cytometry of the marrow further demonstrated decreased erythropoiesis (Figure 3.11D-E). Electron microscopy on bone marrow revealed smaller mitochondria in erythroblasts from *Mcoln1*$^{-/-}$ mice (Figure 3.11F-G). This defect was erythroid-specific as granulocytes from *Mcoln1*$^{-/-}$ mice demonstrated larger mitochondria than those in wild type granulocytes.

Similar expression patterns of genes can provide insight into cooperative functions. In the BloodSpot (http://servers.binf.ku.dk/bloodspot) normal human hematopoiesis (DMAP) database, transcripts of *MCOLN1* show dynamic lineage- and stage- specific

modulation identical to that of *TFR2 (*Figure 3.12A) (251). *CTSB*, the gene encoding the lysosomal Cathepsin B protease, and *SLC11A2*, the gene encoding DMT1, demonstrated similar modulation of expression (Figure 3.13A), supporting the existence of a cohort of co-regulated lysosomal and mitochondrial genes involved in stage-specific events in erythropoiesis. To identify additional candidate factors involved in erythroid mitochondrial iron delivery, we used the BloodSpot Gene Correlations function, which calculates the Pearson's correlation of all gene signatures, to identify the top genes that correlated in expression pattern with *MCOLN1* (251). The top two genes were *MFN2*, encoding Mitofusin-2, a mitochondrial outer membrane protein involved in mitochondria-endoplasmic reticulum contacts (252), and *ATPV0C*, a V-ATPase that contributes to vesicular acidification and lysosomal activity (Figure 3.12B) (251, 253). Visualizing *MFN2* expression on a hierarchical differentiation tree heatmap revealed an expression pattern identical to those of *TFR2* and *MCOLN1*, with dramatic upregulation in the intermediate-stage CD34- CD71+ GPA+ erythroid progenitors, followed by strong downregulation in later-stage CD34- CD71lo GPA+ erythroid cells (Figure 3.13B).

Prior implication of Mitofusin-2 in mitochondrial contacts with the endoplasmic reticulum (252) and lysosomal fusion with autophagosomes (254) suggested a potential role in the formation of mitochondria-lysosomal contacts in erythroblasts. To examine this possibility, lentiviral shRNA knockdowns were performed on primary human erythroid progenitors (Figure 3.12C), followed by ultrastructural analysis. In these experiments, Mitofusin-2 knockdown reduced the numbers of direct contacts between mitochondria and lysosomes (Figure 3.12D-E). Analysis of total heme content in these cells demonstrated reduced heme with Mitofusin-2 knockdown (Figure 3.12F). Further,

knocking down Mitofusin-2 in stage-fixed K562 and HUDEP-2 cells similarly reduced total heme content (Figure 3.12F). Flow cytometry of transduced progenitors differentiated down the erythroid lineage demonstrated impaired upregulation of GPA and CD36 with MFN-2 knockdown, suggesting blockade of erythroid differentiation (Figure 3.12G).

We sought to examine the potential for a physical interaction between TfR2, MFN2, and Rab7, a lysosome-associated protein. Analyzing lysates from K562 cells, we observed coimmunoprecipitation between endogenous TfR2 and Rab7, additionally observing some immunoprecipitation of TfR2 with Mitofusin-2 (Figure 3.13C). Immunoprecipitation of tagged recombinant TfR2 verified the physical interaction with Rab7 (Figure 3.13D). Antibody limitations precluded the study of endogenous MCOLN1.

Discussion

Intracellular trafficking of iron and transferrin has been extensively studied, with many of the critical pathway components identified. Erythroid cells, however, display unique requirements for high-efficiency mitochondrial iron delivery to support rapid and abundant heme synthesis while minimizing exposure to oxidative stress. A key aspect of this specialized “pipeline” appears to consist of inter-organellar transfer in which iron transits from endosomes to mitochondria while bypassing exposure to the chelatable cytosolic compartment (226). An erythroid role for the canonical TfR1-mediated recycling endosomal pathway has been supported by the profound anemias associated with mutations in *Tfrc*, *Slc11a2*, *Steap3*, or Sec15l1 (255). However, the molecular basis for directed transfer of iron from endosomes to mitochondria remains unclear, and erythroid-specific participants in this process have hitherto not been identified. Furthermore, the residual erythropoiesis present in animals lacking TfR1 (*Tfrc*) or DMT1 (*Slc11a2*) supports the existence of additional non-canonical pathways for erythroid mitochondrial iron delivery (102, 104).

Results from this study identify an erythroid-specific, TfR2-dependent route for transferrin uptake and lysosomal delivery. These findings are consistent with the distinguishing characteristics of TfR2 as a tissue-specific receptor that undergoes rapid lysosomal trafficking, in contrast to the ubiquitously expressed TfR1 that undergoes obligate recycling (256). Our data also identify an erythroid-specific organelle configuration involving mitochondrial clustering around a central lysosomal core with

frequent MCS between the two organelle types. Although the pathway may involve additional steps of iron trafficking between the lysosome and mitochondria, these structures may offer a dedicated direct pathway for mitochondrial iron transfer via lysosomal transit. Further supporting the lineage specificity of such a pathway is the dynamic co-regulation with TfR2 of a cohort of factors involved in lysosome function, lysosomal iron export, and mitochondrial contact formation: ATP6V0C, Cathepsin-B, Mucolipin-1, and Mitofusin-2. Specifically, transcripts encoding these factors show highly restricted and coordinated expression in human erythroblasts at the CD34- CD71+ GPA+ stage of development (Figure 3.12). Prior studies in reticulocytes have identified brief, transient endosomal contacts with mitochondria as a potential means of inter-organellar iron delivery (227). Whether this “kiss and run” mechanism pertains to trafficking in polychromatophilic erythroblasts during peak iron flux remains undetermined. The random and sporadic endosomal-mitochondrial contacts associated with “kiss and run” make this mechanism unfit solely to meet all demands associated with high-amplitude heme biosynthesis. Assembly of stable lysosomal-mitochondrial contacts at the stage of peak iron flux provides an erythroid-specific support mechanism to assist in efficient and accurate mitochondrial iron delivery.

Although TfR2 expression is dispensable for erythropoiesis mice with bone marrow knockout of *Tfr2* have microcytic red cells, consistent with impaired iron-loading (146). Our data in human erythroid progenitors show that TfR2 affects intracellular distribution of transferrin but not overall uptake (Figure 3.5), supporting the existence of multiple distinct but overlapping pathways for iron utilization in this lineage. The strong influence of TfR2 on erythroid transferrin trafficking may seem paradoxical in light of its low ligand-

binding affinity as compared with TfR1 (110). However, ligand internalization may also be influenced by surface receptor abundance and internalization rates. Furthermore, plasma levels of circulating holotransferrin are approximately 100 times higher than the dissociation constant (K_d) of the TfR2-holotransferrin interaction, which likely overwhelms affinity differences between TfR2 and TfR1 and predicts full ligand saturation of TfR2. Finally, TfR2 could regulate transferrin trafficking in an indirect manner, through binding and regulating factors involved in endosomal transport.

Our study identifies *MFN2* as a critical erythroid gene coregulated with *TFR2* and required for differentiation. The protein product, Mitofusin-2, participates in several aspects of mitochondrial remodeling including fusion, contact formation with other organelles such as endoplasmic reticulum, and autophagy (252, 254, 257, 258). *MFN2* is downregulated in progenitors from patients with refractory anemia with ring sideroblasts (RARS) (259), a myelodysplastic syndrome with mitochondrial iron overload, suggesting feedback regulation by mitochondrial iron levels. The functions of Mitofusin-2 relevant for erythroid differentiation remain unestablished. One intriguing possibility is that developing erythroblasts co-opt components of the autophagy machinery to promote assembly of lysosomal-mitochondrial networks that support differentiation. Supporting this notion, Mitofusin-2 participates in lysosomal fusion events (254, 260), and additional autophagy factors, ATG7 and Nix, have been found to contribute to early stages of erythropoiesis (50, 51). Importantly, our ultrastructural studies show that the lysosomal-mitochondrial contacts within proliferating erythroblasts do not represent bona fide autophagy. An autophagy-related process of holo-ferritin catabolism, ferritinophagy, has also been implicated as a route for erythroid iron trafficking (90). However, the absence of

hematologic abnormalities in mice lacking ferritin heavy chain suggest this process is dispensable for erythropoiesis (261).

In addition to a role in supporting heme synthesis, TfR2-mediated mitochondrial iron delivery might also provide a sensing mechanism. Extracellular iron sensing by TfR2 is known to regulate hepcidin production and erythropoiesis (146, 202, 203), but the molecular basis for these functions has not been identified. An established sensor highly responsive to intracellular iron fluctuation consists of mitochondrial aconitase, an iron-sulfur cluster enzyme that mediates the erythroid iron restriction response (143, 147, 165). Rapid and continuous mitochondrial delivery of extracellular iron via lysosomal trafficking of TfR2-transferrin would enable ongoing calibration of critical metabolic activity in accordance with extracellular environment. In this manner, TfR2 modulation of mitochondrial aconitase activity could enable dynamic responsiveness of erythropoiesis to circulating iron availability.

Materials and Methods

Cell culture

Purified normal human donor $CD34^+$ progenitors derived from G-CSF-mobilized peripheral blood mononuclear cells were purchased from Fred Hutchinson Cancer Research Center (Seattle, WA). Upon thawing, cells were cultured 72 hours in pre-stimulation medium consisting of Iscove's modified Dulbecco's medium (IMDM, Gibco, Gaithersburg, MD) with BIT 9500 supplement (Stem Cell Technologies, Vancouver, Canada), and a cytokine mix of 100 ng/ml human stem cell factor (SCF) (PeproTech, Rocky Hill, NJ), 100 ng/ml human FMS-like tyrosine kinase 3 ligand (PeproTech), 100 ng/ml human thrombopoietin (PeproTech), and 20 ng/ml human interleukin 3 (IL-3) (PeproTech). Cells were moved to erythroid or granulocytic medium following 72 hour prestimulation. Erythroid medium consisted of IMDM with 2 mM L-glutamine (Gibco), Chelex-100 (Sigma-Aldrich, St. Louis, MO) stripped 0.05% bovine serum albumin (BSA, Sigma-Aldrich), Insulin-Transferrin-Selenium (ITS-A) supplement (Stem Cell Technologies), 0.0012% 1-thioglycerol (Sigma-Aldrich), recombinant human erythropoietin at 4.5 U/ml (Procrit, Beerse, Belgium), and 25 ng/ml human SCF. Granulocytic medium consisted of IMDM with 2 mM L-glutamine, Chelex-100-stripped 0.05% bovine serum albumin, ITS-A supplement, 0.0012% 1-thioglycerol, 10 ng/ml granulocyte colony-stimulating factor (G-CSF) (PeproTech), 10 ng/ml IL-3, and 25 ng/ml SCF. For all experiments, cells underwent analysis after three days in erythroid or granulocytic culture medium. For heme studies, Bafilomycin (Sigma-Aldrich) or DMSO

control were added to 3-day erythroid cultures for 16 hours prior to analysis. HUDEP-2 cells were cultured in StemSpan SFEM (Stem Cell Technologies) with 50 ng/ml human SCF, 3 U/ml Epo (Procrit), 1 μM dexamethasone (Sigma-Aldrich), and 1 μg/ml doxycycline (Sigma-Aldrich). K562 cells (ATCC, Manassas, VA) were grown in RPMI medium (Gibco) with 10% fetal bovine serum (FBS) (Gibco), 2 mM L-glutamine (Gibco), and Anti-Anti antibiotic supplement (Gibco). HEK293T cells (ATCC) were grown in DMEM (Gibco) with 10% FBS (Gibco), 2 mM L-glutamine (Gibco), and Anti-anti (Gibco).

Transferrin uptake assays

Analysis of transferrin internalization was performed using fluorochrome- and gold-conjugated holotransferrin. Transferrin conjugates with Alexa Fluor® 594 (T13343), fluorescein (T2871), and pHrodo® Red (P35376) were purchased from ThermoFisher Scientific. 10 nm and 30 nm gold-conjugated transferrin (AC-10-07) was purchased from Cytodiagnostics, Ontario, Canada. Biotin-conjugated transferrin (T23363) was purchased from ThermoFisher Scientific. For fluorescence microscopy, 2 x 10^5 erythroid or granulocytic cells were incubated twenty minutes at 37°C in 100 μl IMDM with 0.05% BSA and 25 μg/ml fluorochrome-labeled transferrin. The cells were then washed in PBS, resuspended in IMDM at a density of 10^6/ml, cytospun onto a glass slide (10^5 cells per slide), and fixed with 4% paraformaldehyde (PFA) in PBS for 15 minutes at room temperature. For electron microscopy, 2 x 10^5 erythroid cells were incubated one hour at 37°C in 100 μl IMDM with 0.05% BSA and 25 μg/ml biotin-conjugated transferrin or four hours at 37°C in 100 μl IMDM with 0.05% BSA and 25 μg/ml gold-labeled transferrin. The

cells were then washed in PBS and resuspended in 2% paraformaldehyde (PFA) and 2% glutaraldehyde in PBS for 20 minutes at room temperature.

Cell extraction and immunoblot

For SDS-PAGE of whole cell lysates, cell pellets were combined with equal volumes of 2X Laemmli sample buffer (60 mM Tris HCl pH 6.8, 2% SDS, 100 µM DTT, 10% glycerol, 0.01% bromophenol blue) supplemented with cOmplete® Protease Inhibitors (11836170001, Roche Diagnostics, Indianapolis, IN) and PhosSTOP® Phosphatase Inhibitors (04906845001, Roche Diagnostics), followed by DNA shearing using tuberculin syringes and boiling for five minutes. After electrophoresis and transfer, nitrocellulose membranes were probed overnight at 4°C with primary antibodies at a 1:1000 dilution in Tris-buffered saline with 0.1% Tween 20 (TBS-T) with 1% non-fat dried milk. HRP-conjugated secondary antibodies (Bethyl Labs, Montgomery, TX) were applied for one hour at a 1:5000 dilution. HRP detection was performed using chemiluminescent SuperSignal West Pico substrate (ThermoFisher Scientific, Waltham, MA) and SuperSignal West Femto Maximum Sensitivity Substrate (ThermoFisher Scientific).

For cell surface biotinylation experiments, primary human progenitors were washed with PBS and resuspended at 10^7 cells/ml in the surface-impermeable biotinylation EZ-Link™ Sulfo-NHS-LC-Biotin (#21335, ThermoFisher Scientific), dissolved at 1 mg/ml in PBS pH 8.0. The cell suspension was incubated on ice for 30 minutes, washed twice with PBS pH 8.0 with 100 mM glycine, and returned to culture medium at 37°C for 0-3 hours incubation. At the indicated time points, the cells were

resuspended at a density of 10^6 cells per 150 µl in biotin lysis buffer (150 mM NaCl, 5 mM EDTA, and 10 mM Tris HCl [pH 7.4] with 1% Triton X-100), incubated for 15 minutes on ice, and centrifuged at 17,000 rpm for ten minutes at 4°C. A portion of supernatant was directly analyzed by immunoblot as input, and the remainder combined with pre-washed NeutrAvidin resin (ThermoFisher Scientific) at a ratio of 3:1 lysate:bead slurry. Slurry/lysate mixtures were rotated for one hour at 4°C, washed twice in biotin lysis buffer, resuspended in Laemmli buffer, and eluates (“PD”) underwent immunoblot as above.

For immunoprecipitations, K562 cells were washed in PBS and resuspended in IP lysis buffer (150 mM NaCl, 2 mM MgCl2, 10 mM HEPES (Gibco), 0.5% NP40, cOmplete® protease inhibitor (Roche Diagnostics), and PhosSTOP® phosphatase inhibitor (Roche Diagnostics)) at a density of 2 x 10^6 per 100 µl. Transfected HEK293T cells were washed and lysed in 500 µl IP lysis buffer per semi-confluent 10cm plate. Lysates were incubated on ice for 15 minutes then centrifuged 10 minutes at 15,000 rpm at 4°C. Protein content in the supernatant was quantified by BCA while samples were stored on ice. For immunoprecipitation of endogenous proteins in K562s, 6 µg of antibody was added to 3 mg of protein extract in 1 ml lysis buffer overnight, using the following antibodies: rabbit IgG (ab27478 from Abcam, Cambridge, UK), rabbit polyclonal anti-MFN2 (ab56889, Abcam), and rabbit monoclonal anti-TfR2 (ab185550, Abcam). Immunoprecipitations with unconjugated antibodies were captured with a 1:1 mixture of protein A (#88846 ThermoFisher Scientific) and protein G (#88847 ThermoFisher Scientific) magnetic beads, pre-washed three times in lysis buffer and added at a volume of 25 µl packed beads per 1ml sample. For immunoprecipitation of epitope-tagged recombinant proteins, 30 µl of Myc-tag Mouse monoclonal magnetic bead conjugated slurry (#5698, Cell

Signaling Technology, Danvers, MA) was added to 3 mg of protein extract in 1ml lysis buffer. Bead suspensions were rotated two hours at 4°C, quickly washed twice in lysis buffer, slowly washed twice with 15 minutes of rotation in 4°C lysis buffer, again quickly washed twice in lysis buffer, resuspended in 50 µl Laemmli buffer, boiled, and analyzed by immunoblot as described.

Primary antibodies consisted of: mouse monoclonal anti-human TfR2 (sc-32271 from Santa Cruz Biotechnology, Santa Cruz, CA), rabbit polyclonal anti-TfR1 (sc-9099 from Santa Cruz Biotechnology), mouse monoclonal anti-TfR1 (sc-32272 from Santa Cruz Biotechnology), mouse monoclonal anti-Tubulin (clone DM1A, #T9026 from Sigma-Aldrich), rabbit polyclonal anti-MFN2 (ab56889 from Abcam, Cambridge, UK), and mouse anti-Rab7 (ab50533 from Abcam).

Flow cytometry and Amnis ImageStream® analysis

For flow cytometry of cultured human progenitors, cells were centrifuged, washed, and re-suspended in PBS + 1% FBS with a conjugated antibody cocktail. Antibodies were added at 2 µl per 100 µl buffer. After 30 minutes staining on ice, samples were washed with PBS + 1% FBS and run on a CyAn ADP Analyzer (Beckman Coulter, Brea, CA) or a FACS Calibur flow cytometer (BD, Franklin Lakes, NJ), followed by compensation and analysis using FlowJo 8.8.7 software (FlowJo, Ashland, OR). Live cell gating was conducted using FSC/SSC and exclusion of Zombie-Violet (#423113, Biolegend, San Diego, CA). For flow cytometry of mouse bone marrow, femurs were flushed with PBS with 5 mM EDTA, passed through a 70 µm filter mesh, incubated five minutes at room

temperature in ammonium chloride lysis buffer to remove red blood cells, and washed with PBS. Marrow was then stained with a conjugated antibody cocktail and analyzed as above, with specific gating on FSC/SSCLow erythroid cells. Fluorochrome-conjugated antibodies to human markers (CD235, CD13, CD36) and murine markers (Ter119, CD71) were purchased from BD-Pharmingen (San Jose, CA).

For Amnis ImageStream® analysis, cells were initially subjected to MitoTracker Deep Red FM® (M22426, ThermoFisher Scientific) staining at 200 nM in serum-free RPMI medium for 30 minutes. The cells were washed with PBS and stained for GPA or CD13 as described for flow cytometry, followed by fixation in 4% fresh PFA for 15 minutes at room temperature. The cells were then washed with PBS and permeabilized 30 minutes at room temperature with intracellular staining buffer: 0.06% Triton X-100, 2% BSA, and 2% FBS in PBS. Following staining for one hour at room temperature with a 1:100 dilution of FITC-conjugated anti-human-Lamp1 (#53107942 Ebioscience), the cells were washed with intracellular staining buffer, followed by incubation with 1 μg/ml DAPI for ten minutes and final washing in intracellular staining buffer. For acquisition, the samples were re-suspended at 106 cells per 50 μl and analyzed on an Amnis ImageStreamX Mark II cytometer (EMD Millipore, Billerca, MA). Data analysis was conducted using the IDEAS® software package (EMD Millipore) with gating on viable, singlet, in-focus, GPA+ or CD13+ cells.

Heme content

Total cellular heme was detecting according to previously described methods.(262-264) Cells were lysed at a density of 10^6 per ml in 2 M oxalic acid (Sigma Aldrich). Lysates were heated to 100°C for 30 minutes and fluorometrically read at excitation/emission wavelengths of 400nm/662nm (SpectraMAX Gemini EM, Molecular Devices, Sunnyvale, CA).

Transfections and transduction

pLKO.1 shRNA vectors were co-transfected with pCMV-dR8.74 (GAG/POL/TAT/REV) and pMD2.G (VSV-G) in HEK293T cells to generate replication defective lentivirus. Transduction of cells and puromycin selection was performed as previously described(265). HEK293T cells were grown to 60% confluency in 10 cm plates (for preparation of lentivirus) and transfected in their culture medium using a calcium phosphate precipitation kit in accordance with manufacturer's instructions (#631312, Clontech, Mountain View, CA). For lentiviral packaging, pCMV-dR8.74 and pMD2.G were co-transfected with pLKO.1 shRNA vectors at a mass ratio of 3:1:4 for pCMV-dR8.74:pMD2.G:pLKO.1. pLKO.1 vectors expressing shRNAs active against TFR2 (TRCN0000063628), MFN2 (TRCN0000082683), and TfR1 (TRCN0000057658) were purchased from GE Dharmacon (Lafayette, CO). 16 hours after transfection, the medium was exchanged with Opti-MEM™ I (Gibco), and supernatants were collected 40 hours following initiation of transfection. Viral supernatants were filtered with 0.45 μm syringe filters and stored at -80°C until use. For K562 transduction, cells were incubated with viral supernatants for 24 hours, followed by puromycin selection at 2 μg/ml in growth medium

for at least 48 hours. For human primary progenitors, cells were expanded in pre-stimulation medium for 48 hours and transferred to retronectin-coated 12-well plates containing viral supernatants supplemented with prestimulation cytokines. For HUDEP-2 transduction, cells were incubated with viral supernatants for 24 hours, followed by puromycin selection at 2 μg/ml in growth medium for at least 48 hours. After 2 hours at 37°C, plates were spun at 500 g for 90 minutes. Following overnight culture at 37°C, cells were transferred to fresh viral supernatants with prestimulation cytokines for a second round of incubation, spinoculation, and overnight culture. The cells were then subjected to 48 hours of puromycin selection at 2 μg/ml in prestimulation medium, and live cells were enriched by centrifugation on Ficoll-Paque PLUSTM medium (#17-1440-02, GE Healthcare, Pittsburgh, PA). Viable mononuclear cells were washed in IMDM and subjected to erythroid culture.

For immunoprecipitation of transfectants, HEK293T cells were transfected with 20 μg plasmid using a calcium phosphate precipitation kit and harvested for protein extracts 40 hours following initiation of transfection. The following expression constructs were used for cotransfection and coimmunoprecipitation in HEK293T cells: pcDNA6/myc and pcDNA6/myc human TfR2 from Dr. Paul Schmidt (Boston Children's Hospital); Mfn2-Myc, a gift from David Chan (Addgene plasmid #23213)(257); pEYFP-C1; Rab7-GFP, a gift from Merino Zerial(266).

Murine models

All animal experiments were approved by the University of Virginia Institutional Animal Care and Use Committee (IACUC). The *Tfr2*^{Y245X} mutant strain was developed in the Fleming lab as descried(267). *Mcoln1*$^{-/-}$ mice (B6.Cg-*Mcoln1*^{tm1Sasl}/J) were purchased from Jackson Laboratories (Bar Harbor, ME). Age-matched and sex-matched litter mates were used for all studies. Retro-orbital bleeds into EDTA-coated collection tubes were analyzed for complete blood counts (CBC) on a Hemavet 950 hematology system (Drew Scientific Group, Miami Lakes, FL).

Microscopy

For gross and light microscopic assessment of bone marrow, 12-week-old *Mcoln1*-/- and wild type littermates were euthanized, and femurs were photographed and fixed in formalin for 48 hours, followed by decalcification, paraffin embedding, sectioning, and H&E staining. Slides were imaged on an Olympus BX51 light microscope.

For immunofluorescent staining combined with mitochondria labeling, cells were first incubated with 200 nM MitoTracker Deep Red FM® (M22426, ThermoFisher Scientific) in serum-free RPMI medium for 30 minutes, then washed in PBS and resuspended in IMDM at 10^6 cells/ml. The cells were then cytospun onto a glass slide (10^5 per slide) and fixed with 4% paraformaldehyde (PFA) in PBS for 15 minutes at room temperature. The slides made from cytospins of MitoTracker or fluorescent-tranferrin loaded cells were washed in PBS, then permeabilized/blocked in immunofluorescence (IF) staining buffer (0.06% Triton X-100, 2% BSA, 2% FBS in PBS) for one hour at room

temperature. Staining was performed using FITC-conjugated anti-human-Lamp1 (#53107942 Ebioscience), rabbit polyclonal anti-TfR1 (sc-9099 from Santa Cruz Biotechnology), or mouse monoclonal anti-TfR1 (sc-32272 from Santa Cruz Biotechnology) at dilutions of 1:100 in IF staining buffer overnight in a hybridization chamber at 4°C. Slides were washed three times with IF staining buffer, and Alexa Fluor®-conjugated secondary antibodies (ThermoFisher Scientific) were applied at dilution of 1:500 in IF staining buffer for one hour at room temperature, with DAPI at 1µg/ml included in the final ten minutes of the secondary stain. Slides were washed three times in IF staining buffer, once in PBS, mounted with coverslip and medium (#H-1000 Vectashield, Burlingame, CA), and viewed on a Zeiss LSM-700 confocal microscope with the 63x objective. Images were analyzed using Fiji ImageJ version 2.0.0 software. Colocalization analysis was performed using Fiji ImageJ coloc2 function to obtain Pearson's R value (above threshold) for the Tf and TfR1 signal. The percentage of Tf colocalized with TfR1 was assessed by Imaris 8.4 (Bitplane, Zurich, Switzerland) spot counting function. Spot masks were created for the Tf and TfR1 signal. The TfR1 spot mask was analyzed by distance transformation, and values mapped to the Tf spot mask, such that each Tf vesicle was given a distance value to the most proximal TfR1 vesicle. Distances closer than .4 μm were defined to be colocalized.

For transmission electron microscopy (TEM) of mouse bone marrow cells, femurs were flushed with PBS with 5 mM EDTA; extruded marrow was passed through a 70 µm filter mesh, incubated five minutes at room temperature in ammonium chloride lysis buffer to remove red blood cells, washed in PBS, and fixed in 2% PFA plus 2% glutaraldehyde in PBS for 20 minutes at room temperature. For TEM of cultured human progenitors, cells

were washed in PBS and fixed in 2% PFA plus 2% glutaraldehyde in PBS for 20 minutes at room temperature. All samples were post-fixed in 1% osmium tetroxide for thirty minutes at room temperature, and embedded and polymerized at 65°C for 24 hours. 70 nM sections were placed on 200 mesh grids and stained with uranyl acetate and lead citrate. Secondary staining of biotin-conjugated transferrin was performed using 10 nm gold-conjugated streptavidin (#25269 from Electron Microscopy Sciences, Hatfield, PA) at a 1:5 dilution in incubation buffer of .2% BSA in PBS for two hours. Grids were then washed three times in incubation buffer and three times in water for 5 minutes per wash. Grids were carbon coated to minimize conductance and imaged on a JEOL 1230 (JEOL, Peabody, MA) electron microscope or TITAN Themis (FEI, Hillsboro, OR) at 80 kV. Images were taken with a Scientific Instruments of America 4K X 4K CCD camera. For quantification of gold-conjugated transferrin in organelle compartments, images were taken of unstained, processed sections to best visualize 10 nm gold particles. Images were then de-identified, scrambled and counted in a blinded manner, with MVB/lysosomes being distinguished from endosomes by having three or more intraluminal vesicles (ILVs). For quantification of direct mitochondrial-lysosomal membrane contact sites (MCSs), de-identified, scrambled images of progenitors were counted in a blinded manner, with direct contacts defined by lack of detectable cytosol between mitochondrial and MVB/lysosome membranes. Intra-mitochondrial electron dense foci were similarly counted in a blinded manner. For quantification of mitochondria size, images were subjected to tracing of mitochondria and area measurement via Fiji ImageJ version 2.0.0.

Statistics

All statistical analysis was performed with Prism 6 (GraphPad Software, La Jolla, CA). Graphs are displayed as mean of $\geq$ 3 independent experiments ± standard error of the mean. Data were analyzed by either a two-tailed Student *t* test, one-way ANOVA, or two-way ANOVA, as indicated. Post-hoc analysis was performed using Dunnett's multiple comparisons test for one-way ANOVA and Sidak's multiple comparisons test for two-way ANOVA.

CHAPTER 3 Figures

Figure 3.1. Differentiation of erythroid and granulocytic progenitors from purified CD34+ human bone marrow cells.

Flow cytometry of progenitors cultured four days in erythroid or granulocytic medium.

Figure 3.2. Lysosomal trafficking of transferrin in erythroid progenitors.

(A) Fluorescence microscopy of human erythroid and granulocytic progenitors undergoing pHrodo Red-transferrin uptake (confocal image obtained with 20X objective). (B) Fluorescence microscopy at higher magnification of erythroid progenitors undergoing pHrodo Red-transferrin uptake (confocal image with 63X objective, arrows denote perinuclear clustered vesicles). (C) Fluorescence microscopy for colocalization of Alexa Fluor® 594-transferrin with endogenous Lamp1 in erythroid progenitors (confocal image with 63X oil objective, with boxed region projected at higher magnification). Yellow denotes merge between separate red and green channels. (D) Transmission electron microscopy of erythroid progenitors undergoing 10 nm gold-conjugated transferrin uptake, with boxed regions expanded to highlight MVB/lysosomal accumulation of transferrin particles (arrows denote representative gold-conjugated transferrin particles).

Figure 3.3. Distribution of transferrin in erythroid progenitors.

(A) Transmission electron microscopy of erythroid progenitors subjected to 30 nm gold-conjugated transferrin uptake, with insets highlighting specific MVB/lysosomal accumulation of transferrin particles. (B) Transmission electron microscopy of erythroid

progenitors subjected to biotin-conjugated transferrin uptake followed by gold-conjugated streptavidin staining. Arrows denote gold particles. (C) Quantification of biotin-conjugated transferrin uptake by erythroid cells as in (B) (number of cells counted = 18 per group, $^{**}P < 0.01$).

Figure 3.4. Confirmation of non-colocalization of transferrin with TfR1 in erythroid progenitors.

Immunofluorescent staining for TfR1 using alternative mouse monoclonal anti-TfR1 (sc-32272 from Santa Cruz Biotechnology) on erythroid progenitors subjected to Alexa Fluor® 594-tagged transferrin loading (63X oil objective).

Figure 3.5. TfR2 is required for the lysosomal trafficking of transferrin.

(A) Fluorescence microscopy for colocalization of Alexa Fluor® 594-transferrin with TfR1 in erythroid progenitors (top left: confocal image with 63X oil objective, top right: Inset of image depicting higher magnification) and granulocytic progenitors (bottom left: confocal image with 63X oil objective, bottom right: Inset of image depicting higher magnification). Yellow denotes merge between separate red and green channels. (B) Colocalization of Alexa Fluor® 594-transferrin and TfR1 as measured by Pearson's correlation coefficient (left panel) and percentage of Alexa Fluor® 594-transferrin+ vesicles co-occupied by TfR1 (right panel) (number of cells analyzed = 27-58 per group, $^{***}P < 0.001$). (C) Immunoblot of surface-biotinylated proteins from progenitors in erythroid medium with indicated duration of culture in hours post-biotinylation (left panel); Densitometry for TfR2 versus TfR1 fold decline over 3 hours post-biotinylation (right panel) (n = 4, $^{*}P < 0.05$).

(D) Fluorescence microscopy of human erythroid progenitors transduced with lentiviral shRNA constructs and subjected to Alexa Fluor® 594-transferrin uptake (confocal image with 10X objective, insets with 63X objective). (E) Transmission electron microscopy of erythroid progenitors transduced with lentiviral shRNA constructs and subjected to 10 nm gold-conjugated transferrin uptake, with insets highlighting MVB/lysosomal accumulation (left panel) and endosomal accumulation (right panel) of transferrin particles. (F) Summary of transmission electron microscopy studies as in (E) showing number of lysosomal transferrin particles per cell section with indicated lentiviral shRNA transduction (top panel); number of endosomal transferrin particles per cell section with indicated lentiviral shRNA transduction (bottom panel) (number of cells counted = 44-45 per group, ***P < 0.001). (G) Fluorescence microscopy for colocalization of Alexa Fluor® 594-transferrin with TfR1 in erythroid progenitors transduced with lentiviral shRNA constructs (confocal image with 63X oil objective). Yellow denotes merge between separate red and green channels. (H) Colocalization of Alexa Fluor® 594-transferrin and TfR1 as measured by Pearson's correlation coefficient (top panel) and percentage of Alexa Fluor® 594-transferrin+ vesicles co-occupied by TfR1 (bottom panel) (number of cells analyzed = 12-23 per group, ** P < 0.01, *** P < 0.001).

Figure 3.6. TfR2 knockdown in lentivirus-transduced progenitors.

Immunoblot documentation of TfR2 knockdown in erythroid progenitors transduced with lentiviral shRNA constructs (EV: empty vector).

Figure 3.7. Direct membrane contacts sites between erythroid mitochondria and lysosomes.

(A) Imaging flow cytometry showing bright field (BF), glycophorin A (GPA), mitochondria (Mito), nuclei (DAPI) and Lamp1 (L1) in erythroid progenitors. (B) Fluorescence microscopy for Lamp1 and MitoTracker Deep Red FM® in erythroid and granulocytic progenitors (confocal image with 63X oil objective, subjected to additional magnification). (C) Transmission electron microscopy of erythroid progenitors. (D) Transmission electron microscopy of erythroid progenitors. Arrow denotes contorted mitochondrion in direct contact with two MVB/lysosomes. (E) Quantification of membrane contacts observed by transmission electron microscopy of erythroid progenitors as in (D) (number of cells counted = 48 per group, *** $P < 0.001$). (F) Transmission electron microscopy of erythroid progenitors subjected to 10 nm gold-conjugated transferrin uptake, with micrograph depicting mitochondria in direct contact with transferrin-laden MVB/lysosome. (G) Total heme content in erythroid progenitors -/+ overnight treatment with 2nM Bafilomycin (BAF) (n = 4 per group, ** $P < 0.01$). (H) Transmission electron microscopy of erythroid and granulocytic progenitors, with insets highlighting proximity of mitochondria to MVB/lysosome. (I) Quantification of mitochondria-MVB/lysosome membrane contacts observed by transmission electron microscopy of erythroid and granulocytic progenitors as in (H) (number of cells counted = 48-53 per group, * $P < 0.05$)

Figure 3.8. Demonstration by imaging cytometry of differences between erythroid and granulocytic progenitors in lysosomal-mitochondrial organization.

(A) Representative images of erythroid (GPA+) and granulocytic (CD13+) progenitors showing lysosomal (L1), mitochondrial (Mito), and nuclear (DAPI) distribution. Imaging cytometry was conducted using Amnis ImageStream®. (B) Comparison of lysosomal LAMP1 area (left panel) and intensity (right) in gated erythroid and granulocytic progenitors. Mean, median values are shown in upper right corner. (C) Comparisons of nuclear-mitochondrial and nuclear-lysosomal orientations using DAPI-MitoTracker XY delta-centroid (left panel) and DAPI-Lamp1 XY delta-centroid (right) in gated erythroid and granulocytic progenitors. Mean, median values are shown in upper right corner. (D) Comparison of lysosomal-mitochondrial orientation using Lamp1-MitoTracker XY delta-centroid in gated erythroid and granulocytic progenitors. Mean, median values are shown in upper right corner.

Figure 3.9. TfR2 is required for erythroid mitochondrial integrity.

(A) Summary of imaging flow cytometry studies showing relative MitoTracker Deep Red FM® mean fluorescence intensities in lentiviral-transduced K562 cells (n = 4, * $P < 0.05$). (B) Transmission electron microscvopy of bone marrow from adult wild type and *Tfr2*^{Y245X} mutant mice, depicting erythroid progenitors (top panels) and granulocytic progenitors (bottom). (C) Ultrastructural quantitation of mean mitochondrial size in erythroid and granulocytic progenitors from wild type and *Tfr2*^{Y245X} bone marrow as in (B) (number of cells analyzed = 15-23 per group, *** $P < 0.001$, ns not significant). (D) Transmission electron microscopy of erythroid progenitors transduced with lentiviral shRNA constructs. (E) Ultrastructural enumeration of electron-dense foci per mitochondrion in transduced erythroid progenitors as in (D) (number of cells analyzed = 10-13 per group, * $P < 0.05$).

(F) Total heme content in erythroid progenitors transduced with lentiviral shRNA constructs (n = 3 per group, ** $P < 0.01$).

Figure 3.10. TfR1 knockdown in lentivirus-transduced progenitors.

(A) Immunoblot documentation of TfR1 knockdown in erythroid progenitors transduced with lentiviral shRNA constructs (EV: empty vector). (B) Flow cytometry of progenitors subjected to transduction with lentiviral shRNA constructs and cultured four days in erythroid medium.

Figure 3.11. The lysosomal iron channel Mucolipin-1 contributes to erythropoiesis and mitochondrial integrity.

(A) Circulating red blood cell counts, hemoglobin concentration (Hb), and hematocrit (Hct) in littermate adult wild type, *Mcoln1*$^{+/-}$, and *Mcoln1*$^{-/-}$ mice (n = 9 per group, * $P < 0.05$, ** $P < 0.01$). (B) Femur images from adult wild type and *Mcoln1*$^{-/-}$ mice. (C) Light micrographs of hematoxylin and eosin stained bone marrow from adult wild type and *Mcoln1*$^{-/-}$ mice (40x objective). (D) Flow cytometry of wild type and *Mcoln1*$^{-/-}$ bone marrow erythroid progenitors to assess erythroid differentiation. (E) Summary of flow cytometry studies as in (D) showing decrease in percentage of Ter119+ cells in low SSC-gated *Mcoln1*$^{-/-}$ bone marrow (n = 4-8 per group, * $P < 0.05$). (F) Transmission electron microscopy of bone marrow from adult wild type and *Mcoln1*$^{-/-}$ mice, depicting marrow erythroid progenitor (top panels) and marrow granulocytic progenitors (bottom panels); arrows denote mitochondria. (G) Ultrastructural quantitation of mean mitochondrial size

in erythroid and granulocytic progenitors from wild type and *Mcoln1*$^{-/-}$ bone marrow as in (F) (number of cells analyzed = 10 per group, *** $P < 0.001$, ** $P < 0.01$).

Figure 3.12. Mitofusin-2 mediates mitochondria-lysosomal membrane contacts and is required for erythropoiesis.

(A) BloodSpot expression profiles for *TFR2* and *MCOLN1* using DMAP dataset. (B) BloodSpot expression correlation analysis from DMAP dataset listing expression correlation coefficients for the most correlated genes to *MCOLN1*. (C) Immunoblot documentation of Mitofusin-2 knockdown in erythroid progenitors transduced with lentiviral shRNA constructs. (D) Transmission electron microscopy of erythroid progenitors transduced with lentiviral shRNA constructs (arrows denote mitochondria in direct contact with MVB/lysosomes). (E) Ultrastructural quantitation of mitochondria-MVB/lysosome membrane contacts in transduced erythroid progenitors as in (D) (total cells counted = 15 per group, * $P < 0.05$. (F) Total heme content in erythroid progenitors (top panel), K562 cells (middle panel), and HUDEP-2 cells (bottom panel) transduced with lentiviral shRNA constructs (top panel) (n = 4 per group, ** $P < 0.01$, *** $P < 0.001$). (G) Flow cytometry (left panel) of progenitors transduced as in (D) and cultured four days in erythroid medium; summary of flow cytometry experiments on transduced progenitors (right panel) (n = 3, * $P < 0.05$).

Figure 3.13. Interactions between lineage- and stage- specific drivers of iron uptake.

(A) Heatmap depiction of *SLC11A2* (encoding DMT1) and *CTSB* (encoding lysosomal Cathepsin B protease) transcript levels throughout normal human hematopoiesis, with highest expression in GPA+ CD71+ intermediate erythroid progenitors. The DMAP dataset was analyzed using BloodSpot (http://servers.binf.ku.dk/bloodspot). (B) Heatmap depiction of *MFN2* transcript levels throughout normal human hematopoiesis. (C) Immunoprecipitation (IP) with indicated antibodies of K562 cell extracts followed by immunoblot (IB).

(D) Immunoprecipitation (IP) of Myc-tagged recombinant MFN2 and TfR2 from extracts of HEK293T transfectants followed by immunoblot (IB) detection of YFP-tagged Rab7 and control YFP. Input immunoblot in left panel.

Figure 3.1

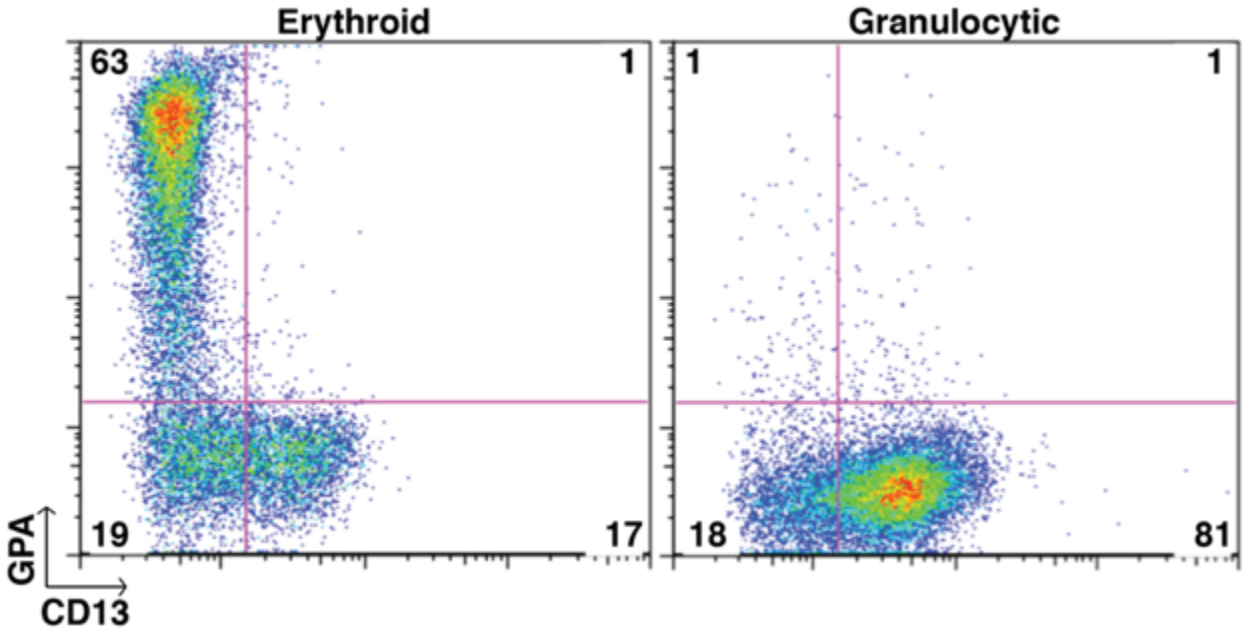

Figure 3.2

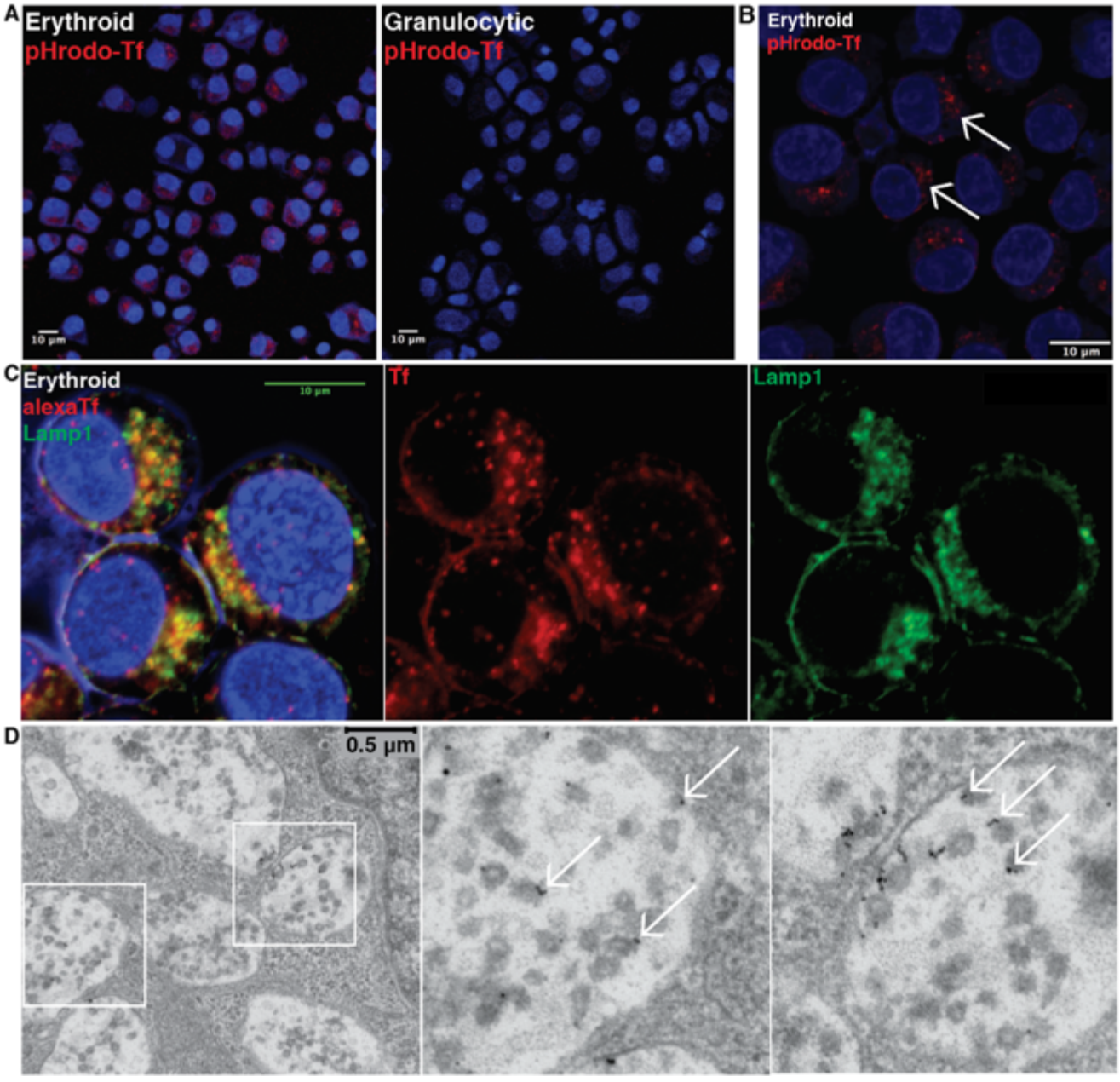
A
Erythroid
pHrodo-Tf
10 μm
Granulocytic
pHrodo-Tf
10 μm
B
Erythroid
pHrodo-Tf
10 μm
C
Erythroid
alexaTf
Lamp1
10 μm
Tf
Lamp1
D
0.5 μm

Figure 3.3

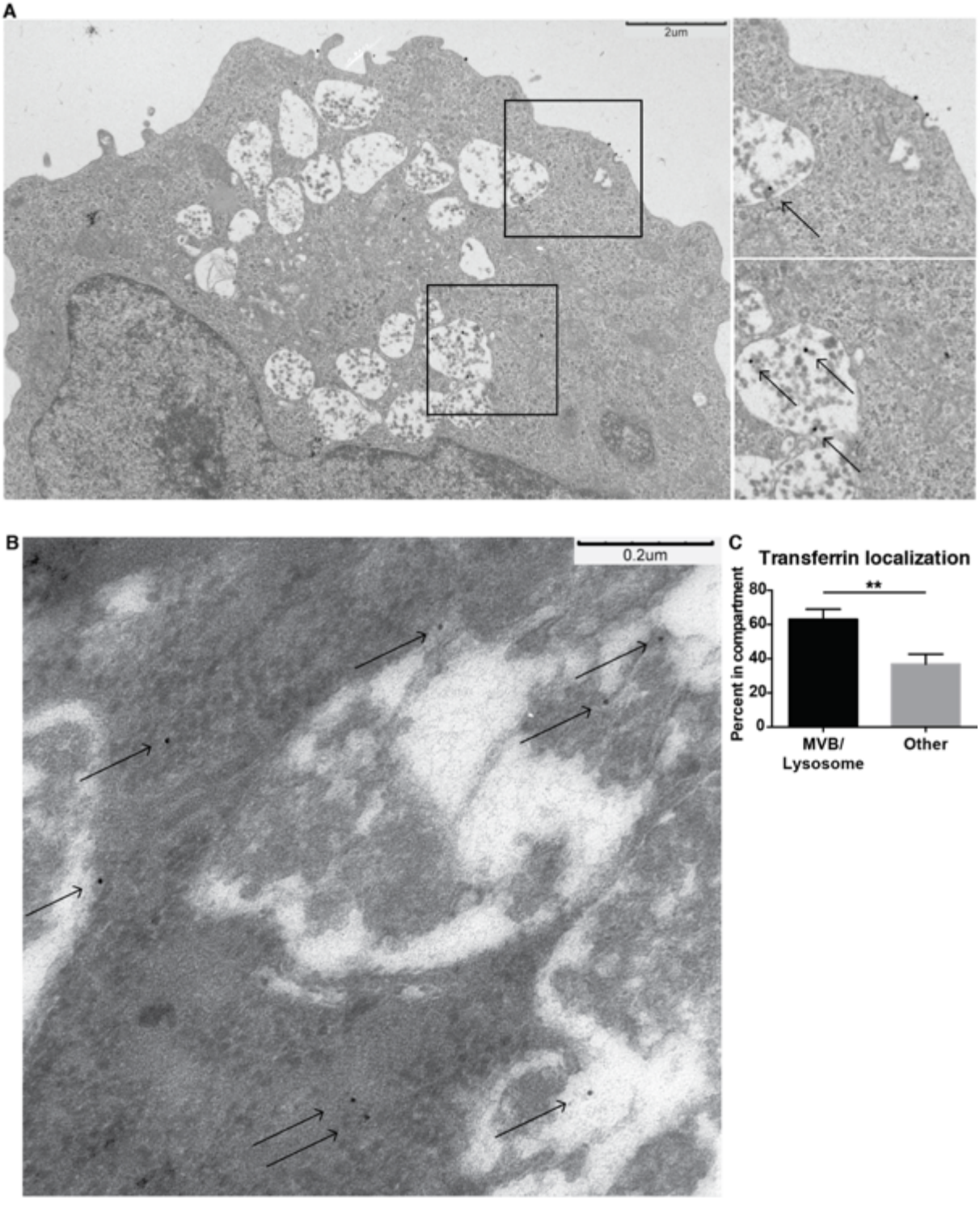
A
2um
B
0.2um
C
Transferrin localization
Percent in compartment
80
60
40
20
0
**
MVB/
Lysosome
Other

Figure 3.4

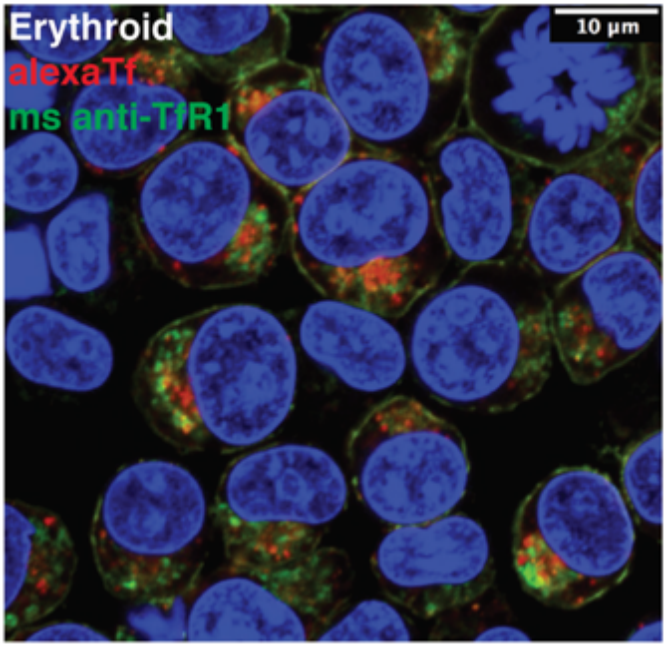

Figure 3.5

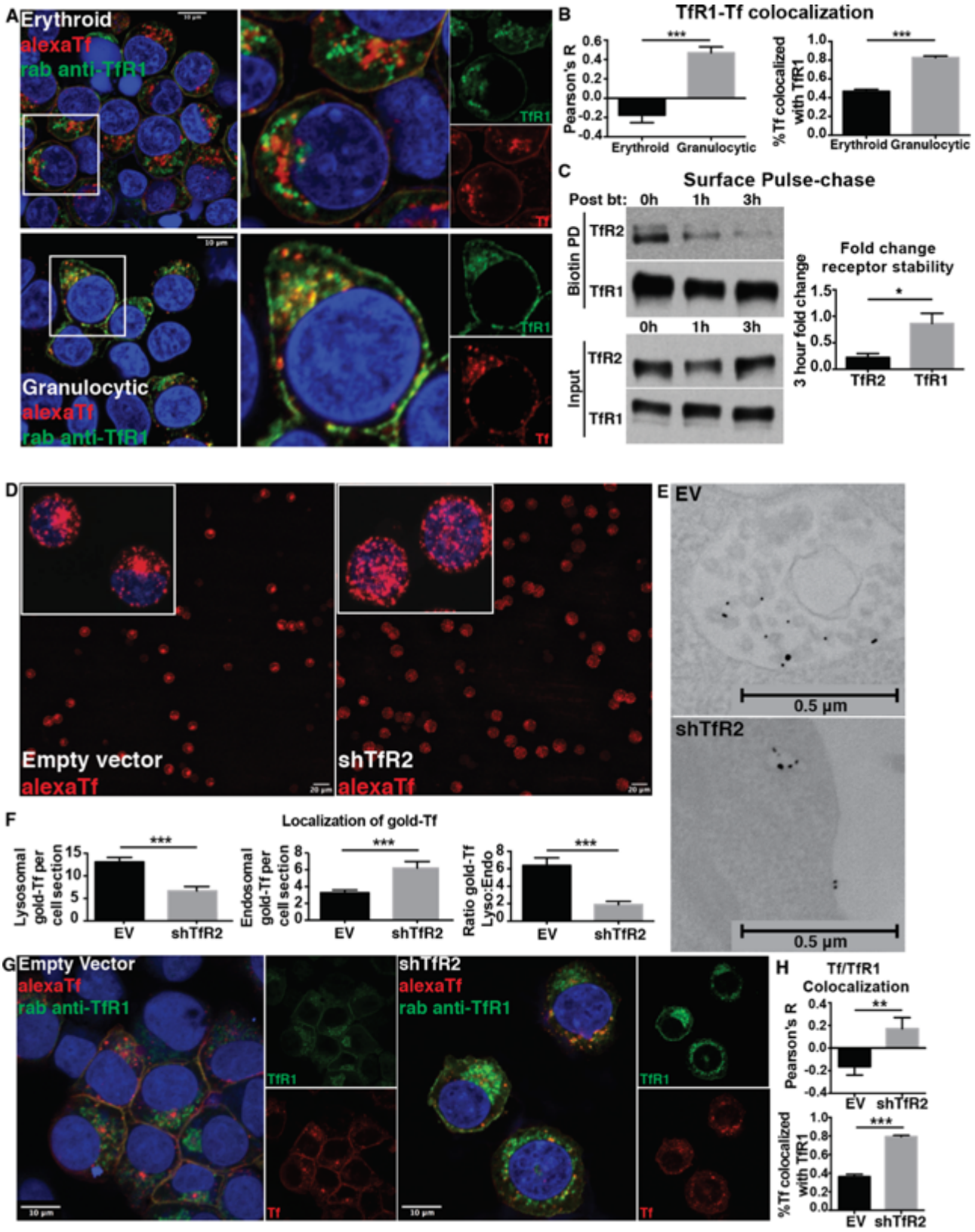
A
Erythroid
alexaTf
rab anti-TfR1
TfR1
Tf
Granulocytic
alexaTf
rab anti-TfR1
B
TfR1-Tf colocalization
Pearson's R
Erythroid
Granulocytic
% Tf colocalized with TfR1
C
Surface Pulse-chase
Post bt: 0h 1h 3h
Biotin PD
TfR2
TfR1
Input
Fold change receptor stability
3 hour fold change
D
Empty vector
alexaTf
shTfR2
alexaTf
E
EV
0.5 µm
shTfR2
0.5 µm
F
Localization of gold-Tf
Lysosomal gold-Tf per cell section
Endosomal gold-Tf per cell section
Ratio gold-Tf Lyso:Endo
EV
shTfR2
G
Empty Vector
alexaTf
rab anti-TfR1
shTfR2
alexaTf
rab anti-TfR1
H
Tf/TfR1 Colocalization
Pearson's R
% Tf colocalized with TfR1

Figure 3.6

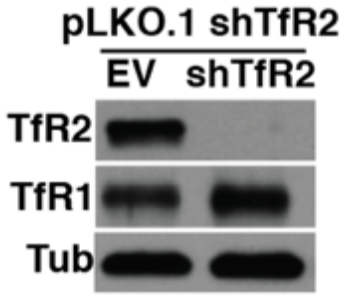

Figure 3.7

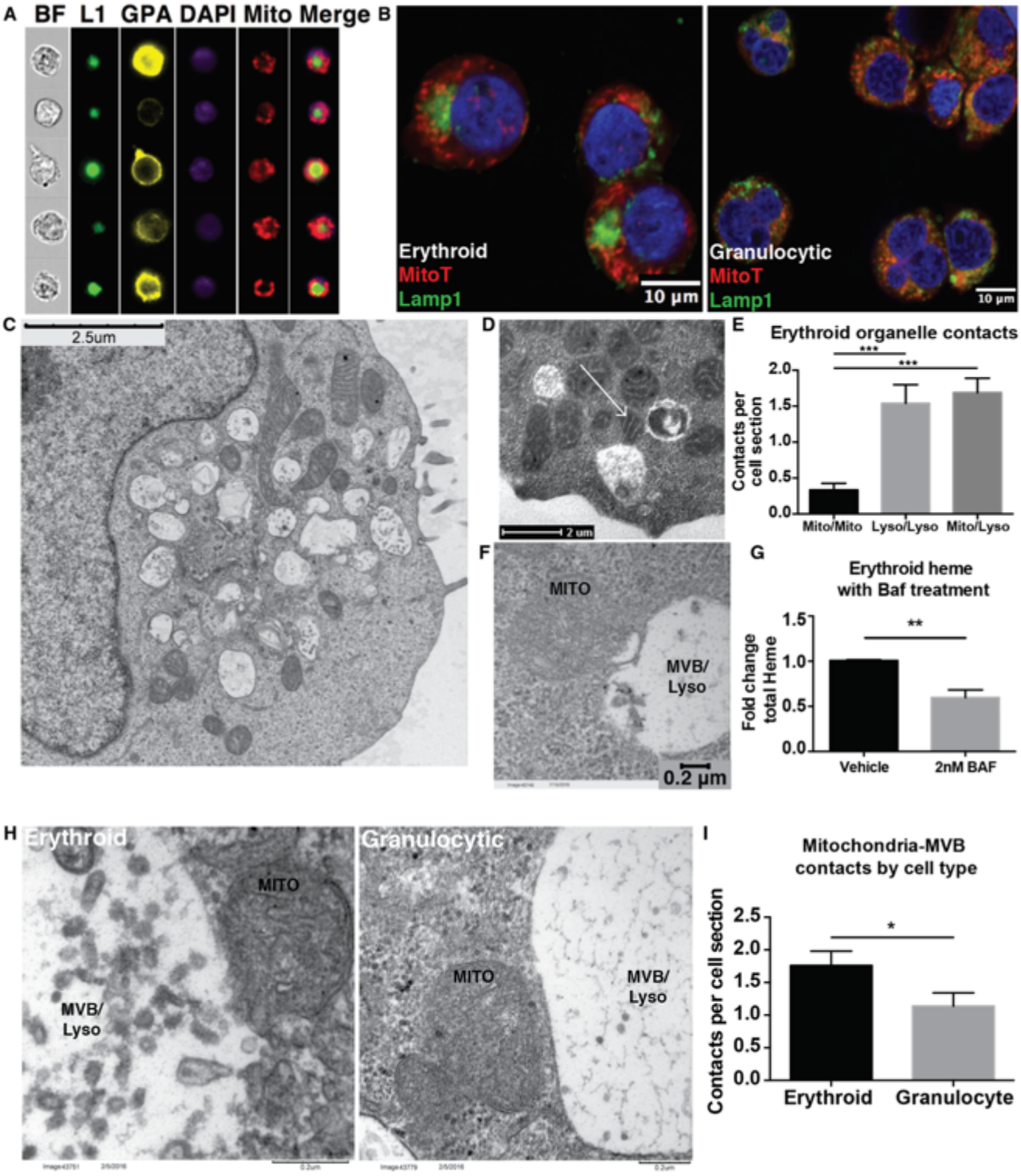
A
BF L1 GPA DAPI Mito Merge
B
Erythroid
MitoT
Lamp1
10 µm
Granulocytic
MitoT
Lamp1
10 µm
C
2.5um
D
2 um
E
Erythroid organelle contacts
***
***
Contacts per cell section
2.0
1.5
1.0
0.5
0.0
Mito/Mito
Lyso/Lyso
Mito/Lyso
F
MITO
MVB/ Lyso
0.2 µm
G
Erythroid heme with Baf treatment
**
Fold change total Heme
1.5
1.0
0.5
0.0
Vehicle
2nM BAF
H
Erythroid
MITO
MVB/ Lyso
Granulocytic
MITO
MVB/ Lyso
I
Mitochondria-MVB contacts by cell type
*
Contacts per cell section
2.5
2.0
1.5
1.0
0.5
0.0
Erythroid
Granulocyte

Figure 3.8

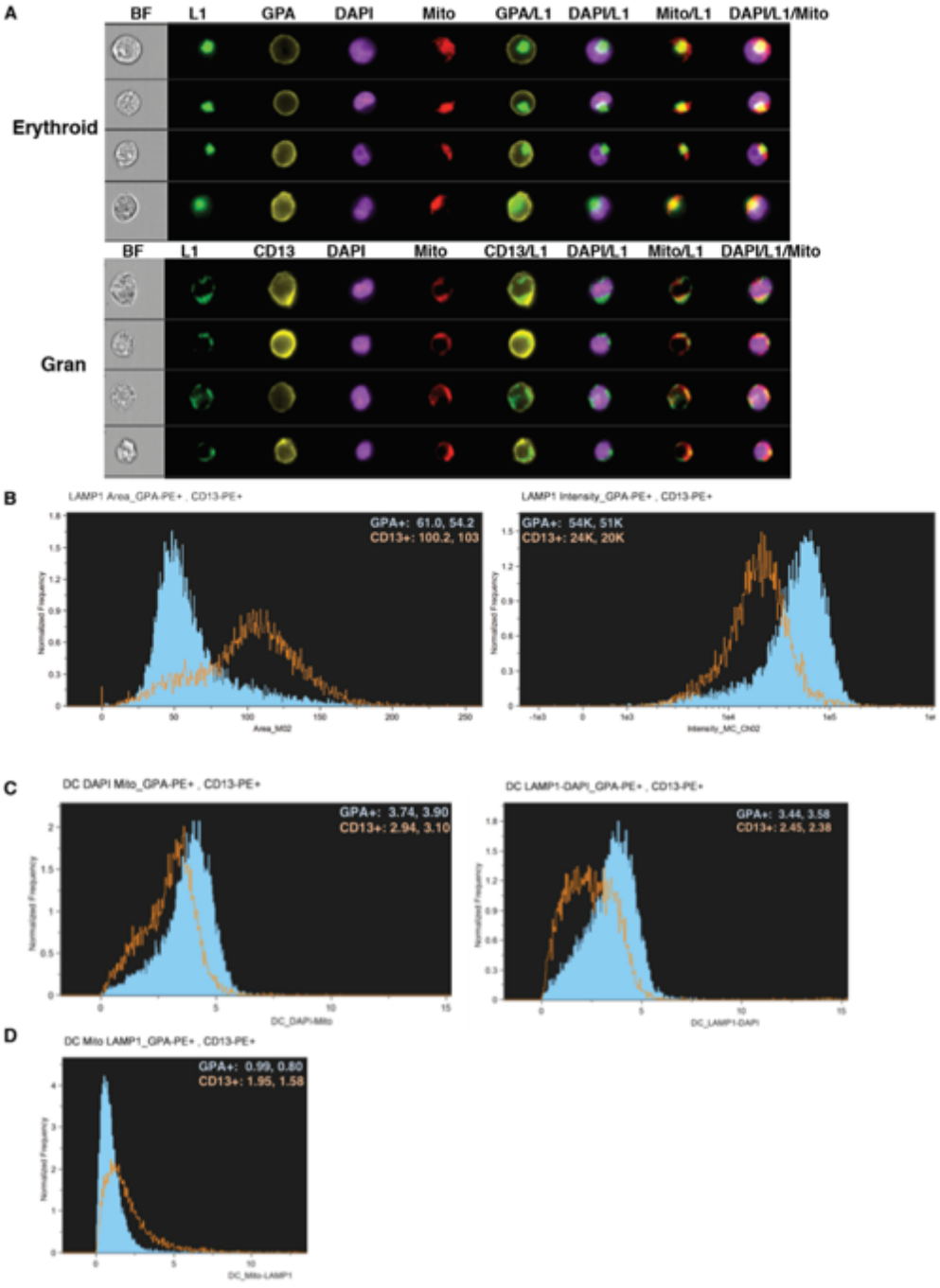
A
BF
L1
GPA
DAPI
Mito
GPA/L1
DAPI/L1
Mito/L1
DAPI/L1/Mito
Erythroid
BF
L1
CD13
DAPI
Mito
CD13/L1
DAPI/L1
Mito/L1
DAPI/L1/Mito
Gran
B
LAMP1 Area_GPA-PE+ , CD13-PE+
GPA+: 61.0, 54.2
CD13+: 100.2, 103
LAMP1 Intensity_GPA-PE+ , CD13-PE+
GPA+: 54K, 51K
CD13+: 24K, 20K
C
DC DAPI Mito_GPA-PE+ , CD13-PE+
GPA+: 3.74, 3.90
CD13+: 2.94, 3.10
DC LAMP1-DAPI_GPA-PE+ , CD13-PE+
GPA+: 3.44, 3.58
CD13+: 2.45, 2.38
D
DC Mito LAMP1_GPA-PE+ , CD13-PE+
GPA+: 0.99, 0.80
CD13+: 1.95, 1.58

Figure 3.9

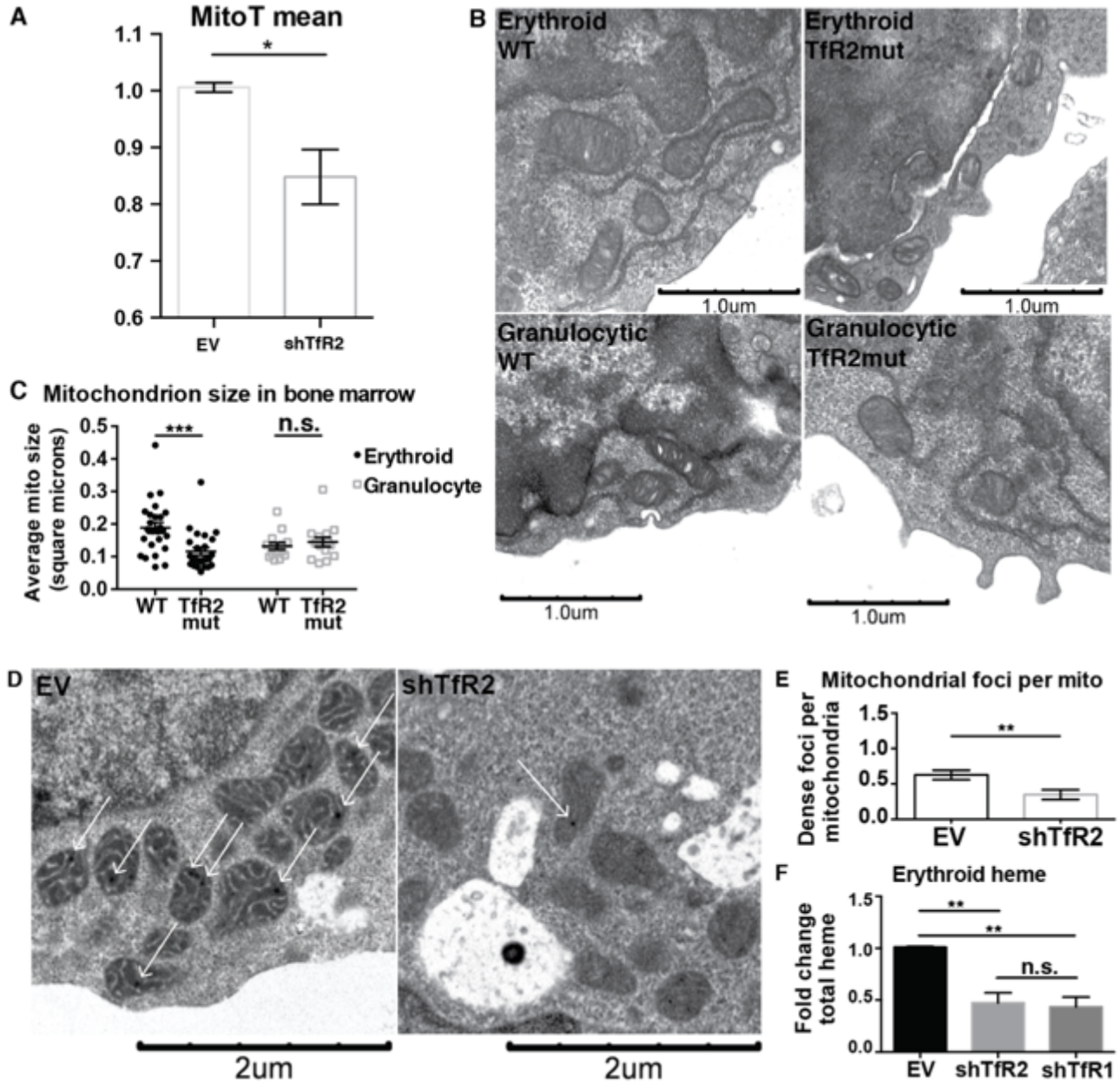
A
MitoT mean
1.1
1.0
0.9
0.8
0.7
0.6
*
EV
shTfR2
B
Erythroid WT
Erythroid TfR2mut
Granulocytic WT
Granulocytic TfR2mut
1.0um
C
Mitochondrion size in bone marrow
Average mito size (square microns)
0.5
0.4
0.3
0.2
0.1
0.0
***
n.s.
Erythroid
Granulocyte
WT
TfR2 mut
D
EV
shTfR2
2um
E
Mitochondrial foci per mito
Dense foci per mitochondria
1.5
1.0
0.5
0.0
**
F
Erythroid heme
Fold change total heme
shTfR1

Figure 3.10

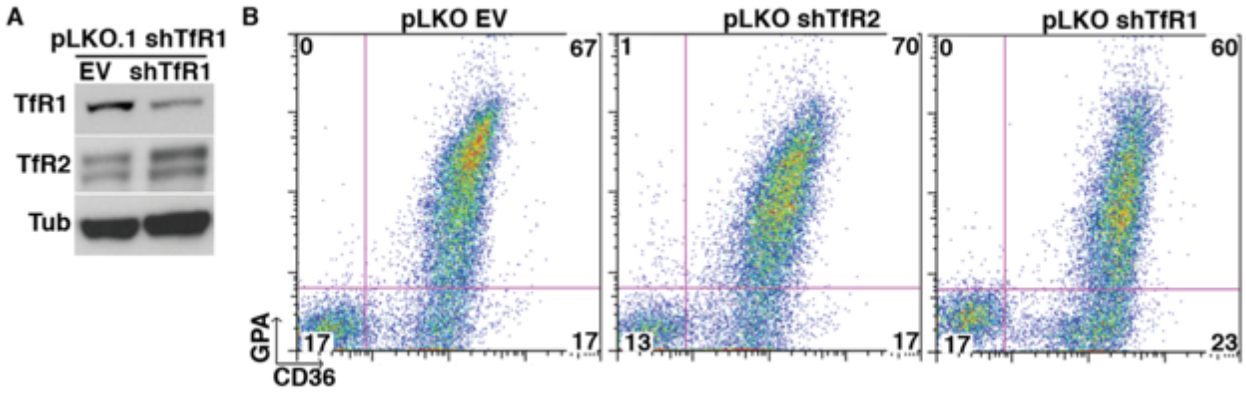
A
pLKO.1 shTfR1
EV shTfR1
TfR1
TfR2
Tub
B
pLKO EV
pLKO shTfR2
pLKO shTfR1
0
67
17
17
1
70
13
17
0
60
17
23
GPA
CD36

Figure 3.11

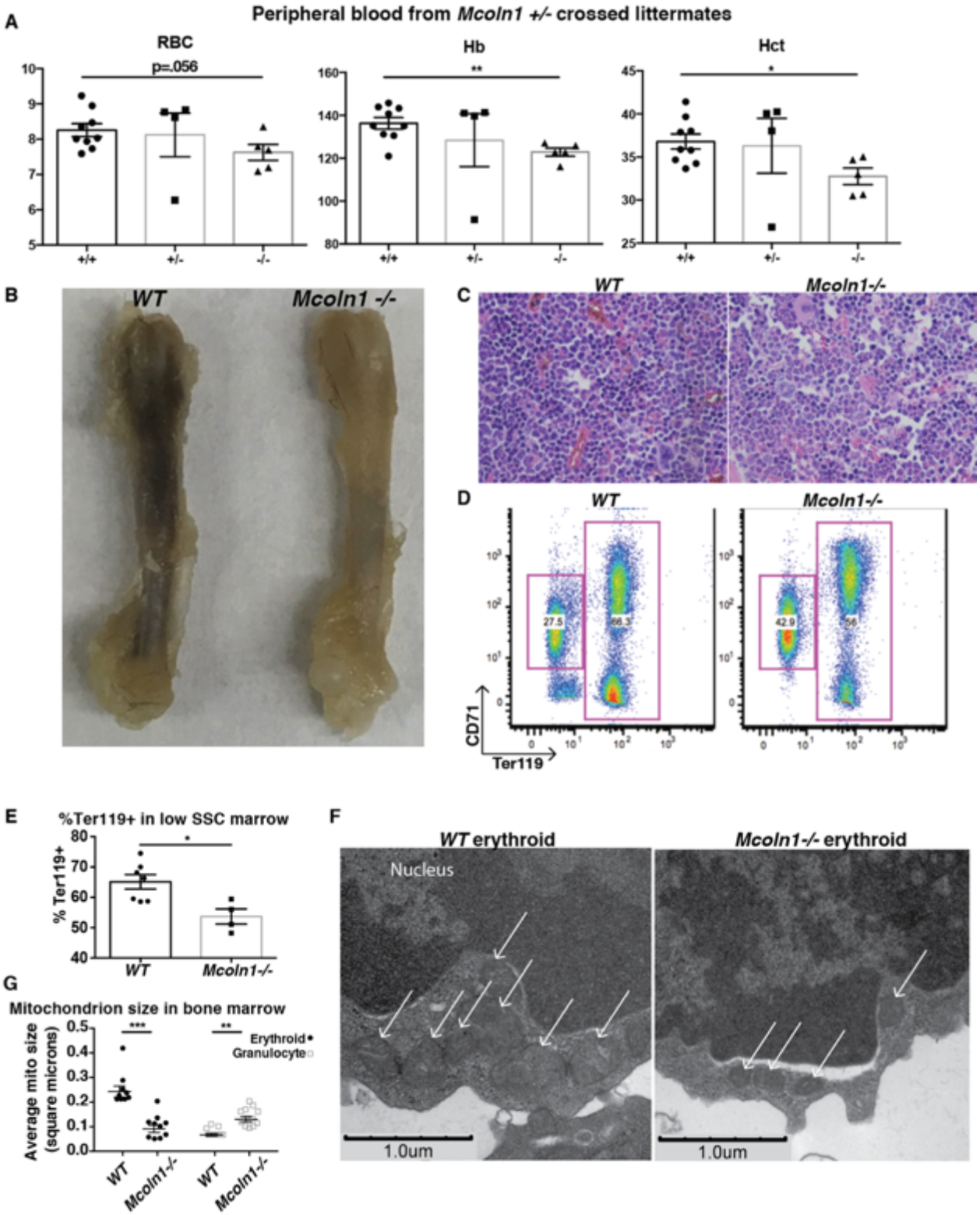
A
Peripheral blood from Mcoln1 +/- crossed littermates
RBC
p=.056
Hb
**
Hct
*
+/+
+/-
-/-
B
WT
Mcoln1 -/-
C
WT
Mcoln1-/-
D
WT
Mcoln1-/-
27.5
66.3
42.9
56
CD71
Ter119
E
%Ter119+ in low SSC marrow
% Ter119+
WT
Mcoln1-/-
F
WT erythroid
Mcoln1-/- erythroid
Nucleus
1.0um
1.0um
G
Mitochondrion size in bone marrow
Average mito size (square microns)
***
**
Erythroid
Granulocyte
WT
Mcoln1-/-
WT
Mcoln1-/-

Figure 3.12

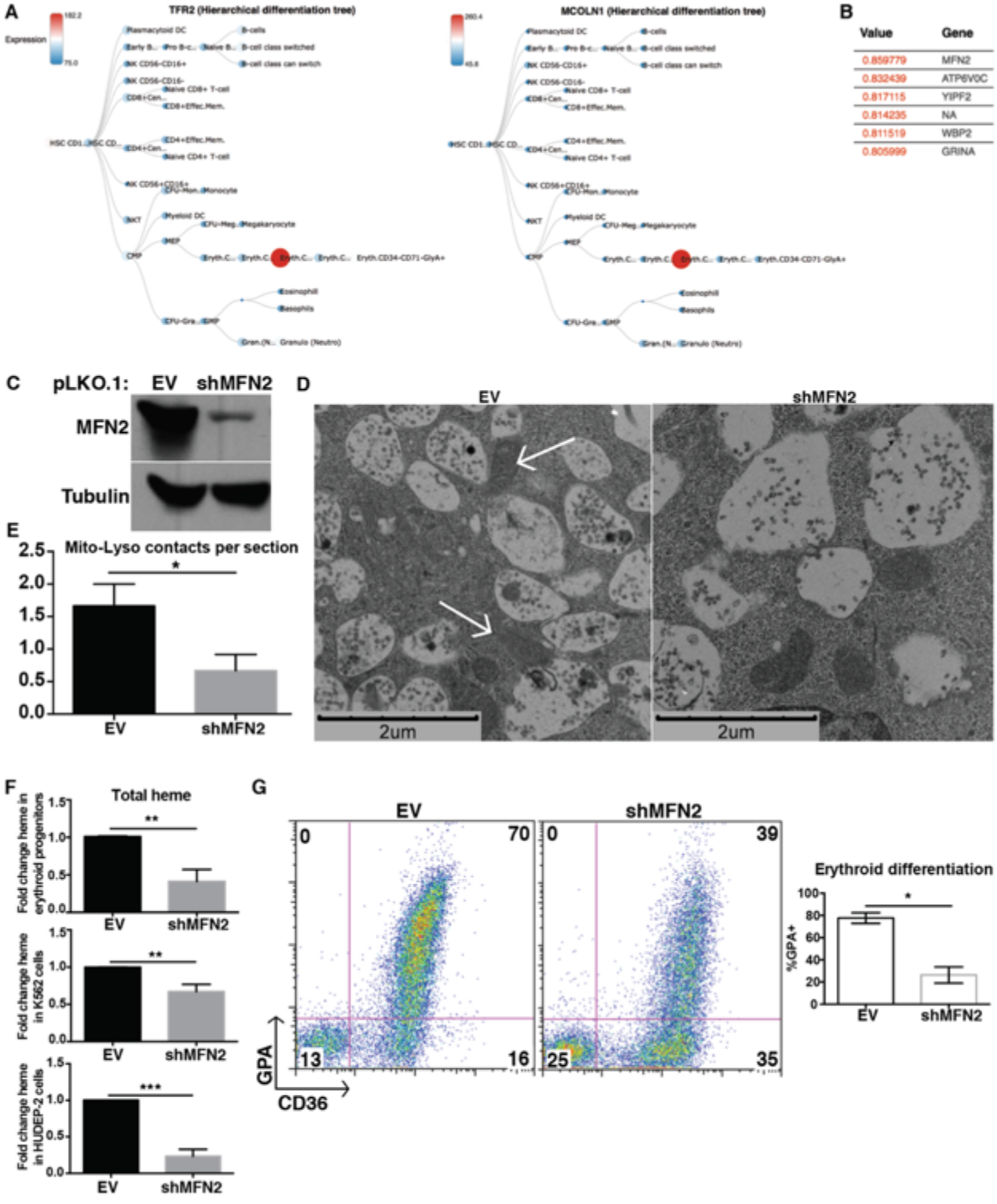
A
TFR2 (Hierarchical differentiation tree)
MCOLN1 (Hierarchical differentiation tree)
B
Value
Gene
0.859779
MFN2
0.832439
ATP6V0C
0.817115
YIPF2
0.814235
NA
0.811519
WBP2
0.805999
GRINA
C
pLKO.1: EV shMFN2
MFN2
Tubulin
D
EV
shMFN2
2um
2um
E
Mito-Lyso contacts per section
EV
shMFN2
F
Total heme
Fold change heme in erythroid progenitors
Fold change heme in K562 cells
Fold change heme in HUDEP-2 cells
G
EV
shMFN2
GPA
CD36
Erythroid differentiation
%GPA+

Figure 3.13

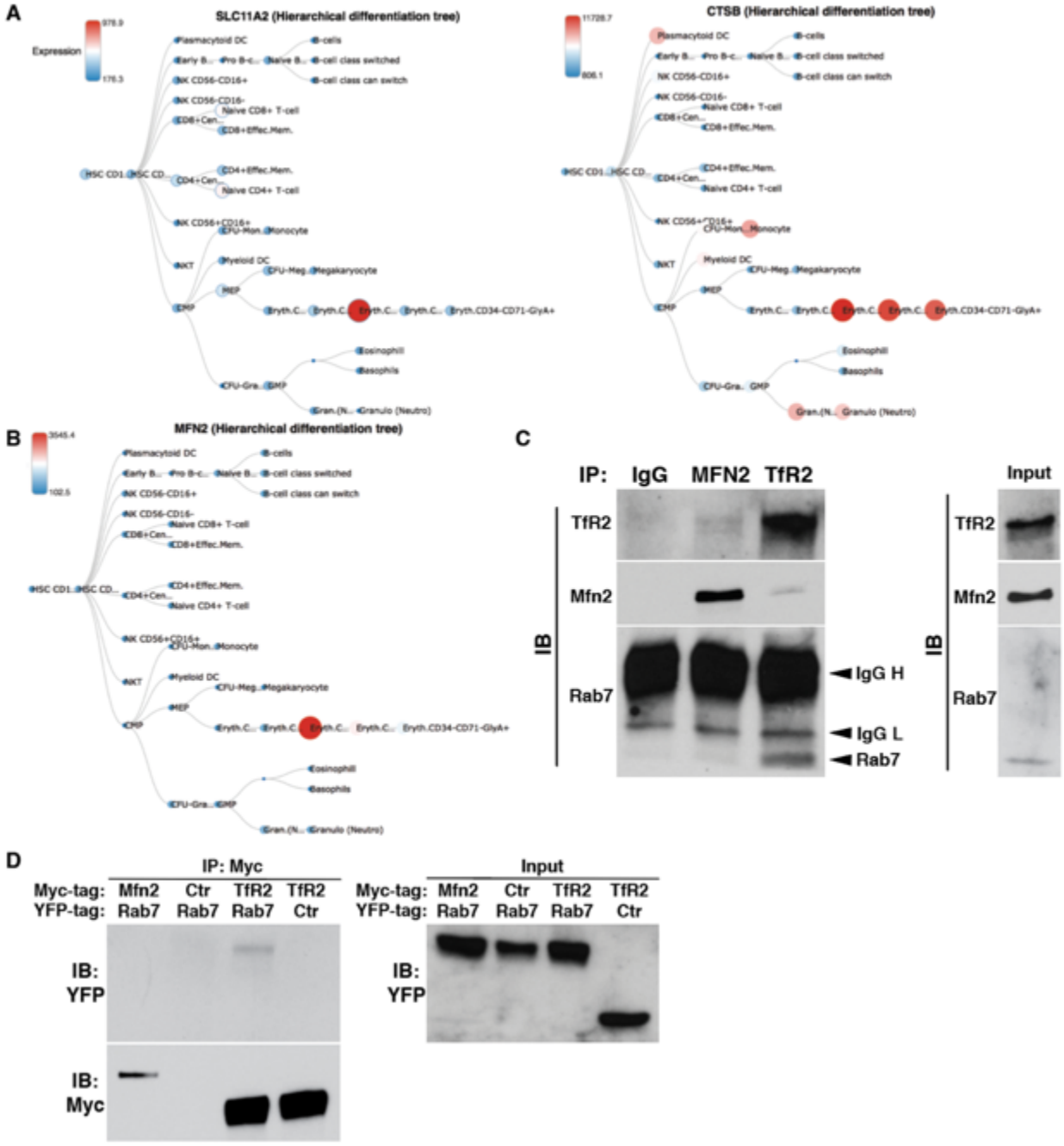
A
SLC11A2 (Hierarchical differentiation tree)
Expression
978.9
176.3
CTSB (Hierarchical differentiation tree)
11728.7
606.1
B
MFN2 (Hierarchical differentiation tree)
3545.4
102.5
C
IP: IgG MFN2 TfR2
Input
IB
TfR2
Mfn2
Rab7
IgG H
IgG L
Rab7
D
IP: Myc
Input
Myc-tag: Mfn2 Ctr TfR2 TfR2
YFP-tag: Rab7 Rab7 Rab7 Ctr
IB: YFP
IB: Myc

CHAPTER 4:

General Discussion

TfR2: Balancing Iron Uptake with Sensing

The experimental results described herein provide a mechanistic basis of the erythroid iron deprivation response, in addition to shedding light upon long-standing questions of erythroid iron uptake. Regarding the erythroid iron deprivation response, we have uncovered a pathway by which TfR2 senses extracellular iron, ultimately affecting the surface expression and signaling of EpoR, the major receptor regulating erythropoiesis. This mechanism allows for cell-autonomous sensing of iron stores by the tissue that utilizes most of the body's iron, sparing iron stores in the face of depletion. Notably, despite impaired EpoR surface expression, signaling through Epo is modulated such that the limited EpoR surface repertoire hyperactivates Akt signaling, thus allowing for cell survival and failed proliferation. The erythroid iron deprivation response is the pathogenic basis of many human anemias, including iron deficiency anemia, anemia of chronic disease, and anemia of kidney disease. By uncovering the common pathogenic process underlying these diseases, we open the door to novel anemia treatments and pharmacological targets. One such treatment includes isocitrate, which our studies identify as the metabolite regulating TfR2 degradation.

TfR2 sensing, interestingly, occurs through alternate trafficking as opposed to the activation of canonical intracellular signaling pathways. Under iron replete conditions, TfR2 traffics to the lysosome and undergoes surface recycling. This equilibrium is pushed towards lysosomal trafficking with iron deprivation, thus driving the degradation of TfR2 and its associated binding partners, including Scribble, a master regulator of surface EpoR expression. Questions arose when making the initial observations as to why

erythroid cells undergo a bioenergetically demanding process of synthesizing and trafficking the TfR2 receptor, only to degrade it in the lysosome as part of a sensing mechanism. While this observation can easily be rationalized given the importance of iron sensing, preliminary observations of microcytosis with bone marrow TfR2 knockout provided clues as to an alternate function of TfR2.

Iron must ultimately reach the erythroid mitochondria as part of the biosynthesis of heme. For years, hematologists have observed the lack of cytosolic transit of iron by erythroid progenitors consuming diferric transferrin. This has given rise to the “kiss-and-run” hypothesis of iron uptake: erythroid progenitors endocytose transferrin, delivering the iron-laden endosomes to a position so proximal to mitochondria that the transit of iron is virtually undetectable in the cytosol. The observation that a recognized transferrin receptor in the quiescent state was rapidly trafficking iron to the lysosome provoked the hypothesis that TfR2-mediated lysosomal delivery of transferrin could be the upstream arm of an iron delivery pathway. Ultimately, we were able to uncover a pathway by which TfR2 delivers iron to the mitochondria, which sit peripheral to and directly contact a spherical network of lysosomes in erythroid cells. This contact enables iron transfer into the mitochondria and promotes hemoglobinization. Several molecular players were identified to participate in this process, including MCOLN1, a lysosomal iron channel, and MFN2, a mitochondrial outer membrane protein contributing to mitochondria-lysosomal direct contacts. Remarkably, these genes undergo similar lineage- and stage-specific coregulation, with strong upregulation in CD71+ GPA+ intermediate erythroid progenitors and rapid downregulation upon further maturity. The findings of this study are significant in several ways: First, we identify a novel pathway of iron uptake that is lysosome-

mediated, and driven by TfR2, a receptor recognized for iron sensing but dismissed in uptake. Second, the collective data provides a solution to the problem of limited cytosolic iron transit with erythroid iron uptake. Finally, we are the first to identify functional direct contacts between mitochondria and lysosomes – subcellular structures which likely mediate cellular processes extending beyond iron trafficking.

Thus, TfR2 is a receptor efficiently solving two erythroid problems at once. On one hand, TfR2 is essential for normal iron uptake by erythroid cells, and traffics iron to the lysosome in its journey to the mitochondria. On the other hand, this process is dynamically regulated by transferrin concentrations: with iron deprivation, lysosomal transit and degradation is accelerated, driving a molecular cascade that ultimately pauses erythropoiesis. This model can be understood from the perspective of fluctuating iron levels in the circulation. Ultimately, there are two phases to the iron deprivation response: initial iron deprivation results in rapid TfR2 trafficking to the lysosome, such that increased iron uptake and delivery can sustain the nutrient demand of the actively hemoglobinizing erythroid cell. Sustained iron deprivation and consequent TfR2/Scribble depletion, however, blocks the surface expression of EpoR to pause erythropoiesis. Many questions are brought forth by these studies pertinent to the process of erythroid iron uptake and the mechanism of erythroid iron sensing. These problems include understanding the role other erythroid organelles in erythropoiesis, exploring the interaction between aconitase/TfR2/isocitrate, and assessing the trafficking and post-translational modifications of Scribble. Several of these problems, and associated potential methodological approaches in answering these problems, are addressed in this general discussion.

Organelle Apparatus in Erythroid Iron Uptake

TfR2 is observed to undergo lysosomal transport and degradation, as assessed by pharmacological inhibition of translation and of lysosomal cathepsin activity. Iron deprivation accelerates the rate of TfR2 degradation, while isocitrate stabilizes TfR2 under these circumstances. Whether isocitrate and iron deprivation are affecting a general pathway of lysosomal transport or acting specifically upon TfR2 has yet to be determined. Visualization of general lysosomal transport is possible using protease-sensitive fluorophores. The addition of Magic Red cathepsin substrates to erythroid cells cultured in iron deprived conditions and with isocitrate can identify whether generic lysosomal transport and cathepsin activity is perturbed by iron deprivation. If such imaging fails to identify a difference, it would implicate specific TfR2 trafficking, and not generic lysosomal trafficking and degradation, as the upstream target of the erythroid iron deprivation response. To directly address the hypothesis that TfR2 degradation is specifically regulated, GFP-tagged recombinant TfR2 or fluorophore-labeled anti-TfR2 antibody can be applied to erythroid progenitors and assessed via imaging for lysosomal co-localization and degradation.

Additional questions arise from the nature of the association between TfR2 and transferrin. TfR1 binds holotransferrin to initiate clathrin-mediate endocytosis; it is unclear whether TfR2 must also bind holotransferrin to initiate internalization. With lower transferrin saturation, we would predict fewer molecules of transferrin to bind TfR2; however, TfR2 is accelerated in its degradation. We hypothesize that given the high concentration of transferrin in circulation and in culture medium, TfR2 would remain

occupied. To ask this question, fluorophore-conjugated transferrin could be imaged in conjunction with tagged recombinant TfR2 or fluorophore-labeled anti-TfR2. It would be informative to recognize the fate of surface TfR2 under conditions of iron deprivation and isocitrate rescue. To this end, surface biotinylation of a cohort of TfR2 receptors can be performed on cells cultured in all conditions, following by re-introduction to culture media and harvesting of lysates. Streptavidin pulldown of cell lysates can inform whether TfR2 on the cell surface, in direct contact with transferrin, is accelerated in degradation.

Analysis of total heme content in erythroid progenitors following TfR2 knockdown confirmed the contribution of TfR2 to mitochondrial delivery of iron. However, although suggested, it remains inconclusive whether iron is directly transferred to the mitochondria from the lysosome, and whether iron (and not transferrin) can be observed in the lysosome. The iron-chelatable dyes RPA and RDA label the mitochondria, with fluorescence quenched by mitochondrial iron. Staining erythroid cells with RPA/RDA and subjecting them to fluorophore-conjugated transferrin uptake would allow for live imaging of iron flux from vesicular cell compartments to the mitochondria. To further characterize TfR2-dependent erythroid iron transport, transferrin containing radiolabeled iron can be administered to cells, followed by fractionation of the cytosol, lysosome, and mitochondria. Capturing the movement of iron with time would allow for an understanding of specific iron movement through the different cellular compartments, in addition to providing additional evidence of direct mitochondrial transfer.

Electron microscopy of erythroid progenitors identified a unique configuration of centralized golgi stacks, budding into lysosomal clusters that are peripherally shielded by mitochondria. While in most cells golgi stacks are flat and emanating from the

endoplasmic reticulum, erythroid cells contained non-traditional golgi stacks, circularized to form a perinuclear globe. Adding to the peculiarity of erythroid golgi stacks, the cellular material at the center of the golgi is of darker, more homogenous electron density than the cytosol (Figure 4.1). Further, Mitotracker staining of the mitochondria highlights a network of peripheral mitochondria, projecting Mitotracker+ processes towards the center that connect to a surprisingly Mitotracker+ golgi center (Figure 4.2). These unique properties of the erythroid golgi apparatus suggest additional interaction and function associated with the mitochondria. Additional characterization of erythroid organelles is essential to properly understand the unique layout and properties of the golgi apparatus. By electron microscopy, endoplasmic reticulum is seen throughout the cytosol, but not projecting from the nuclear membrane or interacting with the golgi. Given that the golgi creates a globe, it is likely that the endoplasmic reticulum is projecting as a stem into the golgi at a narrow point. Immunofluorescence studies of calreticulin, golgin97 (marker of the trans golgi network), and gp74 (marker of the cis golgi network) localization in erythroid cells can identify a potential interaction between the golgi and endoplasmic reticulum, in addition to defining the cis and trans faces of the golgi. Co-immunostaining mitochondrial outer membrane proteins such as MFN-2 and lysosome markers such as Lamp1 would provide a comprehensive picture of erythroid cellular anatomy as it pertains to iron uptake. Whether the layout and interaction between the organelles are affected by iron deprivation can be assessed by immunofluorescence and electron microscopy in cells subjected to iron deprivation. Specifically, we would expect the frequency of membrane contact sites between mitochondria and lysosomes to be increased with initial iron deprivation, as cells attempt to obtain more mitochondrial iron.

As described in chapter 2, Scribble is identified in the membranous and cytosolic fractions of erythroid progenitors. Immunofluorescence of Scribble and Golgin97 confirms some Scribble colocalization with the golgi, suggesting that the golgi may be involved in Scribble modulation by the iron deprivation response. In support of this concept, Golgin97 intensity is reduced with iron deprivation in erythroid cells (Figure 4.3), suggesting "golgiopathy" as a pathogenic mechanism in the erythroid iron deprivation response. It is unclear how the golgi can be manipulated by iron, or whether this contributes to the iron deprivation response. Potentially, TfR2 stability or degradation, through its trafficking to the lysosome, may be contributing to the integrity of the golgi. Erythroid cells subjected to TfR2 knockdown and concomitant iron deprivation can be analyzed for the extent of golgi reduction, thus assessing the contribution of TfR2 to iron-dependent erythroid golgiopathy. In a similar manner, the contribution of TfR2 to the lysosome can be analyzed through knockdown and imaging, with attention to changes in ILV content, lysosome number, and vesicular size.

Mitochondria-Lysosomal Contacts

Direct contacts between mitochondria and lysosomes are observed in erythroid cells as part of an iron uptake pathway. Although this is the first observation of such structures, erythroid cells are not the only cells burdened with high iron demand in specific cellular compartments, and such organelle contacts may be observed in other cell types. Myoblasts and myocytes synthesize heme in the production of myoglobin, and examining the pattern of transferrin uptake and interaction between mitochondria and lysosomes in such cells would be interesting. Myocytes do not express TfR2, suggesting that if this pathway does exist, lysosomal trafficking of transferrin must be mediated by other players. Mitochondria-lysosomal MCSs were observed in granulocytes, suggesting that these structures may be part of the generic transferrin uptake pathway, and potentially enriched in cells responsible for iron handling: macrophages, enterocytes, and hepatocytes. Immunofluorescence and electron microscopy conducted on these cells will inform whether MCS density is associated with iron function.

Although we describe TfR2 as mediating transferrin delivery to the lysosome, we are curious whether lysosomal iron delivery may be a generalized trafficking pathway. In many cell types studied, the expression of DMT1, the channel responsible for ferrous export from the endosome to the cytosol, has high co-localization with the lysosome. This provides the potential for iron to remain in the vesicular pathway all the way to the lysosome in non-erythroid cells. Lysosomal delivery and export of iron may be a specialized pathway for organelle-specific delivery of iron beyond the mitochondria and should be investigated further.

In our studies of mitochondria-lysosomal MCS, we identify MFN2 knockdown as significantly reducing the number of contacts between mitochondria and lysosomes. MFN2 is known to physically bind other MFN2 molecules in mediating MCS, but in performing immunofluorescence studies of our mitochondria, we were only able to observe MFN2 on mitochondria (Figure 4.2). Experiments could be carried out on candidate lysosomal membrane proteins to assess whether they physically interact with MFN2. Such studies would identify novel MFN2 binding partners and mediators of organelle contacts. While MFN2 knockdown significantly reduced the frequency of MCS, direct contacts were not entirely ablated, suggesting alternative molecular players in mediating mitochondria-lysosomal contacts. There are a number of mitochondrial outer membrane proteins involved in mediating membrane contacts, which can be systemically profiled for their contributions to erythroid mitochondria-lysosomal MCS. One potential candidate in maintaining erythroid mitochondria-lysosomal MCS is mitochondrial fission protein Fission 1 homologue (FIS1). FIS1 is expressed on the mitochondria and involved in mitochondria-ER interactions through binding of the ER protein Bap31 (268). Intriguingly, FIS1 follows the same pattern of hematopoietic expression as TfR2 and MCOLN1, with sharp upregulation in intermediate GPA+ CD71+ progenitors followed by immediate downregulation with further maturation. Performing immunofluorescence and knockdown studies of FIS1 could test whether the outer membrane protein is relevant in iron uptake and organelle contacts.

Several genes involved in the pathway of lysosomal iron delivery are co-expressed with identical lineage- and stage- specific upregulation in erythropoiesis. Given that these genes undergo remarkably similar co-regulation, we hypothesize that the collection of these genes may be regulated by one or few erythroid transcription factors. Analyzing promoter sequences of *TfR2, CTSB, MFN2,* and *MCOLN1* genes could identify binding motifs in common that may be associated with erythroid transcription factors. NF-E2, GATA1, SCL/Tal1, KLF1 are all major transcription factors involved in erythropoiesis that are activated in early/intermediate erythropoiesis, with comparable expression patterns to the genes in question (Figure 4.4). As such, they represent candidate transcription factors for coordinating the upregulation of players in lysosomal iron trafficking. ChIP-Seq experiments could confirm the interaction between these transcription factors and the genes in question.

To appreciate the pathways in question, physical interactions could be assessed between the different players of the pathway. TRPML1 may directly bind MFN2 and function in mediating mitochondria-lysosomal MCS. Further, the expression of the proteins may be interconnected: knockdown of TfR2 and MFN2 may be associated with compensatory changes in the protein levels of other participants of the pathways. The levels of MFN2 itself appear dynamically regulated: in the disease Myelodysplatic syndrome with ring sideroblasts (MDS-RARS), which is associated with profound anemia and improper iron handling, MFN2 is found upregulated. This may be a compensatory process to drive efficient iron uptake and suggests that erythroid cells may modulate the levels of MFN2 and other proteins to match their needs.

Finally, we have observed toxicity with erythroid MCOLN1 and MFN2 lentiviral knockdown (data not shown). Properly categorizing the nature of this toxicity, through annexin V and PI staining with different erythroid markers would shed light on the pathogenic process that results from knockdown. No toxicity is observed with TfR2 or TfR1 knockdown, leading us to propose two alternative hypotheses: either iron uptake is critical for survival in these cells and TfR2 and TfR1 are performing redundant functions, or MCOLN1 and MFN2 are preventing iron accumulation in the lysosome, which is associated with impaired lysosomal function and toxicity (269). Performing knockdowns, assessments of iron content/flux, and culture of progenitors in iron deprivation conditions can address both hypotheses and uncover the mechanism by which toxicity occurs.

Mechanism of Isocitrate Rescue

By a mechanism that remains unknown, isocitrate stabilizes TfR2 and completely rescues the erythroid iron deprivation response. To better understand this rescue mechanism, we will first seek to identify whether isocitrate can affect TfR2 stability and Scribble levels under iron-replete conditions. Identifying rescue specifically under iron deprivation conditions will suggest that rescue occurs through the same pathway, likely with similar molecular players, as deprivation. It remains to be conclusively determined whether the mechanism of isocitrate rescue is dependent on isocitrate metabolism or signaling effects by the molecule. Likely, it is not dependent on metabolic effects, as alpha-ketoglutarate, one enzymatic step away from isocitrate, fails to rescue the erythroid iron deprivation phenotype. To further examine whether the efficacy of isocitrate was dependent on metabolism, D-isocitrate and L-isocitrate (the metabolically inactive enantiomer) were applied to iron deprived cells and both found to rescue differentiation to similar levels. While suggesting a signaling (rather than metabolic) effect by isocitrate, there is the potential for L-isocitrate to undergo back conversion to citrate which is achiral and capable of re-entering the metabolic pathway. To rule out unexpected metabolism, radiolabeled D- and L- isocitrate enantiomers can be applied to cells, followed by lysis and assessment of radiolabel in other metabolites. Confirmation that no other radiolabeled metabolites are generated when L-isocitrate is administered would conclusively define the effect of L-isocitrate as signaling-based, rather than metabolic.

It has yet to be determined whether isocitrate is internalized into cells upon treatment, or whether it may exert its effect through activity on the cell surface. To address

this, radiolabeled isocitrate can be applied to cells, followed by cell fractionation and assessment of isocitrate content in the cytosolic and membranous fractions. Identification of isocitrate in both fractions would suggest active uptake into the cytosol from the surface, while identification in specific fractions would argue for specificity of isocitrate activity and effect. Potentially, isocitrate efficacy may be derived through direct binding to TfR2 or transferrin, resulting in stabilization. To this end, labeled isocitrate can be incubated with recombinant transferrin, recombinant TfR2, or lysates containing TfR2/transferrin. Immunoprecipitation followed by assessment of isocitrate content would identify a direct binding interaction and provide hints as to the mechanism. Another potential mechanism of isocitrate efficacy may be through affecting osmolarity and ion exchange. Isocitrate effects are seen at high concentrations: erythroid progenitors demonstrate rescue with 20mM isocitrate supplemented to culture media. This concentration may perturb the osmolarity of erythroid cells, resulting in compensatory ion exchange that functions to rescue the phenotype. Measurements of cellular size, nuclear shape, nuclear size, and intracellular ion concentration would assess osmotic stress in erythroid progenitors subjected to isocitrate treatment.

Finally, the mechanism by which aconitase activity interacts with TfR2 remains to be explored. Fluoroacetate treatment recapitulates features of the iron deprivation response in erythroid progenitors, but fails to be rescued by additional treatment of isocitrate. While isocitrate rescue of iron deprivation is conditionally dependent upon TfR2 expression, fluoroacetate treatment blocks differentiation in cells both expressing and knocked down for TfR2. The lack of an isocitrate effect with TfR2 knockdown is likely due to Scribble upregulation at baseline, but may result from other effects: in particular, if

isocitrate functions through an interaction with aconitase, TfR2 may “license” aconitase sensing of iron. In chapter 2, we describe compensatory changes in transferrin uptake associated with TfR2 knockdown. One such mechanism may include switching to aconitase-independent iron sensing (as mitochondrial iron flux becomes impaired), such that isocitrate and aconitase activity no longer function in sensing. To test this, aconitase activity can be quantified via enzymography and in erythroid progenitors subjected to TfR2 knockdown. Finally, we observe that TfR2 nascent surface presentation, in addition to degradation, is critically dependent upon aconitase activity (data not shown). Although isocitrate fails to rescue the fluoroacetate-mediated differentiation phenotype, analysis of whether TfR2 surface kinetics can be rescued by isocitrate when added to fluoroacetate will help identify the interactions between both the fluoroacetate and isocitrate pathways. Other fluoroacetate-driven phenotypes, such as the loss of Scribble, impaired EpoR surface expression, can additionally be examined for isocitrate rescue.

Post-translational Modifications of Scribble

As described in chapter 2, Scribble can be identified in the cytosolic and membranous fractions, with slightly more observed in the cytosol. Our findings have identified membrane-associated Scribble as the more sensitive form which is actively regulated by iron, aconitase, and TfR2. Scribble regulation of cell polarity has been recently identified to be affected by Scribble palmitoylation and consequent localization of Scribble (270). Given that the membranous fraction is the dynamic fraction in the setting of the erythroid iron deprivation response, Scribble palmitoylation, may be associated with the iron deprivation response. By immunofluorescence and western blotting, we identify rapid flux of Scribble from the cytosolic to the membranous fractions with short-term treatment of a depalmitoylation inhibitor, suggesting that Scribble dynamically undergoes depalmitoylation to flicker from the membranous to the cytosolic fraction (Figure 4.5). Further, palmitoylation is associated with nuclear localization of Scribble, which may be associated with modulation of transcriptional activity. Given that the membranous Scribble pool appears to drive the iron deprivation phenotype, we hypothesize that altering the equilibrium of cytosolic and membranous Scribble may rescue the iron deprivation response. To address this, low-dose depalmitoylation inhibitor can be added to erythroid cultures in iron deprivation, followed by flow cytometric analysis of erythroid differentiation. Further, the kinetics and localization of Scribble can be compared following pharmacological inhibition of palmitoylation and depalmitoylation in iron replete, iron deprived, and isocitrate-treated conditions to assess whether the modifications of Scribble are dependent upon iron or isocitrate. Expression levels of palmitolyases and

depalmitoylases, including ZDHHC7, a candidate palmitoylase expressed throughout the erythropoietic lineage, can be assessed for changes with iron deprivation.

Three distinct bands were observed with western blotting of Scribble. These bands were confirmed to be Scribble by blotting with three separate anti-Scribble antibodies, as well as confirming the loss of all bands with shRNA-mediated Scribble knockdown. Treatment of progenitors with a de-ubiquitylase inhibitor and consequent accumulation of the top band suggests the three bands are differentially ubiquitylated proteins undergoing dynamic ubiquitylation and deubiquitylation. Mass spectrometry of overexpressed Scribble could enable specific identification of the three separate bands. Further, immunoprecipitation of Scribble followed by blotting with an anti-ubiquitin antibody can identify ubiquitin modifications in the higher molecular weight bands. Whether the ubiquitylated bands are associated with Scribble localization can be studied by treating cells with deubiquitylase and ubiquitylase inhibitors, followed by immunofluorescence of Scribble. Similarly, cycloheximide treatment of cells in conjunction with deubiquitylase and ubiquitylase inhibition can identify whether longer-term treatment with inhibitors can stabilize or destabilize Scribble.

Given that Scribble could modify surface presentation and signaling through EpoR, we asked whether a reciprocal association could be identified. Treatment of erythroid progenitors with Epo following Epo withdrawal resulted in the rapid and specific loss of membranous (not cytosolic) Scribble (Figure 4.6). Cytosolic Scribble levels were not appreciably increased, either due to frank degradation of membranous Scribble or limitations as to the detectability of fraction shifting of Scribble due to the enormity of the cytosolic Scribble pool. This phenomenon may have greater implications in erythroid

physiology, as it suggests that progenitors temporarily deprived of Epo can be permanently perturbed. We hypothesize that the Epo-induced degradation of Scribble functions as a feedback system to limit Epo signaling, as diminished Scribble levels can then regulate the density of surface EpoR. However, given that Scribble inhibits Akt signaling, the loss of Scribble may function to hyperactivate Epo-dependent Akt signaling in erythroid cells subjected to Epo restimulation. To address both concepts, cells can be analyzed for surface EpoR expression following Epo re-stimulation to identify whether EpoR is failing to reach the surface given the fewer molecules of Scribble. Signaling of STAT5 and Akt can be compared in Epo-restimulated cells versus the quiescent state to see whether signaling is perturbed upon re-stimulation. It remains to be determined how Epo stimulation can affect Scribble. First, we would like to identify whether this effect is TfR2-dependent, as TfR2 regulated Scribble and is a known binding partner of EpoR. Second, we can examine whether this effect is iron dependent, by performing restimulation in the presence and absence of iron. Finally, to address whether Scribble loss is signaling dependent, Epo restimulation can be performed under conditions of pharmacologic Jak inhibition, to identify whether Jak-dependent signaling is required for the response.

Compensation to TfR2 Knockdown

Although TfR2-dependent lysosomal transferrin uptake defines a novel pathway of erythroid iron trafficking, TfR2 knockdown was associated with re-patterning, and not reduction, of transferrin uptake. Therefore, absence of this ancillary pathway of transferrin uptake results in a compensatory program to maintain erythroid iron uptake. Likely, because of the enhancement of endosomal transferrin uptake, this is occurring through TfR1, although initial studies do not appear to demonstrate TfR1 protein upregulation with TfR2 knockdown. There are several experimental approaches that can help characterize whether TfR2 knockdown is associated with a TfR1-centric compensatory pathway.

First, repeat studies of TfR2 knockdown and TfR1 blotting in primary erythroid progenitors and immortalized cell types can confirm whether or not TfR1 levels are modulated upon TfR2 knockdown. Changes in TfR1 levels may occur through IRP1-mediated stabilization of TfR1 transcript, a process that can be assessed by looking at IRP1/IRE binding, IRP1 activity, and the expression of TfR1 and other IRE-containing transcripts following TfR2 knockdown. If TfR1 levels are confirmed to be unaffected by TfR2 knockdown, it would suggest that the kinetics of TfR1 trafficking are affected by TfR2 knockdown. In chapter 2, we have described Scribble upregulation upon TfR2 knockdown. Given that Scribble generally contributes to receptor trafficking, we hypothesize that Scribble upregulation upon TfR2 knockdown can enhance TfR1 trafficking, ultimately driving the uptake of transferrin into the endosomes. Studies using fluorophore-conjugated anti-TfR1 could assess the velocity of TfR1. Studies employing protease-cleavage of surface proteins followed by recovery of TfR1 upon reintroduction

to culture media would assess the surface presentation and surface recycling of TfR1. Whether Scribble is involved in this compensatory pathway can be assessed by performing a double-knockdown of TfR2 and Scribble, looking at transferrin uptake, TfR1 trafficking, and potential toxicity. It should be noted that although compensatory programs are put in place upon TfR2 knockdown, cells are ultimately less hemoglobinized and smaller, suggesting that enhanced non-lysosomal transferrin uptake is less efficient in mitochondrial delivery than TfR2-dependent transferrin uptake. Intriguingly, TfR2 knockdown cells continue to differentiate under conditions of low iron, failing to demonstrate a normal iron deprivation response. In this situation, assessments of size, total cellular heme, toxicity, TfR1 protein levels, and transferrin uptake could provide insight as to whether compensation in iron uptake to TfR2 knockdown can adequately additionally respond to fluctuations in iron.

Second, combined knockdown can be performed on progenitors followed by measurements of iron uptake, transferrin uptake, and differentiation. Preliminary studies using an shRNA hairpin that knocks down both TfR1 and TfR2 demonstrate robust impairment in erythroid differentiation with combined knockdown (Figure 4.7). Thus, while TfR1 and TfR2 uptake pathways appear largely redundant, combined loss may deprive cells entirely of both iron uptake pathways.

Third, TfR2 knockdown may be associated with perturbations at the ultrastructural level. Electron microscopy of erythroid progenitors subjected to TfR2 knockdown may provide insight as to whether the golgi, mitochondria, or endoplasmic reticulum are affected. Potentially, the density, size, and integrity of the golgi and lysosome may be affected. Further, despite a precipitous reduction in the flux of transferrin to the lysosome,

heme can still be synthesized, suggesting that iron delivery to the mitochondria continues to occur in erythroid progenitors subjected to TfR2 knockdown. Whether this delivery involves cytosolic transit or not can be assessed by overnight treatments with a cytosolic iron chelator, followed by an assessment of total cellular heme. If no cytosolic iron is detected, it would suggest the presence of endosome-mitochondria interactions, which may be detected by electron microscopy and immunofluorescence studies.

Finally, TfR2 may be intimately associated with lysosomal function and integrity. Preliminary studies suggest that TfR2 overexpression in HEK293T cells is associated with an upregulation of Lamp1 (data not shown). The association between TfR2 expression and Lamp1 levels can be further confirmed through experimental repeats and assessed in cells subjected to TfR2 knockdown. Further, immunofluorescence of Lamp1 may depict changes upon TfR2 knockdown. Studies described in chapter 3 identified a physical interaction between TfR2 and Rab7. This interaction potentially describes the process by which TfR2 can traffic to the lysosome, but may also be involved in recruiting proteins and other factors to the lysosome for proper lysosome function and formation. Lysosensor-based live imaging and the administration of Magic Red protease substrates to erythroid progenitors subjected to TfR2 knockdown and TfR2 overexpression could identify changes in lysosomal pH and protease activity. Further, western blotting of lysosomal markers and proteins, including cathepsins, V-type H^+ ATPases, and DRC2 in both the knockdown and overexpression condition could identify changes in total lysosomal protein levels.

Iron Re-exposure

Reports from our and other laboratories support the notion that iron deprivation impairs erythroid differentiation while sparing survival. Epo signaling drives proliferation, differentiation, and survival of erythroid progenitors. Although iron deprivation is associated with reduced surface presentation of EpoR, iron deprivation-induced Scribble loss is associated with Akt hyperactivation. Thus, the limited repertoire of surface EpoR molecules function to promote adequate Akt signaling in the presence of extracellular Epo. We hypothesize that preserved Akt signaling enables progenitor survival during iron deprivation. This can be tested by subjecting erythroid cells to concomitant iron deprivation and pharmacological Akt inhibition and assessing viability. Further, S473A Akt mutants can be developed to block Akt phosphorylation of this site, and again assessing viability with iron deprivation.

From a physiological standpoint, iron deprived erythroid progenitors entering a state of “suspended animation” rather than cell death efficiently matches iron status with erythropoiesis with the wasted bioenergetics of progenitor death. However, this assumes the ability of iron-deprived cells to re-differentiate when again exposed to iron. The concept of erythroid iron re-exposure has not been explored. Taking erythroid progenitors and subjecting them to temporary iron deprivation, followed by flow cytometric study of erythroid differentiation markers will allow for an assessment of whether iron-deprived cells are capable of differentiating with re-introduction to iron. Further, iron-deprived progenitors may be poised to re-differentiate when introduced to iron replete culture conditions and outperform iron-loaded counterparts. Human erythroid differentiation, from

HSC to circulating erythrocyte, occurs over the course of several days. Therefore, it can be possible for erythroid cells to face multiple temporary episodes of iron deprivation. Performing serial episodes of iron deprivation and re-exposure will assess whether progenitors truly enter a state of suspended animation when iron-deprived or whether they carry the burden of iron deprivation throughout terminal erythropoiesis. If progenitors demonstrate normal or enhanced differentiation following iron re-exposure, this is likely to be associated with recovery of the surface milieu of EpoR and TfR2. Western blotting of cellular fractions can confirm total and surface the levels both receptors and Scribble.

Surface exposure of TfR2 is regulated by Scribble levels. Thus, with iron-deprivation, a reduction in both surface EpoR and TfR2 levels are expected to be driven by Scribble loss. Thus, with iron re-exposure, sensing of iron is likely to initially occur through a TfR2-independent process. Iron may be taken into the cell by TfR1, where it can be sensed ultimately by aconitase activity. If progenitors are observed to successfully differentiate following iron re-exposure, exploring the mechanism underlying this process may yield novel intracellular iron-sensing molecular mechanisms.

Hepatocyte Iron Sensing

Hepatocytes are the other cell type to express significant levels of TfR2. Hepcidin expression and plasma levels are dependent on hepatocyte TfR2, suggesting its function in hepatic iron sensing. However, hepatocytes contain significant iron stores and are involved in iron handling beyond hepcidin expression. Whether TfR2 in hepatocytes functions in either lysosomal iron trafficking or iron sensing through a Scribble-mediated pathway remains to be determined.

To assess whether TfR2 may play similar roles in hepatocytes as to the functions identified in erythroid iron sensing, primary hepatocytes can be cultured in the presence and absence of iron, followed by measurements of TfR2 and Scribble total levels. Total levels of TfR2 and Scribble should decrease, in a TfR2-dependent manner, if the pathway similarly exists in hepatocytes. If changes in TfR2, Scribble, or both proteins are not observed, it may be due to the absence of other erythroid proteins. EpoR and Jak overexpression in HEK293T cells was found to enhance the association between Scribble and TfR2. Thus, the EpoR module may facilitate the interactions necessary for TfR2 and Scribble to undergo lysosomal co-catabolism. This hypothesis can be tested by overexpression of EpoR and EpoR-associated proteins in hepatocytes, followed by assessments of iron-dependent Scribble and TfR2 stability.

Finally, the lysosome may play an essential role in iron uptake and release in hepatocytes. Treatment of normal and TfR2-knockdown hepatocytes with fluorophore-conjugated transferrin can identify patterns of transferrin uptake in hepatocytes. The lysosome is already recognized as playing a role in the release of ferritin-associated iron.

Examination of ferritin stores, including mitochondrial ferritin, may identify direct contacts between organelles as observed in erythroid progenitors.

Soluble TfR1 as an ERFE Effector

Recently, the erythroid gene *Fam123* was identified to encode the long-sought connection between enhanced erythropoiesis and hepcidin suppression. This link allows for enhanced iron uptake to occur following accelerated erythropoiesis, matching immediate iron uptake with expected iron consumption by differentiating erythroid progenitors. The encoded protein, named Erythroferrone (ERFE), was suspected of being a circulating hormone with direct hepcidin-suppressing activity on hepatocytes. *Fam123* transcript was upregulated with phlebotomy, and *Fam123 -/-* mice demonstrate impaired recovery from anemia and higher levels of hepcidin following phlebotomy.

Several observations suggest that ERFE may not provide a complete story as to the link between erythropoiesis and hepcidin suppression. First, ERFE was not observed in the plasma and a receptor for ERFE was not identified on hepatocytes. Further, treatment of hepatocytes with recombinant ERFE failed to suppress hepcidin expression. This was attributed to precipitation of ERFE protein. However, conditioned culture media from HeLa cells transfected to overexpress ERFE was capable of suppressing hepcidin in hepatocytes. Finally, ELISA assays, which are being generated for clinical and scientific use, fail to detect ERFE in the plasma at baseline, attributed to poor sensitivity of the assay. The collection of this data points to a second messenger in communicating ERFE to hepatocytes.

Soluble TfR1, upregulated with erythropoiesis, is measured clinically to assess erythropoiesis, although the mechanism underlying the upregulation of soluble TfR1 has remained largely uncharacterized. TfR1, not expressed on circulating erythrocytes, can

be shed from the erythroid membrane via cleavage (271, 272), with some demonstration of membrane association (273, 274) and exosome release (275). One possible function for plasma soluble TfR1 may be as a decoy receptor to transferrin, thus absorbing diferric transferrin from the circulation and reducing the functional transferrin saturation. Therefore, the presence of soluble TfR1 may deceive hepatocytes into perceiving reduced transferrin saturation, thus reducing hepcidin expression.

First, although TfR1 is membrane associated, the precise nature of plasma TfR1 complexes are not understood. Many proteins identified in the extracellular space are associated with exosomes. Whether TfR1 is associated with other clusters can be analyzed by size-filtering of plasma and looking for the expression of TfR1. Exosomes can further be prepared using ultracentrifugation and analyzed for the expression of TfR1. The function of soluble TfR1 can be assessed by analyzing soluble TfR1 levels in wild type and *Fam123 -/-* mice following phlebotomy, with the expectation of observing TfR1 upregulation in wild type but not *Fam123 -/-* animals. Further, levels of soluble TfR1 can be measured in conditioned culture media in an ERFE overexpression system. If soluble TfR1 is identified to be exosome associated, exosomes can be isolated from plasma or erythroblast culture, administered in vivo and in vitro, and assessed for efficacy in reducing hepcidin expression. Removal of TfR1+ exosomes can be performed by anti-TfR1 precipitation to see whether the effect is lost, thus implicating TfR1+ exosomes in hepcidin modulation.

miRNAs in Circulating Erythrocytes

Mature circulating erythrocytes are transcriptionally inert, utilizing existing intracellular hemoglobin stores to shuttle gases between the body's tissues. Void of nuclear material, RNA transcripts, and ribosomes, they are transcriptionally and translationally inactive, having synthesized the proteins required for function as erythroblasts. However, recent observations have identified miRNAs as a large intracellular component of circulating erythrocytes (276, 277). Analyses have concluded that the majority of miRNAs identified in the circulation are contained within erythrocytes. miRNAs canonically exert control over gene expression through the regulation of translation. Given that translation is inactive in erythrocytes, is it suspected that miRNAs exist in erythrocytes as vestigial remnants of erythropoiesis. However, miRNA profiles radically shift throughout terminal erythropoiesis (277), maintaining the possibility that the miRNA content of mature erythrocytes can have function. The possibility that miRNAs in circulating erythrocytes may have physiological purpose has remained unexplored.

Any physiological function of miRNA likely occurs through internalization into a separate translationally active cell. The setting in which intracellular miRNAs may interact with another cell type is likely to involve erythrocyte cell death. Potentially, the phagocytosis of erythrocytes may expose the engulfing cell. Although limited in experimental evidence, there is some precedent to the concept that engulfed cells may communicate genetic material to the phagocyte (278, 279). Given that erythrocytes are the major phagocytosed cell in the body, we hypothesize that circulating erythrocytes may communicate to macrophages via intracellular miRNA content. Testing this hypothesis

can be done via transfusing mice with normal and *Dicer -/-* blood, followed by assessing erythrocyte clearance and circulating blood cell parameters. Dye-labeling of transfused blood could allow for quantification of erythrocyte clearance. The phenotype can be exaggerated by phlebotomizing mice immediately before blood transfer such that the major cellular component in circulation is derived from the transfusion. Studies can be performed of the spleen and liver to assess whether the macrophage number or morphology are affected. A phenotype between wild type and *Dicer -/-* circulating erythrocytes may not be evident with normal physiology: alternative models include inducing dermal injury or intravascular clotting such that erythrocyte clearance occurs under a disease setting of leukocyte recruitment to a clot.

CHAPTER 4 Figures

Figure 4.1. Interaction between centralized golgi and lysosomes in erythroid progenitors.

Transmission electron microscopy of erythroid progenitors.

Figure 4.2. Interaction between centratlized golgi and mitochondria in erythroid progenitors.

Mitotracker and immunofluorescent staining for MFN2 on erythroid progenitors.

Figure 4.3. Impaired erythroid trans-golgi-network with iron deprivation.

Immunofluorescent staining for Golgin97 in erythroid progenitors cultured in 100% or 10% transferrin saturation (63X oil objective).

Figure 4.4. Stage-specific expression of major erythroid transcription factors.

Heatmap depiction of NFE2, GATA1, Tal1, and Klf1 transcript levels throughout normal human hematopoiesis, with highest expression in GPA+ CD71+ intermediate erythroid progenitors. The DMAP dataset was analyzed using BloodSpot (http://servers.binf.ku.dk/bloodspot).

Figure 4.5. Scribble localization and palmitoylation.

Immunofluorescent staining for Scribble and Golgin97 in erythroid progenitors cultured in 100% transferrin saturation and subjected to 10-minute treatment with the de-palmitoylase inhibitor palmostatin B (63X oil objective).

Figure 4.6. Membranous Scribble with epo restimulation.

Immunoblots of membrane fractions from erythroid progenitors subjected to 16 hours of overnight Epo deprivation followed by Epo stimulation for 0, 1, and 3 hours; densitometry (bottom panel) from multiple experiments for fold change in membranous Scribble relative to ATP1A1 at 1 hour and 3 hours Epo stimulation (n = 3, one-way ANOVA, **, $P < 0.01$; ***, $P < 0.001$).

Figure 4.7. TfR1 and TfR2 knockdown in lentivirus-transduced progenitors.

Flow cytometry of progenitors subjected to transduction with indicated lentiviral shRNA constructs and cultured four days in erythroid medium.

Figure 4.1

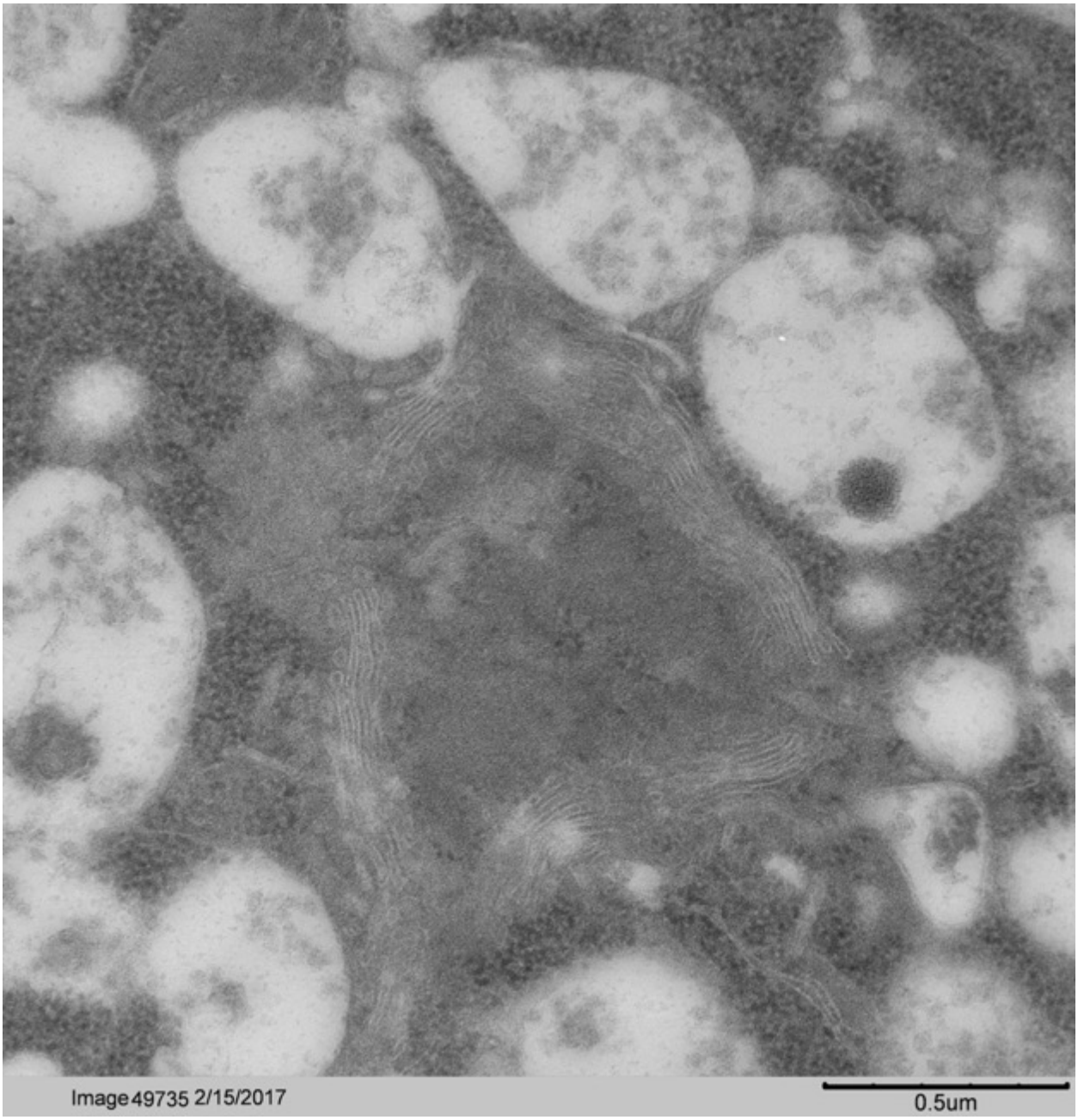

Figure 4.2

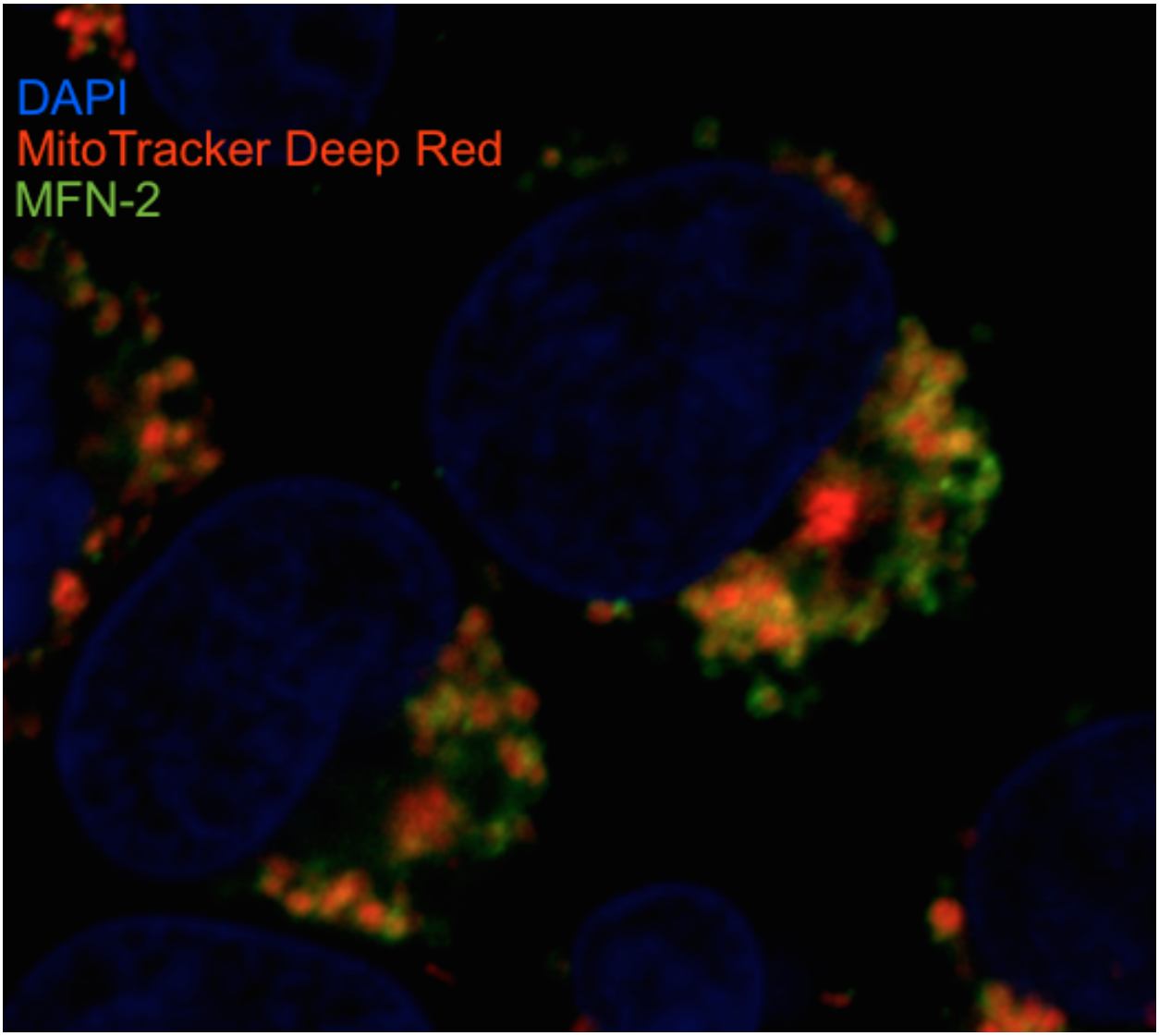

Figure 4.3

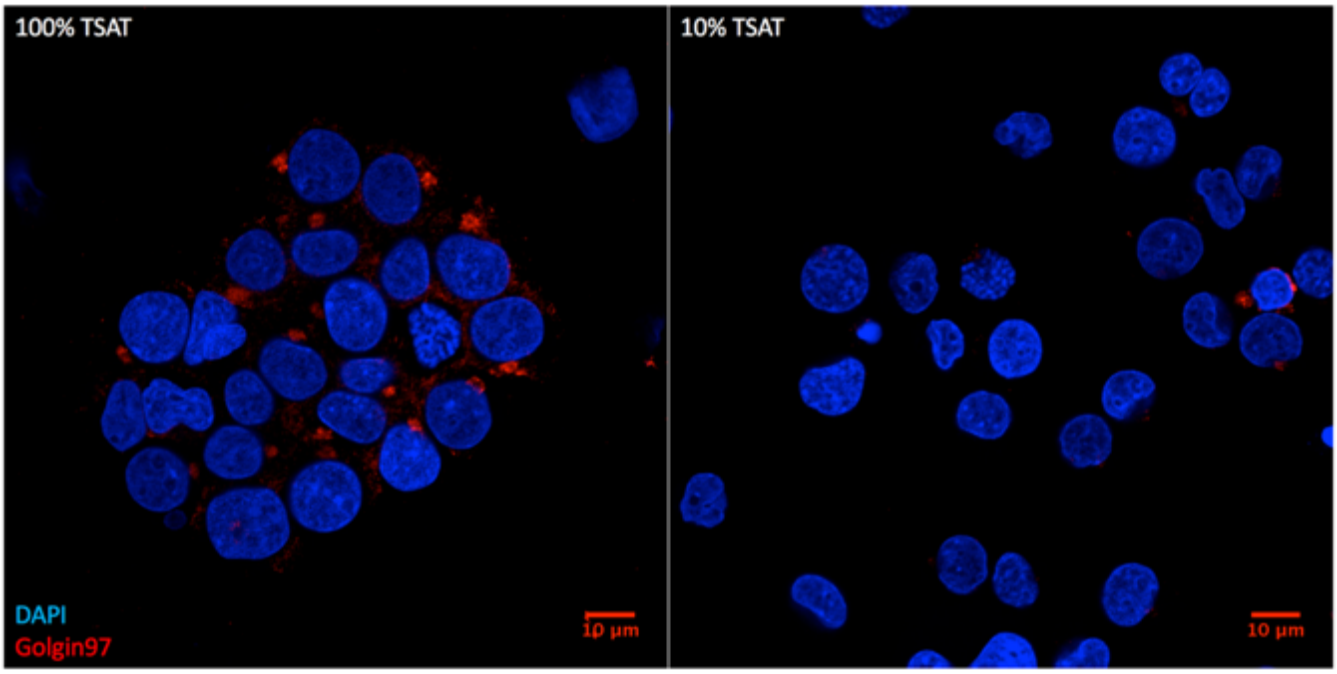

Figure 4.4

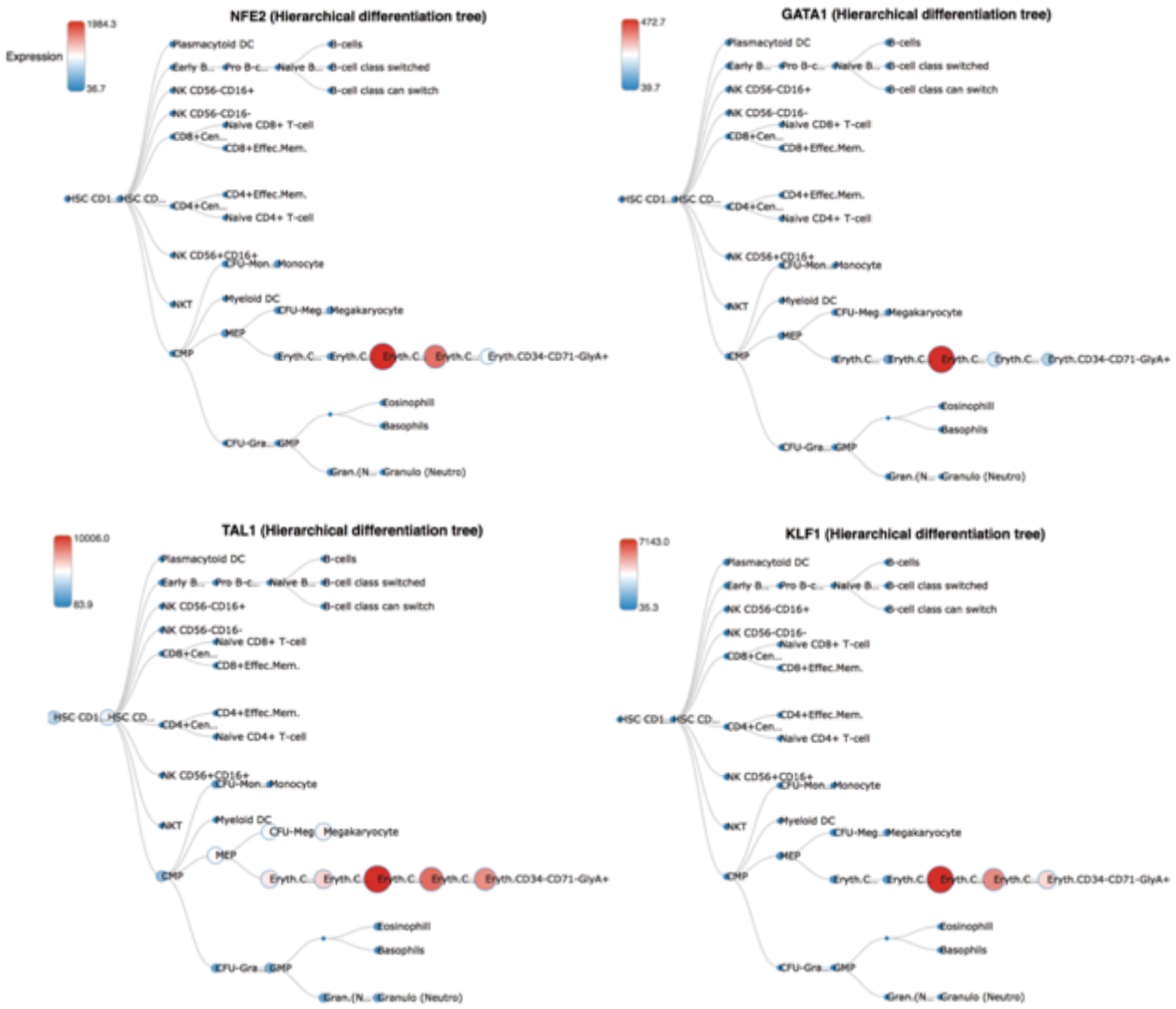
NFE2 (Hierarchical differentiation tree)
Expression
1984.3
36.7
Plasmacytoid DC
B-cells
Early B...
Pro B-c...
Naive B...
B-cell class switched
B-cell class can switch
NK CD56-CD16+
NK CD56-CD16-
Naive CD8+ T-cell
CD8+Cen...
CD8+Effec.Mem.
HSC CD1...
HSC CD...
CD4+Effec.Mem.
CD4+Cen...
Naive CD4+ T-cell
NK CD56+CD16+
CFU-Mon...
Monocyte
NKT
Myeloid DC
CFU-Meg...
Megakaryocyte
MEP
CMP
Eryth.C...
Eryth.CD34-CD71-GlyA+
Eosinophill
Basophils
CFU-Gra...
GMP
Gran.(N...
Granulo (Neutro)
GATA1 (Hierarchical differentiation tree)
472.7
39.7
TAL1 (Hierarchical differentiation tree)
10006.0
83.9
KLF1 (Hierarchical differentiation tree)
7143.0
35.3

Figure 4.5

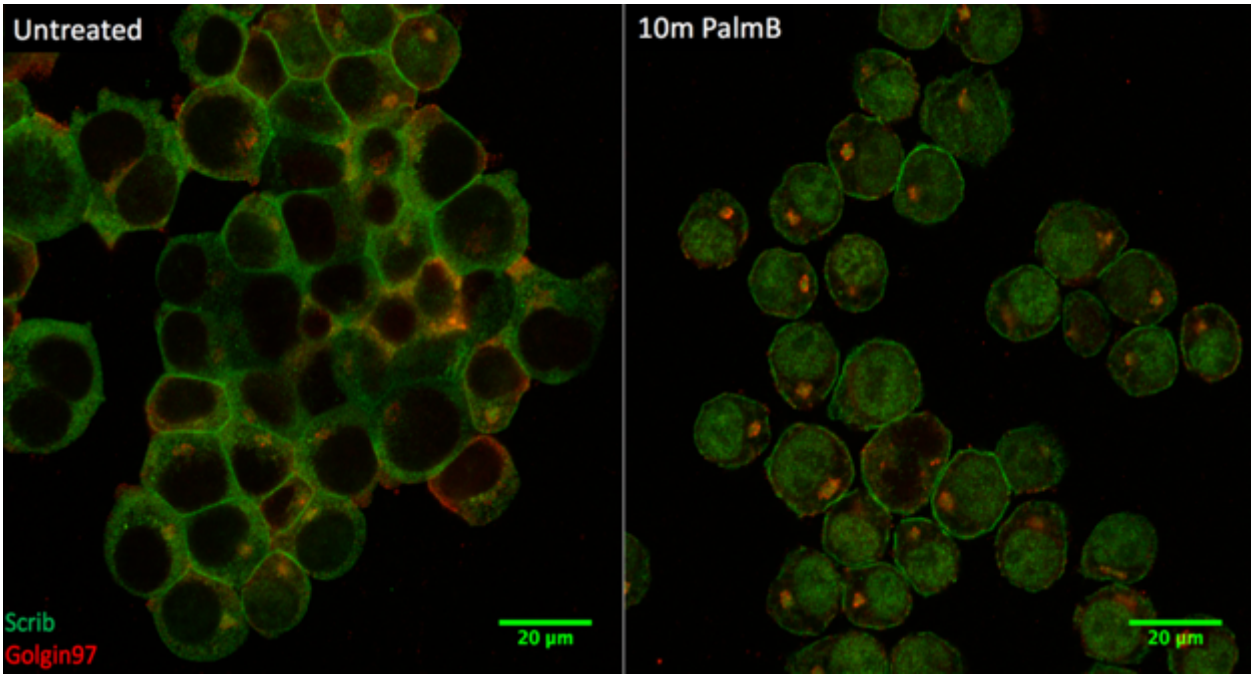

Figure 4.6

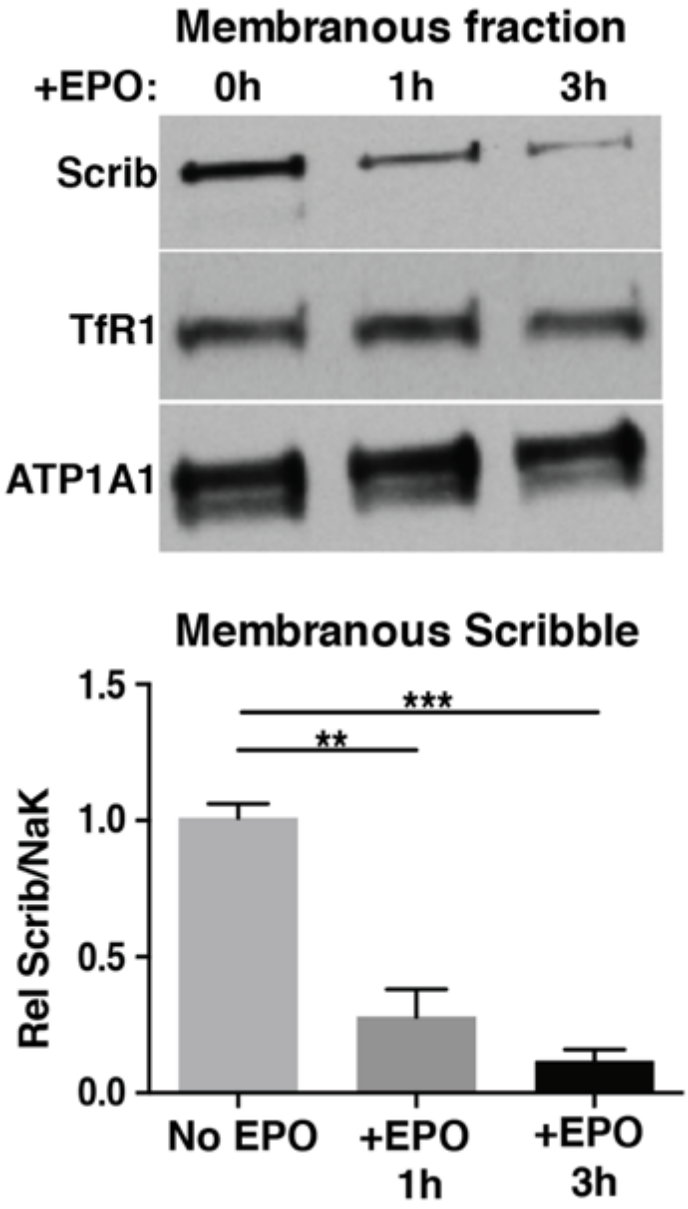
Membranous fraction
+EPO:
0h
1h
3h
Scrib
TfR1
ATP1A1
Membranous Scribble
Rel Scrib/NaK
1.5
1.0
0.5
0.0
***
**
No EPO
+EPO 1h
+EPO 3h

Figure 4.7

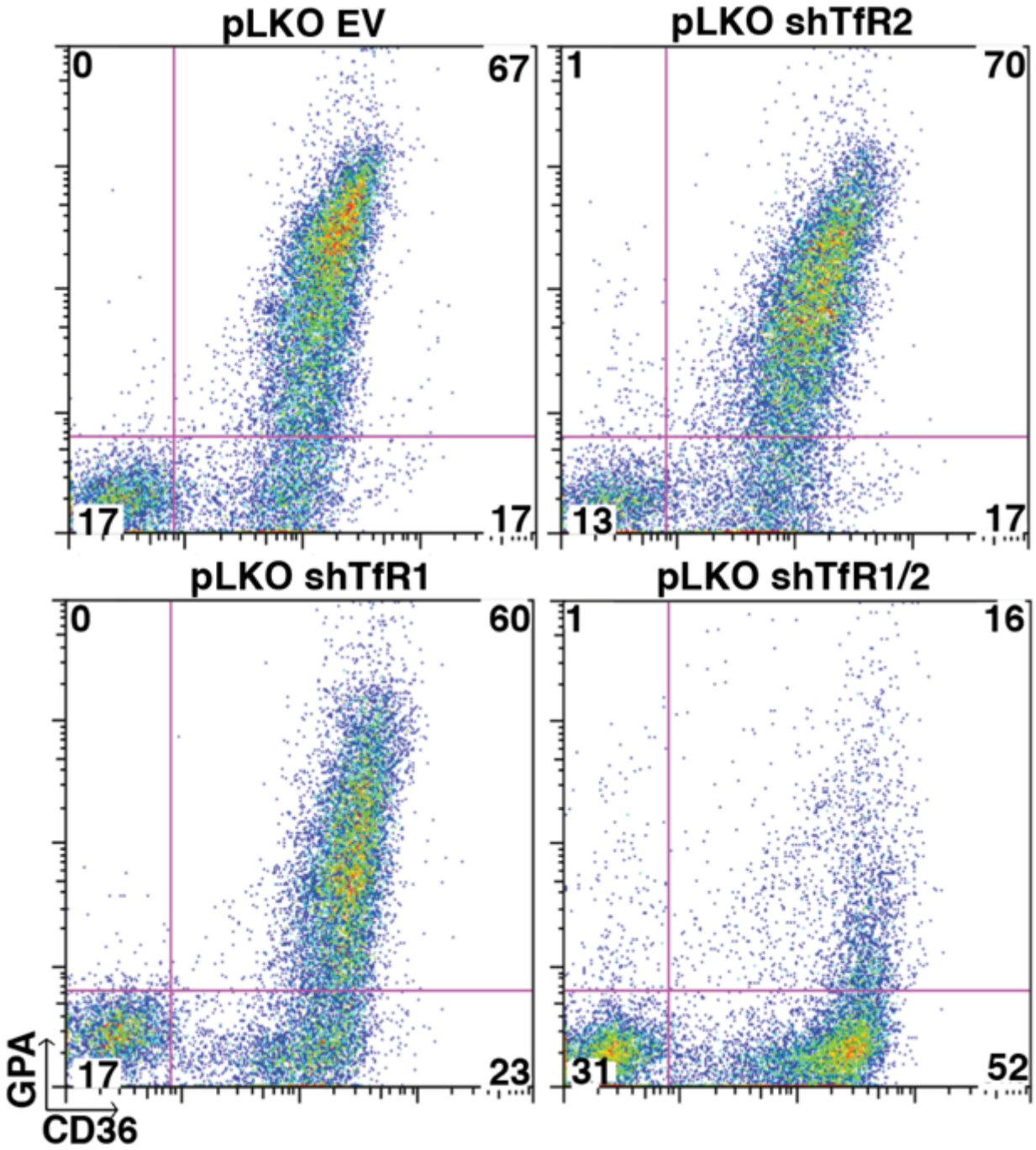
pLKO EV
0
67
17
17
pLKO shTfR2
1
70
13
17
pLKO shTfR1
0
60
17
23
pLKO shTfR1/2
1
16
31
52
GPA
CD36

References

1. Perdiguero EG, and Geissmann F. The development and maintenance of resident macrophages. *Nat Immunol.* 2016;17(1):2-8.
2. Perdiguero EG, Klapproth K, Schulz C, Busch K, de Bruijn M, Rodewald HR, and Geissmann F. The Origin of Tissue-Resident Macrophages: When an Erythro-myeloid Progenitor Is an Erythro-myeloid Progenitor. *Immunity.* 2015;43(6):1023-4.
3. Medvinsky A, and Dzierzak E. Definitive hematopoiesis is autonomously initiated by the AGM region. *Cell.* 1996;86(6):897-906.
4. Muller AM, Medvinsky A, Strouboulis J, Grosveld F, and Dzierzak E. Development of hematopoietic stem cell activity in the mouse embryo. *Immunity.* 1994;1(4):291-301.
5. Chen MJ, Yokomizo T, Zeigler BM, Dzierzak E, and Speck NA. Runx1 is required for the endothelial to haematopoietic cell transition but not thereafter. *Nature.* 2009;457(7231):887-91.
6. Zovein AC, Hofmann JJ, Lynch M, French WJ, Turlo KA, Yang Y, Becker MS, Zanetta L, Dejana E, Gasson JC, et al. Fate tracing reveals the endothelial origin of hematopoietic stem cells. *Cell Stem Cell.* 2008;3(6):625-36.
7. Kumar V, Abul K. Abbas, Nelson Fausto, Stanley L. Robbins, and Ramzi S. Cotran. Robbins and Cotran pathologic basis of disease. 2005.
8. Reagan MR, and Rosen CJ. Navigating the bone marrow niche: translational insights and cancer-driven dysfunction. *Nat Rev Rheumatol.* 2016;12(3):154-68.

9. Gattazzo F, Urciuolo A, and Bonaldo P. Extracellular matrix: a dynamic microenvironment for stem cell niche. *Biochim Biophys Acta.* 2014;1840(8):2506-19.

10. Sugiyama T, Kohara H, Noda M, and Nagasawa T. Maintenance of the hematopoietic stem cell pool by CXCL12-CXCR4 chemokine signaling in bone marrow stromal cell niches. *Immunity.* 2006;25(6):977-88.

11. Raaijmakers MH, Mukherjee S, Guo S, Zhang S, Kobayashi T, Schoonmaker JA, Ebert BL, Al-Shahrour F, Hasserjian RP, Scadden EO, et al. Bone progenitor dysfunction induces myelodysplasia and secondary leukaemia. *Nature.* 2010;464(7290):852-7.

12. Katayama Y, Battista M, Kao WM, Hidalgo A, Peired AJ, Thomas SA, and Frenette PS. Signals from the sympathetic nervous system regulate hematopoietic stem cell egress from bone marrow. *Cell.* 2006;124(2):407-21.

13. Itkin T, Gur-Cohen S, Spencer JA, Schajnovitz A, Ramasamy SK, Kusumbe AP, Ledergor G, Jung Y, Milo I, Poulos MG, et al. Distinct bone marrow blood vessels differentially regulate haematopoiesis. *Nature.* 2016;532(7599):323-8.

14. Kunisaki Y, Bruns I, Scheiermann C, Ahmed J, Pinho S, Zhang D, Mizoguchi T, Wei Q, Lucas D, Ito K, et al. Arteriolar niches maintain haematopoietic stem cell quiescence. *Nature.* 2013;502(7473):637-43.

15. Naveiras O, Nardi V, Wenzel PL, Hauschka PV, Fahey F, and Daley GQ. Bone-marrow adipocytes as negative regulators of the haematopoietic microenvironment. *Nature.* 2009;460(7252):259-63.

16. Bruns I, Lucas D, Pinho S, Ahmed J, Lambert MP, Kunisaki Y, Scheiermann C, Schiff L, Poncz M, Bergman A, et al. Megakaryocytes regulate hematopoietic stem cell quiescence through CXCL4 secretion. *Nat Med.* 2014;20(11):1315-20.

17. Essers MA, Offner S, Blanco-Bose WE, Waibler Z, Kalinke U, Duchosal MA, and Trumpp A. IFNalpha activates dormant haematopoietic stem cells in vivo. *Nature.* 2009;458(7240):904-8.

18. Baldridge MT, King KY, Boles NC, Weksberg DC, and Goodell MA. Quiescent haematopoietic stem cells are activated by IFN-gamma in response to chronic infection. *Nature.* 2010;465(7299):793-7.

19. Kollet O, Shivtiel S, Chen YQ, Suriawinata J, Thung SN, Dabeva MD, Kahn J, Spiegel A, Dar A, Samira S, et al. HGF, SDF-1, and MMP-9 are involved in stress-induced human CD34+ stem cell recruitment to the liver. *J Clin Invest.* 2003;112(2):160-9.

20. Rosen CJ, Ackert-Bicknell C, Rodriguez JP, and Pino AM. Marrow fat and the bone microenvironment: developmental, functional, and pathological implications. *Crit Rev Eukaryot Gene Expr.* 2009;19(2):109-24.

21. Shemin D, and Rittenberg D. The life span of the human red blood cell. *J Biol Chem.* 1946;166(2):627-36.

22. Boas FE, Forman L, and Beutler E. Phosphatidylserine exposure and red cell viability in red cell aging and in hemolytic anemia. *Proc Natl Acad Sci U S A.* 1998;95(6):3077-81.

23. Ghashghaeinia M, Cluitmans JC, Akel A, Dreischer P, Toulany M, Koberle M, Skabytska Y, Saki M, Biedermann T, Duszenko M, et al. The impact of erythrocyte age on eryptosis. *Br J Haematol.* 2012;157(5):606-14.

24. Oldenborg PA, Zheleznyak A, Fang YF, Lagenaur CF, Gresham HD, and Lindberg FP. Role of CD47 as a marker of self on red blood cells. *Science.* 2000;288(5473):2051-4.

25. Fossati-Jimack L, Azeredo da Silveira S, Moll T, Kina T, Kuypers FA, Oldenborg PA, Reininger L, and Izui S. Selective increase of autoimmune epitope expression on aged erythrocytes in mice: implications in anti-erythrocyte autoimmune responses. *J Autoimmun.* 2002;18(1):17-25.

26. Burger P, Hilarius-Stokman P, de Korte D, van den Berg TK, and van Bruggen R. CD47 functions as a molecular switch for erythrocyte phagocytosis. *Blood.* 2012;119(23):5512-21.

27. Fraser ST, Isern J, and Baron MH. Maturation and enucleation of primitive erythroblasts during mouse embryogenesis is accompanied by changes in cell-surface antigen expression. *Blood.* 2007;109(1):343-52.

28. Kingsley PD, Malik J, Fantauzzo KA, and Palis J. Yolk sac-derived primitive erythroblasts enucleate during mammalian embryogenesis. *Blood.* 2004;104(1):19-25.

29. Beksac M, and Preffer F. Is it time to revisit our current hematopoietic progenitor cell quantification methods in the clinic? *Bone Marrow Transplant.* 2012;47(11):1391-6.

30. Seita J, and Weissman IL. Hematopoietic stem cell: self-renewal versus differentiation. *Wiley Interdiscip Rev Syst Biol Med.* 2010;2(6):640-53.

31. Clarke BJ, and Housman D. Characterization of an erythroid precursor cell of high proliferative capacity in normal human peripheral blood. *Proc Natl Acad Sci U S A.* 1977;74(3):1105-9.

32. Li J, Hale J, Bhagia P, Xue F, Chen L, Jaffray J, Yan H, Lane J, Gallagher PG, Mohandas N, et al. Isolation and transcriptome analyses of human erythroid progenitors: BFU-E and CFU-E. *Blood.* 2014;124(24):3636-45.

33. Nijhof W, and Wierenga PK. Isolation and characterization of the erythroid progenitor cell: CFU-E. *J Cell Biol.* 1983;96(2):386-92.

34. Chen K, Liu J, Heck S, Chasis JA, An X, and Mohandas N. Resolving the distinct stages in erythroid differentiation based on dynamic changes in membrane protein expression during erythropoiesis. *Proc Natl Acad Sci U S A.* 2009;106(41):17413-8.

35. Hu J, Liu J, Xue F, Halverson G, Reid M, Guo A, Chen L, Raza A, Galili N, Jaffray J, et al. Isolation and functional characterization of human erythroblasts at distinct stages: implications for understanding of normal and disordered erythropoiesis in vivo. *Blood.* 2013;121(16):3246-53.

36. Lee SH, Crocker PR, Westaby S, Key N, Mason DY, Gordon S, and Weatherall DJ. Isolation and immunocytochemical characterization of human bone marrow stromal macrophages in hemopoietic clusters. *J Exp Med.* 1988;168(3):1193-8.

37. Sadahira Y, and Mori M. Role of the macrophage in erythropoiesis. *Pathol Int.* 1999;49(10):841-8.

38. Chasis JA, and Mohandas N. Erythroblastic islands: niches for erythropoiesis. *Blood.* 2008;112(3):470-8.

39. Sadahira Y, Yoshino T, and Monobe Y. Very late activation antigen 4-vascular cell adhesion molecule 1 interaction is involved in the formation of erythroblastic islands. *J Exp Med.* 1995;181(1):411-5.

40. Soni S, Bala S, Gwynn B, Sahr KE, Peters LL, and Hanspal M. Absence of erythroblast macrophage protein (Emp) leads to failure of erythroblast nuclear extrusion. *J Biol Chem.* 2006;281(29):20181-9.

41. Hanspal M, Smockova Y, and Uong Q. Molecular identification and functional characterization of a novel protein that mediates the attachment of erythroblasts to macrophages. *Blood.* 1998;92(8):2940-50.

42. Manwani D, and Bieker JJ. The erythroblastic island. *Curr Top Dev Biol.* 2008;82(23-53.

43. Yoshida H, Kawane K, Koike M, Mori Y, Uchiyama Y, and Nagata S. Phosphatidylserine-dependent engulfment by macrophages of nuclei from erythroid precursor cells. *Nature.* 2005;437(7059):754-8.

44. De Maria R, Testa U, Luchetti L, Zeuner A, Stassi G, Pelosi E, Riccioni R, Felli N, Samoggia P, and Peschle C. Apoptotic role of Fas/Fas ligand system in the regulation of erythropoiesis. *Blood.* 1999;93(3):796-803.

45. De Maria R, Zeuner A, Eramo A, Domenichelli C, Bonci D, Grignani F, Srinivasula SM, Alnemri ES, Testa U, and Peschle C. Negative regulation of erythropoiesis by caspase-mediated cleavage of GATA-1. *Nature.* 1999;401(6752):489-93.

46. Zeuner A, Eramo A, Testa U, Felli N, Pelosi E, Mariani G, Srinivasula SM, Alnemri ES, Condorelli G, Peschle C, et al. Control of erythroid cell production via caspase-mediated cleavage of transcription factor SCL/Tal-1. *Cell Death Differ.* 2003;10(8):905-13.

47. Zermati Y, Garrido C, Amsellem S, Fishelson S, Bouscary D, Valensi F, Varet B, Solary E, and Hermine O. Caspase activation is required for terminal erythroid differentiation. *J Exp Med.* 2001;193(2):247-54.

48. Carlile GW, Smith DH, and Wiedmann M. Caspase-3 has a nonapoptotic function in erythroid maturation. *Blood.* 2004;103(11):4310-6.

49. Zhao B, Mei Y, Schipma MJ, Roth EW, Bleher R, Rappoport JZ, Wickrema A, Yang J, and Ji P. Nuclear Condensation during Mouse Erythropoiesis Requires Caspase-3-Mediated Nuclear Opening. *Dev Cell.* 2016;36(5):498-510.

50. Sandoval H, Thiagarajan P, Dasgupta SK, Schumacher A, Prchal JT, Chen M, and Wang J. Essential role for Nix in autophagic maturation of erythroid cells. *Nature.* 2008;454(7201):232-5.

51. Zhang J, Randall MS, Loyd MR, Dorsey FC, Kundu M, Cleveland JL, and Ney PA. Mitochondrial clearance is regulated by Atg7-dependent and -independent mechanisms during reticulocyte maturation. *Blood.* 2009;114(1):157-64.

52. Mortensen M, Ferguson DJ, Edelmann M, Kessler B, Morten KJ, Komatsu M, and Simon AK. Loss of autophagy in erythroid cells leads to defective removal of mitochondria and severe anemia in vivo. *Proc Natl Acad Sci U S A.* 2010;107(2):832-7.

53. Ohmizono Y, Sakabe H, Kimura T, Tanimukai S, Matsumura T, Miyazaki H, Lyman SD, and Sonoda Y. Thrombopoietin augments ex vivo expansion of human cord blood-derived hematopoietic progenitors in combination with stem cell factor and flt3 ligand. *Leukemia.* 1997;11(4):524-30.

54. McIver SC, Kang YA, DeVilbiss AW, O'Driscoll CA, Ouellette JN, Pope NJ, Camprecios G, Chang CJ, Yang D, Bouhassira EE, et al. The exosome complex establishes a barricade to erythroid maturation. *Blood.* 2014;124(14):2285-97.

55. McIver SC, Katsumura KR, Davids E, Liu P, Kang YA, Yang D, and Bresnick EH. Exosome complex orchestrates developmental signaling to balance proliferation and differentiation during erythropoiesis. *Elife.* 2016;5(

56. Sawada K, Krantz SB, Dai CH, Koury ST, Horn ST, Glick AD, and Civin CI. Purification of human blood burst-forming units-erythroid and demonstration of the evolution of erythropoietin receptors. *J Cell Physiol.* 1990;142(2):219-30.

57. Rankin EB, Wu C, Khatri R, Wilson TL, Andersen R, Araldi E, Rankin AL, Yuan J, Kuo CJ, Schipani E, et al. The HIF signaling pathway in osteoblasts directly modulates erythropoiesis through the production of EPO. *Cell.* 2012;149(1):63-74.

58. Camacho J, Arnalich F, Zamorano AF, and Vazquez JJ. Serum erythropoietin levels in the anaemia of chronic disorders. *J Intern Med.* 1991;229(1):49-54.

59. Choi D, Schroer SA, Lu SY, Wang L, Wu X, Liu Y, Zhang Y, Gaisano HY, Wagner KU, Wu H, et al. Erythropoietin protects against diabetes through direct effects on pancreatic beta cells. *J Exp Med.* 2010;207(13):2831-42.

60. Nairz M, Schroll A, Moschen AR, Sonnweber T, Theurl M, Theurl I, Taub N, Jamnig C, Neurauter D, Huber LA, et al. Erythropoietin contrastingly affects bacterial infection and experimental colitis by inhibiting nuclear factor-kappaB-inducible immune pathways. *Immunity.* 2011;34(1):61-74.

61. Spivak JL, Gascon P, and Ludwig H. Anemia management in oncology and hematology. *Oncologist.* 2009;14 Suppl 1(43-56.

62. Koury MJ, and Bondurant MC. Erythropoietin retards DNA breakdown and prevents programmed death in erythroid progenitor cells. *Science.* 1990;248(4953):378-81.

63. Grover A, Mancini E, Moore S, Mead AJ, Atkinson D, Rasmussen KD, O'Carroll D, Jacobsen SE, and Nerlov C. Erythropoietin guides multipotent hematopoietic progenitor cells toward an erythroid fate. *J Exp Med.* 2014;211(2):181-8.

64. Grebien F, Kerenyi MA, Kovacic B, Kolbe T, Becker V, Dolznig H, Pfeffer K, Klingmuller U, Muller M, Beug H, et al. Stat5 activation enables erythropoiesis in the absence of EpoR and Jak2. *Blood.* 2008;111(9):4511-22.

65. Wilson A, Murphy MJ, Oskarsson T, Kaloulis K, Bettess MD, Oser GM, Pasche AC, Knabenhans C, Macdonald HR, and Trumpp A. c-Myc controls the balance between hematopoietic stem cell self-renewal and differentiation. *Genes Dev.* 2004;18(22):2747-63.

66. Wagner KU, Claudio E, Rucker EB, 3rd, Riedlinger G, Broussard C, Schwartzberg PL, Siebenlist U, and Hennighausen L. Conditional deletion of the Bcl-x gene from erythroid cells results in hemolytic anemia and profound splenomegaly. *Development.* 2000;127(22):4949-58.

67. Kozar K, Ciemerych MA, Rebel VI, Shigematsu H, Zagozdzon A, Sicinska E, Geng Y, Yu Q, Bhattacharya S, Bronson RT, et al. Mouse development and cell proliferation in the absence of D-cyclins. *Cell.* 2004;118(4):477-91.

68. Wojchowski DM, Sathyanarayana P, and Dev A. Erythropoietin receptor response circuits. *Curr Opin Hematol.* 2010;17(3):169-76.

69. Klingmuller U, Wu H, Hsiao JG, Toker A, Duckworth BC, Cantley LC, and Lodish HF. Identification of a novel pathway important for proliferation and differentiation of primary erythroid progenitors. *Proc Natl Acad Sci U S A.* 1997;94(7):3016-21.

70. Chen C, and Sytkowski AJ. Erythropoietin activates two distinct signaling pathways required for the initiation and the elongation of c-myc. *J Biol Chem.* 2001;276(42):38518-26.

71. Dev A, Byrne SM, Verma R, Ashton-Rickardt PG, and Wojchowski DM. Erythropoietin-directed erythropoiesis depends on serpin inhibition of erythroblast lysosomal cathepsins. *J Exp Med.* 2013;210(2):225-32.

72. Li K, Menon MP, Karur VG, Hegde S, and Wojchowski DM. Attenuated signaling by a phosphotyrosine-null Epo receptor form in primary erythroid progenitor cells. *Blood.* 2003;102(9):3147-53.

73. Zang H, Sato K, Nakajima H, McKay C, Ney PA, and Ihle JN. The distal region and receptor tyrosines of the Epo receptor are non-essential for in vivo erythropoiesis. *EMBO J.* 2001;20(12):3156-66.

74. Sulahian R, Cleaver O, and Huang LJ. Ligand-induced EpoR internalization is mediated by JAK2 and p85 and is impaired by mutations responsible for primary familial and congenital polycythemia. *Blood.* 2009;113(21):5287-97.

75. Bulut GB, Sulahian R, Ma Y, Chi NW, and Huang LJ. Ubiquitination regulates the internalization, endolysosomal sorting, and signaling of the erythropoietin receptor. *J Biol Chem.* 2011;286(8):6449-57.

76. Singh S, Verma R, Pradeep A, Leu K, Mortensen RB, Young PR, Oyasu M, Schatz PJ, Green JM, and Wojchowski DM. Dynamic ligand modulation of EPO receptor pools,

and dysregulation by polycythemia-associated EPOR alleles. *PLoS One.* 2012;7(1):e29064.

77. Walrafen P, Verdier F, Kadri Z, Chretien S, Lacombe C, and Mayeux P. Both proteasomes and lysosomes degrade the activated erythropoietin receptor. *Blood.* 2005;105(2):600-8.

78. Yen CH, Yang YC, Ruscetti SK, Kirken RA, Dai RM, and Li CC. Involvement of the ubiquitin-proteasome pathway in the degradation of nontyrosine kinase-type cytokine receptors of IL-9, IL-2, and erythropoietin. *J Immunol.* 2000;165(11):6372-80.

79. Becker V, Schilling M, Bachmann J, Baumann U, Raue A, Maiwald T, Timmer J, and Klingmuller U. Covering a broad dynamic range: information processing at the erythropoietin receptor. *Science.* 2010;328(5984):1404-8.

80. Rivella S. Ineffective erythropoiesis and thalassemias. *Curr Opin Hematol.* 2009;16(3):187-94.

81. Wu CJ, Krishnamurti L, Kutok JL, Biernacki M, Rogers S, Zhang W, Antin JH, and Ritz J. Evidence for ineffective erythropoiesis in severe sickle cell disease. *Blood.* 2005;106(10):3639-45.

82. Hurrell R, and Egli I. Iron bioavailability and dietary reference values. *Am J Clin Nutr.* 2010;91(5):1461S-7S.

83. Finch CA, Deubelbeiss K, Cook JD, Eschbach JW, Harker LA, Funk DD, Marsaglia G, Hillman RS, Slichter S, Adamson JW, et al. Ferrokinetics in man. *Medicine (Baltimore).* 1970;49(1):17-53.

84. Green R, Charlton R, Seftel H, Bothwell T, Mayet F, Adams B, Finch C, and Layrisse M. Body iron excretion in man: a collaborative study. *Am J Med.* 1968;45(3):336-53.

85. Le Blanc S, Garrick MD, and Arredondo M. Heme carrier protein 1 transports heme and is involved in heme-Fe metabolism. *Am J Physiol Cell Physiol.* 2012;302(12):C1780-5.

86. Quigley JG, Yang Z, Worthington MT, Phillips JD, Sabo KM, Sabath DE, Berg CL, Sassa S, Wood BL, and Abkowitz JL. Identification of a human heme exporter that is essential for erythropoiesis. *Cell.* 2004;118(6):757-66.

87. West AR, and Oates PS. Mechanisms of heme iron absorption: current questions and controversies. *World J Gastroenterol.* 2008;14(26):4101-10.

88. Latunde-Dada GO, Van der Westhuizen J, Vulpe CD, Anderson GJ, Simpson RJ, and McKie AT. Molecular and functional roles of duodenal cytochrome B (Dcytb) in iron metabolism. *Blood Cells Mol Dis.* 2002;29(3):356-60.

89. Ohgami RS, Campagna DR, McDonald A, and Fleming MD. The Steap proteins are metalloreductases. *Blood.* 2006;108(4):1388-94.

90. Mancias JD, Pontano Vaites L, Nissim S, Biancur DE, Kim AJ, Wang X, Liu Y, Goessling W, Kimmelman AC, and Harper JW. Ferritinophagy via NCOA4 is required for erythropoiesis and is regulated by iron dependent HERC2-mediated proteolysis. *Elife.* 2015;4(

91. Mancias JD, Wang X, Gygi SP, Harper JW, and Kimmelman AC. Quantitative proteomics identifies NCOA4 as the cargo receptor mediating ferritinophagy. *Nature.* 2014;509(7498):105-9.

92. Abboud S, and Haile DJ. A novel mammalian iron-regulated protein involved in intracellular iron metabolism. *J Biol Chem.* 2000;275(26):19906-12.

93. Donovan A, Brownlie A, Zhou Y, Shepard J, Pratt SJ, Moynihan J, Paw BH, Drejer A, Barut B, Zapata A, et al. Positional cloning of zebrafish ferroportin1 identifies a conserved vertebrate iron exporter. *Nature.* 2000;403(6771):776-81.

94. Donovan A, Lima CA, Pinkus JL, Pinkus GS, Zon LI, Robine S, and Andrews NC. The iron exporter ferroportin/Slc40a1 is essential for iron homeostasis. *Cell Metab.* 2005;1(3):191-200.

95. DiRusso SC, Check IJ, and Hunter RL. Quantitation of apo-, mono-, and diferric transferrin by polyacrylamide gradient gel electrophoresis in patients with disorders of iron metabolism. *Blood.* 1985;66(6):1445-51.

96. Li H, and Ginzburg YZ. Crosstalk between Iron Metabolism and Erythropoiesis. *Adv Hematol.* 2010;2010(605435.

97. Mayle KM, Le AM, and Kamei DT. The intracellular trafficking pathway of transferrin. *Biochim Biophys Acta.* 2012;1820(3):264-81.

98. Grant BD, and Donaldson JG. Pathways and mechanisms of endocytic recycling. *Nat Rev Mol Cell Biol.* 2009;10(9):597-608.

99. Luck AN, and Mason AB. Transferrin-mediated cellular iron delivery. *Curr Top Membr.* 2012;69(3-35.

100. Andrews NC. Probing the iron pool. Focus on "Detection of intracellular iron by its regulatory effect". *Am J Physiol Cell Physiol.* 2004;287(6):C1537-8.

101. Dautry-Varsat A, Ciechanover A, and Lodish HF. pH and the recycling of transferrin during receptor-mediated endocytosis. *Proc Natl Acad Sci U S A.* 1983;80(8):2258-62.

102. Gunshin H, Fujiwara Y, Custodio AO, Direnzo C, Robine S, and Andrews NC. Slc11a2 is required for intestinal iron absorption and erythropoiesis but dispensable in placenta and liver. *J Clin Invest.* 2005;115(5):1258-66.

103. Horvathova M, Kapralova K, Zidova Z, Dolezal D, Pospisilova D, and Divoky V. Erythropoietin-driven signaling ameliorates the survival defect of DMT1-mutant erythroid progenitors and erythroblasts. *Haematologica.* 2012;97(10):1480-8.

104. Levy JE, Jin O, Fujiwara Y, Kuo F, and Andrews NC. Transferrin receptor is necessary for development of erythrocytes and the nervous system. *Nat Genet.* 1999;21(4):396-9.

105. Chen AC, Donovan A, Ned-Sykes R, and Andrews NC. Noncanonical role of transferrin receptor 1 is essential for intestinal homeostasis. *Proc Natl Acad Sci U S A.* 2015;112(37):11714-9.

106. Prasad AR, and Dailey HA. Effect of cellular location on the function of ferrochelatase. *J Biol Chem.* 1995;270(31):18198-200.

107. Das A, Nag S, Mason AB, and Barroso MM. Endosome-mitochondria interactions are modulated by iron release from transferrin. *J Cell Biol.* 2016;214(7):831-45.

108. Pantopoulos K. Function of the hemochromatosis protein HFE: Lessons from animal models. *World J Gastroenterol.* 2008;14(45):6893-901.

109. Silvestri L, Nai A, Pagani A, and Camaschella C. The extrahepatic role of TFR2 in iron homeostasis. *Front Pharmacol.* 2014;5(93.

110. Kawabata H, Germain RS, Vuong PT, Nakamaki T, Said JW, and Koeffler HP. Transferrin receptor 2-alpha supports cell growth both in iron-chelated cultured cells and in vivo. *J Biol Chem.* 2000;275(22):16618-25.

111. Kawabata H, Fleming RE, Gui D, Moon SY, Saitoh T, O'Kelly J, Umehara Y, Wano Y, Said JW, and Koeffler HP. Expression of hepcidin is down-regulated in TfR2 mutant mice manifesting a phenotype of hereditary hemochromatosis. *Blood.* 2005;105(1):376-81.

112. Nemeth E, Roetto A, Garozzo G, Ganz T, and Camaschella C. Hepcidin is decreased in TFR2 hemochromatosis. *Blood.* 2005;105(4):1803-6.

113. Gao J, Chen J, Kramer M, Tsukamoto H, Zhang AS, and Enns CA. Interaction of the hereditary hemochromatosis protein HFE with transferrin receptor 2 is required for transferrin-induced hepcidin expression. *Cell Metab.* 2009;9(3):217-27.

114. Schmidt PJ, Toran PT, Giannetti AM, Bjorkman PJ, and Andrews NC. The transferrin receptor modulates Hfe-dependent regulation of hepcidin expression. *Cell Metab.* 2008;7(3):205-14.

115. De Domenico I, Ward DM, and Kaplan J. Hepcidin regulation: ironing out the details. *J Clin Invest.* 2007;117(7):1755-8.

116. D'Alessio F, Hentze MW, and Muckenthaler MU. The hemochromatosis proteins HFE, TfR2, and HJV form a membrane-associated protein complex for hepcidin regulation. *J Hepatol.* 2012;57(5):1052-60.

117. Finberg KE, Whittlesey RL, and Andrews NC. Tmprss6 is a genetic modifier of the Hfe-hemochromatosis phenotype in mice. *Blood.* 2011;117(17):4590-9.

118. Silvestri L, Pagani A, Nai A, De Domenico I, Kaplan J, and Camaschella C. The serine protease matriptase-2 (TMPRSS6) inhibits hepcidin activation by cleaving membrane hemojuvelin. *Cell Metab.* 2008;8(6):502-11.

119. Camaschella C, and Roetto A. In: Pagon RA, Adam MP, Ardinger HH, Wallace SE, Amemiya A, Bean LJH, Bird TD, Ledbetter N, Mefford HC, Smith RJH, et al. eds. *GeneReviews(R)*. Seattle (WA); 1993.

120. Pietrangelo A. Hereditary hemochromatosis: pathogenesis, diagnosis, and treatment. *Gastroenterology.* 2010;139(2):393-408, e1-2.

121. Skaar EP. The battle for iron between bacterial pathogens and their vertebrate hosts. *PLoS Pathog.* 2010;6(8):e1000949.

122. Nemeth E, Rivera S, Gabayan V, Keller C, Taudorf S, Pedersen BK, and Ganz T. IL-6 mediates hypoferremia of inflammation by inducing the synthesis of the iron regulatory hormone hepcidin. *J Clin Invest.* 2004;113(9):1271-6.

123. Peyssonnaux C, Zinkernagel AS, Datta V, Lauth X, Johnson RS, and Nizet V. TLR4-dependent hepcidin expression by myeloid cells in response to bacterial pathogens. *Blood.* 2006;107(9):3727-32.

124. Armitage AE, Eddowes LA, Gileadi U, Cole S, Spottiswoode N, Selvakumar TA, Ho LP, Townsend AR, and Drakesmith H. Hepcidin regulation by innate immune and infectious stimuli. *Blood.* 2011;118(15):4129-39.

125. Wrighting DM, and Andrews NC. Interleukin-6 induces hepcidin expression through STAT3. *Blood.* 2006;108(9):3204-9.

126. Liu XB, Nguyen NB, Marquess KD, Yang F, and Haile DJ. Regulation of hepcidin and ferroportin expression by lipopolysaccharide in splenic macrophages. *Blood Cells Mol Dis.* 2005;35(1):47-56.

127. Ganz T, and Nemeth E. Hepcidin and iron homeostasis. *Biochim Biophys Acta.* 2012;1823(9):1434-43.

128. Elliott J, Mishler D, and Agarwal R. Hyporesponsiveness to erythropoietin: causes and management. *Adv Chronic Kidney Dis.* 2009;16(2):94-100.

129. Zaritsky J, Young B, Wang HJ, Westerman M, Olbina G, Nemeth E, Ganz T, Rivera S, Nissenson AR, and Salusky IB. Hepcidin--a potential novel biomarker for iron status in chronic kidney disease. *Clin J Am Soc Nephrol.* 2009;4(6):1051-6.

130. Ganz T, Olbina G, Girelli D, Nemeth E, and Westerman M. Immunoassay for human serum hepcidin. *Blood.* 2008;112(10):4292-7.

131. De Domenico I, Ward DM, Langelier C, Vaughn MB, Nemeth E, Sundquist WI, Ganz T, Musci G, and Kaplan J. The molecular mechanism of hepcidin-mediated ferroportin down-regulation. *Mol Biol Cell.* 2007;18(7):2569-78.

132. Nemeth E, Tuttle MS, Powelson J, Vaughn MB, Donovan A, Ward DM, Ganz T, and Kaplan J. Hepcidin regulates cellular iron efflux by binding to ferroportin and inducing its internalization. *Science.* 2004;306(5704):2090-3.

133. Anderson SA, Nizzi CP, Chang YI, Deck KM, Schmidt PJ, Galy B, Damnernsawad A, Broman AT, Kendziorski C, Hentze MW, et al. The IRP1-HIF-2alpha axis coordinates iron and oxygen sensing with erythropoiesis and iron absorption. *Cell Metab.* 2013;17(2):282-90.

134. Mastrogiannaki M, Matak P, Keith B, Simon MC, Vaulont S, and Peyssonnaux C. HIF-2alpha, but not HIF-1alpha, promotes iron absorption in mice. *J Clin Invest.* 2009;119(5):1159-66.

135. Shah YM, Matsubara T, Ito S, Yim SH, and Gonzalez FJ. Intestinal hypoxia-inducible transcription factors are essential for iron absorption following iron deficiency. *Cell Metab.* 2009;9(2):152-64.

136. Brasse-Lagnel C, Karim Z, Letteron P, Bekri S, Bado A, and Beaumont C. Intestinal DMT1 cotransporter is down-regulated by hepcidin via proteasome internalization and degradation. *Gastroenterology.* 2011;140(4):1261-71 e1.

137. Sham RL, Phatak PD, Nemeth E, and Ganz T. Hereditary hemochromatosis due to resistance to hepcidin: high hepcidin concentrations in a family with C326S ferroportin mutation. *Blood.* 2009;114(2):493-4.

138. Tanno T, and Miller JL. Iron Loading and Overloading due to Ineffective Erythropoiesis. *Adv Hematol.* 2010;2010(358283.

139. Kautz L, Jung G, Valore EV, Rivella S, Nemeth E, and Ganz T. Identification of erythroferrone as an erythroid regulator of iron metabolism. *Nat Genet.* 2014;46(7):678-84.

140. Kautz L, Jung G, Du X, Gabayan V, Chapman J, Nasoff M, Nemeth E, and Ganz T. Erythroferrone contributes to hepcidin suppression and iron overload in a mouse model of beta-thalassemia. *Blood.* 2015;126(17):2031-7.

141. Kautz L, Jung G, Nemeth E, and Ganz T. Erythroferrone contributes to recovery from anemia of inflammation. *Blood.* 2014;124(16):2569-74.

142. Hentze MW, Muckenthaler MU, and Andrews NC. Balancing acts: molecular control of mammalian iron metabolism. *Cell.* 2004;117(3):285-97.

143. Bullock GC, Delehanty LL, Talbot AL, Gonias SL, Tong WH, Rouault TA, Dewar B, Macdonald JM, Chruma JJ, and Goldfarb AN. Iron control of erythroid development by a novel aconitase-associated regulatory pathway. *Blood.* 2010;116(1):97-108.

144. Finch CA. Erythropoiesis, erythropoietin, and iron. *Blood.* 1982;60(6):1241-6.

145. Kimura H, Finch CA, and Adamson JW. Hematopoiesis in the rat: quantitation of hematopoietic progenitors and the response to iron deficiency anemia. *J Cell Physiol.* 1986;126(2):298-306.

146. Nai A, Lidonnici MR, Rausa M, Mandelli G, Pagani A, Silvestri L, Ferrari G, and Camaschella C. The second transferrin receptor regulates red blood cell production in mice. *Blood.* 2015;125(7):1170-9.

147. Richardson CL, Delehanty LL, Bullock GC, Rival CM, Tung KS, Kimpel DL, Gardenghi S, Rivella S, and Goldfarb AN. Isocitrate ameliorates anemia by suppressing the erythroid iron restriction response. *J Clin Invest.* 2013;123(8):3614-23.

148. Knight ZA, Schmidt SF, Birsoy K, Tan K, and Friedman JM. A critical role for mTORC1 in erythropoiesis and anemia. *Elife.* 2014;3(e01913.

149. Guo B, Yu Y, and Leibold EA. Iron regulates cytoplasmic levels of a novel iron-responsive element-binding protein without aconitase activity. *J Biol Chem.* 1994;269(39):24252-60.

150. Tong WH, and Rouault TA. Metabolic regulation of citrate and iron by aconitases: role of iron-sulfur cluster biogenesis. *Biometals.* 2007;20(3-4):549-64.

151. Iwai K, Klausner RD, and Rouault TA. Requirements for iron-regulated degradation of the RNA binding protein, iron regulatory protein 2. *EMBO J.* 1995;14(21):5350-7.

152. Wang J, Chen G, Muckenthaler M, Galy B, Hentze MW, and Pantopoulos K. Iron-mediated degradation of IRP2, an unexpected pathway involving a 2-oxoglutarate-dependent oxygenase activity. *Mol Cell Biol.* 2004;24(3):954-65.

153. Guo B, Phillips JD, Yu Y, and Leibold EA. Iron regulates the intracellular degradation of iron regulatory protein 2 by the proteasome. *J Biol Chem.* 1995;270(37):21645-51.

154. Iwai K, Drake SK, Wehr NB, Weissman AM, LaVaute T, Minato N, Klausner RD, Levine RL, and Rouault TA. Iron-dependent oxidation, ubiquitination, and degradation of iron regulatory protein 2: implications for degradation of oxidized proteins. *Proc Natl Acad Sci U S A.* 1998;95(9):4924-8.

155. Muckenthaler MU, Galy B, and Hentze MW. Systemic iron homeostasis and the iron-responsive element/iron-regulatory protein (IRE/IRP) regulatory network. *Annu Rev Nutr.* 2008;28(197-213.

156. Anderson CP, Shen M, Eisenstein RS, and Leibold EA. Mammalian iron metabolism and its control by iron regulatory proteins. *Biochim Biophys Acta.* 2012;1823(9):1468-83.

157. Henderson BR, Menotti E, and Kuhn LC. Iron regulatory proteins 1 and 2 bind distinct sets of RNA target sequences. *J Biol Chem.* 1996;271(9):4900-8.

158. Cairo G, and Recalcati S. Iron-regulatory proteins: molecular biology and pathophysiological implications. *Expert Rev Mol Med.* 2007;9(33):1-13.

159. Zhang DL, Ghosh MC, and Rouault TA. The physiological functions of iron regulatory proteins in iron homeostasis - an update. *Front Pharmacol.* 2014;5(124.

160. Meyron-Holtz EG, Ghosh MC, Iwai K, LaVaute T, Brazzolotto X, Berger UV, Land W, Ollivierre-Wilson H, Grinberg A, Love P, et al. Genetic ablations of iron regulatory proteins 1 and 2 reveal why iron regulatory protein 2 dominates iron homeostasis. *EMBO J.* 2004;23(2):386-95.

161. Smith SR, Ghosh MC, Ollivierre-Wilson H, Hang Tong W, and Rouault TA. Complete loss of iron regulatory proteins 1 and 2 prevents viability of murine zygotes beyond the blastocyst stage of embryonic development. *Blood Cells Mol Dis.* 2006;36(2):283-7.

162. Wilkinson N, and Pantopoulos K. IRP1 regulates erythropoiesis and systemic iron homeostasis by controlling HIF2alpha mRNA translation. *Blood.* 2013;122(9):1658-68.

163. Nijhof W, Wierenga PK, Staal GE, and Jansen G. Changes in activities and isozyme patterns of glycolytic enzymes during erythroid differentiation in vitro. *Blood.* 1984;64(3):607-13.

164. Oburoglu L, Tardito S, Fritz V, de Barros SC, Merida P, Craveiro M, Mamede J, Cretenet G, Mongellaz C, An X, et al. Glucose and glutamine metabolism regulate human hematopoietic stem cell lineage specification. *Cell Stem Cell.* 2014;15(2):169-84.

165. Talbot AL, Bullock GC, Delehanty LL, Sattler M, Zhao ZJ, and Goldfarb AN. Aconitase regulation of erythropoiesis correlates with a novel licensing function in erythropoietin-induced ERK signaling. *PLoS One.* 2011;6(8):e23850.

166. Kim A, Fung E, Parikh SG, Gabayan V, Nemeth E, and Ganz T. Isocitrate treatment of acute anemia of inflammation in a mouse model. *Blood Cells Mol Dis.* 2016;56(1):31-6.

167. Forejtnikova H, Vieillevoye M, Zermati Y, Lambert M, Pellegrino RM, Guihard S, Gaudry M, Camaschella C, Lacombe C, Roetto A, et al. Transferrin receptor 2 is a component of the erythropoietin receptor complex and is required for efficient erythropoiesis. *Blood.* 2010;116(24):5357-67.

168. Chen J, Wang J, Meyers KR, and Enns CA. Transferrin-directed internalization and cycling of transferrin receptor 2. *Traffic.* 2009;10(10):1488-501.

169. Johnson MB, Chen J, Murchison N, Green FA, and Enns CA. Transferrin receptor 2: evidence for ligand-induced stabilization and redirection to a recycling pathway. *Mol Biol Cell.* 2007;18(3):743-54.

170. Johnson MB, and Enns CA. Diferric transferrin regulates transferrin receptor 2 protein stability. *Blood.* 2004;104(13):4287-93.

171. Pagani A, Vieillevoye M, Nai A, Rausa M, Ladli M, Lacombe C, Mayeux P, Verdier F, Camaschella C, and Silvestri L. Regulation of cell surface transferrin receptor-2 by iron-dependent cleavage and release of a soluble form. *Haematologica.* 2015;100(4):458-65.

172. Ding K, Shameer K, Jouni H, Masys DR, Jarvik GP, Kho AN, Ritchie MD, McCarty CA, Chute CG, Manolio TA, et al. Genetic Loci implicated in erythroid differentiation and cell cycle regulation are associated with red blood cell traits. *Mayo Clin Proc.* 2012;87(5):461-74.

173. Ganesh SK, Zakai NA, van Rooij FJ, Soranzo N, Smith AV, Nalls MA, Chen MH, Kottgen A, Glazer NL, Dehghan A, et al. Multiple loci influence erythrocyte phenotypes in the CHARGE Consortium. *Nat Genet.* 2009;41(11):1191-8.

174. Bilder D, and Perrimon N. Localization of apical epithelial determinants by the basolateral PDZ protein Scribble. *Nature.* 2000;403(6770):676-80.

175. Dow LE, Brumby AM, Muratore R, Coombe ML, Sedelies KA, Trapani JA, Russell SM, Richardson HE, and Humbert PO. hScrib is a functional homologue of the Drosophila tumour suppressor Scribble. *Oncogene.* 2003;22(58):9225-30.

176. Brumby AM, and Richardson HE. scribble mutants cooperate with oncogenic Ras or Notch to cause neoplastic overgrowth in Drosophila. *EMBO J.* 2003;22(21):5769-79.

177. Vaira V, Faversani A, Dohi T, Maggioni M, Nosotti M, Tosi D, Altieri DC, and Bosari S. Aberrant overexpression of the cell polarity module scribble in human cancer. *Am J Pathol.* 2011;178(6):2478-83.

178. Elsum IA, Yates LL, Pearson HB, Phesse TJ, Long F, O'Donoghue R, Ernst M, Cullinane C, and Humbert PO. Scrib heterozygosity predisposes to lung cancer and cooperates with KRas hyperactivation to accelerate lung cancer progression in vivo. *Oncogene.* 2014;33(48):5523-33.

179. Pearson HB, Perez-Mancera PA, Dow LE, Ryan A, Tennstedt P, Bogani D, Elsum I, Greenfield A, Tuveson DA, Simon R, et al. SCRIB expression is deregulated in human prostate cancer, and its deficiency in mice promotes prostate neoplasia. *J Clin Invest.* 2011;121(11):4257-67.

180. Godde NJ, Sheridan JM, Smith LK, Pearson HB, Britt KL, Galea RC, Yates LL, Visvader JE, and Humbert PO. Scribble modulates the MAPK/Fra1 pathway to disrupt luminal

and ductal integrity and suppress tumour formation in the mammary gland. *PLoS Genet.* 2014;10(5):e1004323.

181. Cordero JB, Macagno JP, Stefanatos RK, Strathdee KE, Cagan RL, and Vidal M. Oncogenic Ras diverts a host TNF tumor suppressor activity into tumor promoter. *Dev Cell.* 2010;18(6):999-1011.

182. Leong GR, Goulding KR, Amin N, Richardson HE, and Brumby AM. Scribble mutants promote aPKC and JNK-dependent epithelial neoplasia independently of Crumbs. *BMC Biol.* 2009;7(62.

183. Wu M, Pastor-Pareja JC, and Xu T. Interaction between Ras(V12) and scribbled clones induces tumour growth and invasion. *Nature.* 2010;463(7280):545-8.

184. Li X, Yang H, Liu J, Schmidt MD, and Gao T. Scribble-mediated membrane targeting of PHLPP1 is required for its negative regulation of Akt. *EMBO Rep.* 2011;12(8):818-24.

185. Pocha SM, Wassmer T, Niehage C, Hoflack B, and Knust E. Retromer controls epithelial cell polarity by trafficking the apical determinant Crumbs. *Curr Biol.* 2011;21(13):1111-7.

186. de Vreede G, Schoenfeld JD, Windler SL, Morrison H, Lu H, and Bilder D. The Scribble module regulates retromer-dependent endocytic trafficking during epithelial polarization. *Development.* 2014;141(14):2796-802.

187. Qin Y, Capaldo C, Gumbiner BM, and Macara IG. The mammalian Scribble polarity protein regulates epithelial cell adhesion and migration through E-cadherin. *J Cell Biol.* 2005;171(6):1061-71.

188. Elsum IA, Martin C, and Humbert PO. Scribble regulates an EMT polarity pathway through modulation of MAPK-ERK signaling to mediate junction formation. *J Cell Sci.* 2013;126(Pt 17):3990-9.

189. Lamouille S, Xu J, and Derynck R. Molecular mechanisms of epithelial-mesenchymal transition. *Nat Rev Mol Cell Biol.* 2014;15(3):178-96.

190. Ludford-Menting MJ, Oliaro J, Sacirbegovic F, Cheah ET, Pedersen N, Thomas SJ, Pasam A, Iazzolino R, Dow LE, Waterhouse NJ, et al. A network of PDZ-containing proteins regulates T cell polarity and morphology during migration and immunological synapse formation. *Immunity.* 2005;22(6):737-48.

191. Sun Y, Aiga M, Yoshida E, Humbert PO, and Bamji SX. Scribble interacts with beta-catenin to localize synaptic vesicles to synapses. *Mol Biol Cell.* 2009;20(14):3390-400.

192. Eastburn DJ, Zegers MM, and Mostov KE. Scrib regulates HGF-mediated epithelial morphogenesis and is stabilized by Sgt1-HSP90. *J Cell Sci.* 2012;125(Pt 17):4147-57.

193. Lahuna O, Quellari M, Achard C, Nola S, Meduri G, Navarro C, Vitale N, Borg JP, and Misrahi M. Thyrotropin receptor trafficking relies on the hScrib-betaPIX-GIT1-ARF6 pathway. *EMBO J.* 2005;24(7):1364-74.

194. Piguel NH, Fievre S, Blanc JM, Carta M, Moreau MM, Moutin E, Pinheiro VL, Medina C, Ezan J, Lasvaux L, et al. Scribble1/AP2 complex coordinates NMDA receptor endocytic recycling. *Cell Rep.* 2014;9(2):712-27.

195. Koury MJ, and Ponka P. New insights into erythropoiesis: The roles of folate, vitamin B-12, and iron. *Annu Rev Nutr.* 2004;24(105-31.

196. Camaschella C. Iron-Deficiency Anemia. *N Engl J Med.* 2015;373(5):485-6.

197. Drueke T. Hyporesponsiveness to recombinant human erythropoietin. *Nephrol Dial Transplant.* 2001;16 Suppl 7(25-8.

198. Rosati A, Tetta C, Merello JI, Palomares I, Perez-Garcia R, Maduell F, Canaud B, and Aljama Garcia P. Cumulative iron dose and resistance to erythropoietin. *J Nephrol.* 2015;28(5):603-13.

199. Sunder-Plassmann G, and Horl WH. Importance of iron supply for erythropoietin therapy. *Nephrol Dial Transplant.* 1995;10(11):2070-6.

200. Sunder-Plassmann G, and Horl WH. Erythropoietin and iron. *Clin Nephrol.* 1997;47(3):141-57.

201. Gozzelino R, and Arosio P. The importance of iron in pathophysiologic conditions. *Front Pharmacol.* 2015;6(26.

202. Goswami T, and Andrews NC. Hereditary hemochromatosis protein, HFE, interaction with transferrin receptor 2 suggests a molecular mechanism for mammalian iron sensing. *J Biol Chem.* 2006;281(39):28494-8.

203. Herbison CE, Thorstensen K, Chua AC, Graham RM, Leedman P, Olynyk JK, and Trinder D. The role of transferrin receptor 1 and 2 in transferrin-bound iron uptake in human hepatoma cells. *Am J Physiol Cell Physiol.* 2009;297(6):C1567-75.

204. Gao J, Chen J, De Domenico I, Koeller DM, Harding CO, Fleming RE, Koeberl DD, and Enns CA. Hepatocyte-targeted HFE and TFR2 control hepcidin expression in mice. *Blood.* 2010;115(16):3374-81.

205. Auer PL, Teumer A, Schick U, O'Shaughnessy A, Lo KS, Chami N, Carlson C, de Denus S, Dube MP, Haessler J, et al. Rare and low-frequency coding variants in CXCR2 and other genes are associated with hematological traits. *Nat Genet.* 2014;46(6):629-34.

206. Soranzo N, Spector TD, Mangino M, Kuhnel B, Rendon A, Teumer A, Willenborg C, Wright B, Chen L, Li M, et al. A genome-wide meta-analysis identifies 22 loci associated with eight hematological parameters in the HaemGen consortium. *Nat Genet.* 2009;41(11):1182-90.

207. Rishi G, Secondes ES, Wallace DF, and Subramaniam VN. Hematopoietic deletion of transferrin receptor 2 in mice leads to a block in erythroid differentiation during iron-deficient anemia. *Am J Hematol.* 2016;91(8):812-8.

208. Rozman M, Masat T, Feliu E, and Rozman C. Dyserythropoiesis in iron-deficiency anemia: ultrastructural reassessment. *Am J Hematol.* 1992;41(3):147-50.

209. Menon MP, Fang J, and Wojchowski DM. Core erythropoietin receptor signals for late erythroblast development. *Blood.* 2006;107(7):2662-72.

210. Bullock GC, Delehanty LL, Talbot A-L, Gonias SL, Tong W-H, Rouault TA, Dewar B, Macdonald JM, Chruma JJ, and Goldfarb AN. Iron control of erythroid development by a novel aconitase-associated regulatory pathway. *Blood.* 2010;116(1):97-108.

211. Michaelis UR, Chavakis E, Kruse C, Jungblut B, Kaluza D, Wandzioch K, Manavski Y, Heide H, Santoni MJ, Potente M, et al. The polarity protein Scrib is essential for directed endothelial cell migration. *Circ Res.* 2013;112(6):924-34.

212. Nagasaka K, Pim D, Massimi P, Thomas M, Tomaic V, Subbaiah VK, Kranjec C, Nakagawa S, Yano T, Taketani Y, et al. The cell polarity regulator hScrib controls ERK activation through a KIM site-dependent interaction. *Oncogene.* 2010;29(38):5311-21.

213. Nagasaka K, Seiki T, Yamashita A, Massimi P, Subbaiah VK, Thomas M, Kranjec C, Kawana K, Nakagawa S, Yano T, et al. A novel interaction between hScrib and

PP1gamma downregulates ERK signaling and suppresses oncogene-induced cell transformation. *PLoS One.* 2013;8(1):e53752.

214. Igaki T, Pastor-Pareja JC, Aonuma H, Miura M, and Xu T. Intrinsic tumor suppression and epithelial maintenance by endocytic activation of Eiger/TNF signaling in Drosophila. *Dev Cell.* 2009;16(3):458-65.

215. Kurita R, Suda N, Sudo K, Miharada K, Hiroyama T, Miyoshi H, Tani K, and Nakamura Y. Establishment of immortalized human erythroid progenitor cell lines able to produce enucleated red blood cells. *PLoS One.* 2013;8(3):e59890.

216. Harrington AM, Ward PC, and Kroft SH. Iron deficiency anemia, beta-thalassemia minor, and anemia of chronic disease: a morphologic reappraisal. *Am J Clin Pathol.* 2008;129(3):466-71.

217. Zhao B, Mei Y, Yang J, and Ji P. Erythropoietin-regulated oxidative stress negatively affects enucleation during terminal erythropoiesis. *Exp Hematol.* 2016;44(975-81.

218. Ghaffari S, Kitidis C, Zhao W, Marinkovic D, Fleming MD, Luo B, Marszalek J, and Lodish HF. AKT induces erythroid-cell maturation of JAK2-deficient fetal liver progenitor cells and is required for Epo regulation of erythroid-cell differentiation. *Blood.* 2006;107(5):1888-91.

219. Feigin ME, Akshinthala SD, Araki K, Rosenberg AZ, Muthuswamy LB, Martin B, Lehmann BD, Berman HK, Pietenpol JA, Cardiff RD, et al. Mislocalization of the cell polarity protein Scribble promotes mammary tumorigenesis and is associated with basal breast cancer. *Cancer Res.* 2014;74(11):3180-94.

220. Chen B, Zheng B, DeRan M, Jarugumilli GK, Fu J, Brooks YS, and Wu X. ZDHHC7-mediated S-palmitoylation of Scribble regulates cell polarity. *Nature Chem Biol.* 2016;12(9):686-93.

221. Lohia M, Qin Y, and Macara IG. The Scribble polarity protein stabilizes E-cadherin/p120-catenin binding and blocks retrieval of E-cadherin to the Golgi. *PLoS One.* 2012;7(11):e51130.

222. Hilton DJ, Watowich SS, Murray PJ, and Lodish HF. Increased cell surface expression and enhanced folding in the endoplasmic reticulum of a mutant erythropoietin receptor. *Proc Natl Acad Sci U S A.* 1995;92(190-4.

223. Roche JP, Packard MC, Moeckel-Cole S, and Budnik V. Regulation of synaptic plasticity and synaptic vesicle dynamics by the PDZ protein Scribble. *J Neurosci.* 2002;22(15):6471-9.

224. Ganz T, and Nemeth E. Iron metabolism: interactions with normal and disordered erythropoiesis. *Cold Spring Harb Perspect Med.* 2012;2(5):a011668.

225. Anderson GJ, and McLaren G. *Iron physiology and pathophysiology in humans.* New York: Humana; 2009.

226. Richardson DR, Lane DJ, Becker EM, Huang ML, Whitnall M, Suryo Rahmanto Y, Sheftel AD, and Ponka P. Mitochondrial iron trafficking and the integration of iron metabolism between the mitochondrion and cytosol. *Proc Natl Acad Sci U S A.* 2010;107(24):10775-82.

227. Sheftel AD, Zhang AS, Brown C, Shirihai OS, and Ponka P. Direct interorganellar transfer of iron from endosome to mitochondrion. *Blood.* 2007;110(1):125-32.

228. Zhang AS, Sheftel AD, and Ponka P. Intracellular kinetics of iron in reticulocytes: evidence for endosome involvement in iron targeting to mitochondria. *Blood.* 2005;105(1):368-75.

229. Kawabata H, Yang R, Hirama T, Vuong PT, Kawano S, Gombart AF, and Koeffler HP. Molecular cloning of transferrin receptor 2. A new member of the transferrin receptor-like family. *J Biol Chem.* 1999;274(30):20826-32.

230. Robb AD, Ericsson M, and Wessling-Resnick M. Transferrin receptor 2 mediates a biphasic pattern of transferrin uptake associated with ligand delivery to multivesicular bodies. *Am J Physiol Cell Physiol.* 2004;287(6):C1769-75.

231. Wallace DF, Secondes ES, Rishi G, Ostini L, McDonald CJ, Lane SW, Vu T, Hooper JD, Velasco G, Ramsay AJ, et al. A critical role for murine transferrin receptor 2 in erythropoiesis during iron restriction. *Br J Haematol.* 2015;168(6):891-901.

232. Mastroberardino PG, Hoffman EK, Horowitz MP, Betarbet R, Taylor G, Cheng D, Na HM, Gutekunst CA, Gearing M, Trojanowski JQ, et al. A novel transferrin/TfR2-mediated mitochondrial iron transport system is disrupted in Parkinson's disease. *Neurobiol Dis.* 2009;34(3):417-31.

233. Dong XP, Cheng X, Mills E, Delling M, Wang F, Kurz T, and Xu H. The type IV mucolipidosis-associated protein TRPML1 is an endolysosomal iron release channel. *Nature.* 2008;455(7215):992-6.

234. Csordas G, Renken C, Varnai P, Walter L, Weaver D, Buttle KF, Balla T, Mannella CA, and Hajnoczky G. Structural and functional features and significance of the physical linkage between ER and mitochondria. *J Cell Biol.* 2006;174(7):915-21.

235. Csordas G, Varnai P, Golenar T, Roy S, Purkins G, Schneider TG, Balla T, and Hajnoczky G. Imaging interorganelle contacts and local calcium dynamics at the ER-mitochondrial interface. *Mol Cell.* 2010;39(1):121-32.

236. Lam AK, and Galione A. The endoplasmic reticulum and junctional membrane communication during calcium signaling. *Biochim Biophys Acta.* 2013;1833(11):2542-59.

237. Rizzuto R, Pinton P, Carrington W, Fay FS, Fogarty KE, Lifshitz LM, Tuft RA, and Pozzan T. Close contacts with the endoplasmic reticulum as determinants of mitochondrial Ca2+ responses. *Science.* 1998;280(5370):1763-6.

238. Cohen Y, Klug YA, Dimitrov L, Erez Z, Chuartzman SG, Elinger D, Yofe I, Soliman K, Gartner J, Thoms S, et al. Peroxisomes are juxtaposed to strategic sites on mitochondria. *Mol Biosyst.* 2014;10(7):1742-8.

239. Elbaz-Alon Y, Rosenfeld-Gur E, Shinder V, Futerman AH, Geiger T, and Schuldiner M. A dynamic interface between vacuoles and mitochondria in yeast. *Dev Cell.* 2014;30(1):95-102.

240. Honscher C, Mari M, Auffarth K, Bohnert M, Griffith J, Geerts W, van der Laan M, Cabrera M, Reggiori F, and Ungermann C. Cellular metabolism regulates contact sites between vacuoles and mitochondria. *Dev Cell.* 2014;30(1):86-94.

241. Traub LM. The reverse logic of multivesicular endosomes. *EMBO Rep.* 2010;11(2):79-81.

242. West AP, Jr., Bennett MJ, Sellers VM, Andrews NC, Enns CA, and Bjorkman PJ. Comparison of the interactions of transferrin receptor and transferrin receptor 2

with transferrin and the hereditary hemochromatosis protein HFE. *J Biol Chem.* 2000;275(49):38135-8.

243. Davuluri G, Song P, Liu Z, Wald D, Sakaguchi TF, Green MR, and Devireddy L. Inactivation of 3-hydroxybutyrate dehydrogenase 2 delays zebrafish erythroid maturation by conferring premature mitophagy. *Proc Natl Acad Sci U S A.* 2016;113(11):E1460-9.

244. Knight SA, Sepuri NB, Pain D, and Dancis A. Mt-Hsp70 homolog, Ssc2p, required for maturation of yeast frataxin and mitochondrial iron homeostasis. *J Biol Chem.* 1998;273(29):18389-93.

245. Martelli A, and Puccio H. Dysregulation of cellular iron metabolism in Friedreich ataxia: from primary iron-sulfur cluster deficit to mitochondrial iron accumulation. *Front Pharmacol.* 2014;5(130.

246. Miranda CJ, Makui H, Soares RJ, Bilodeau M, Mui J, Vali H, Bertrand R, Andrews NC, and Santos MM. Hfe deficiency increases susceptibility to cardiotoxicity and exacerbates changes in iron metabolism induced by doxorubicin. *Blood.* 2003;102(7):2574-80.

247. Pereira SM, Williams SR, Murray P, and Taylor A. MS-1 magA: Revisiting Its Efficacy as a Reporter Gene for MRI. *Mol Imaging.* 2016;15(

248. Rouault TA, and Tong WH. Iron-sulphur cluster biogenesis and mitochondrial iron homeostasis. *Nat Rev Mol Cell Biol.* 2005;6(4):345-51.

249. Santambrogio P, Erba BG, Campanella A, Cozzi A, Causarano V, Cremonesi L, Galli A, Della Porta MG, Invernizzi R, and Levi S. Over-expression of mitochondrial ferritin

affects the JAK2/STAT5 pathway in K562 cells and causes mitochondrial iron accumulation. *Haematologica.* 2011;96(10):1424-32.

250. Bessis MC, and Breton-Gorius J. Iron metabolism in the bone marrow as seen by electron microscopy: a critical review. *Blood.* 1962;19(635-63.

251. Bagger FO, Sasivarevic D, Sohi SH, Laursen LG, Pundhir S, Sonderby CK, Winther O, Rapin N, and Porse BT. BloodSpot: a database of gene expression profiles and transcriptional programs for healthy and malignant haematopoiesis. *Nucleic Acids Res.* 2016;44(D1):D917-24.

252. de Brito OM, and Scorrano L. Mitofusin 2 tethers endoplasmic reticulum to mitochondria. *Nature.* 2008;456(7222):605-10.

253. Mangieri LR, Mader BJ, Thomas CE, Taylor CA, Luker AM, Tse TE, Huisingh C, and Shacka JJ. ATP6V0C knockdown in neuroblastoma cells alters autophagy-lysosome pathway function and metabolism of proteins that accumulate in neurodegenerative disease. *PLoS One.* 2014;9(4):e93257.

254. Zhao T, Huang X, Han L, Wang X, Cheng H, Zhao Y, Chen Q, Chen J, Cheng H, Xiao R, et al. Central role of mitofusin 2 in autophagosome-lysosome fusion in cardiomyocytes. *J Biol Chem.* 2012;287(28):23615-25.

255. Pantopoulos K, Porwal SK, Tartakoff A, and Devireddy L. Mechanisms of mammalian iron homeostasis. *Biochemistry.* 2012;51(29):5705-24.

256. Kawabata H, Tong X, Kawanami T, Wano Y, Hirose Y, Sugai S, and Koeffler HP. Analyses for binding of the transferrin family of proteins to the transferrin receptor 2. *Br J Haematol.* 2004;127(4):464-73.

257. Chen H, Detmer SA, Ewald AJ, Griffin EE, Fraser SE, and Chan DC. Mitofusins Mfn1 and Mfn2 coordinately regulate mitochondrial fusion and are essential for embryonic development. *J Cell Biol.* 2003;160(2):189-200.

258. Leal NS, Schreiner B, Pinho CM, Filadi R, Wiehager B, Karlstrom H, Pizzo P, and Ankarcrona M. Mitofusin-2 knockdown increases ER-mitochondria contact and decreases amyloid beta-peptide production. *J Cell Mol Med.* 2016;20(9):1686-95.

259. Nikpour M, Pellagatti A, Liu A, Karimi M, Malcovati L, Gogvadze V, Forsblom AM, Wainscoat JS, Cazzola M, Zhivotovsky B, et al. Gene expression profiling of erythroblasts from refractory anaemia with ring sideroblasts (RARS) and effects of G-CSF. *Br J Haematol.* 2010;149(6):844-54.

260. Hailey DW, Rambold AS, Satpute-Krishnan P, Mitra K, Sougrat R, Kim PK, and Lippincott-Schwartz J. Mitochondria supply membranes for autophagosome biogenesis during starvation. *Cell.* 2010;141(4):656-67.

261. Ferreira C, Santambrogio P, Martin ME, Andrieu V, Feldmann G, Henin D, and Beaumont C. H ferritin knockout mice: a model of hyperferritinemia in the absence of iron overload. *Blood.* 2001;98(3):525-32.

262. Nie G, Chen G, Sheftel AD, Pantopoulos K, and Ponka P. In vivo tumor growth is inhibited by cytosolic iron deprivation caused by the expression of mitochondrial ferritin. *Blood.* 2006;108(7):2428-34.

263. Sassa S. Sequential induction of heme pathway enzymes during erythroid differentiation of mouse Friend leukemia virus-infected cells. *J Exp Med.* 1976;143(2):305-15.

264. Doty RT, Phelps SR, Shadle C, Sanchez-Bonilla M, Keel SB, and Abkowitz JL. Coordinate expression of heme and globin is essential for effective erythropoiesis. *J Clin Invest.* 2015;125(12):4681-91.

265. Elagib KE, Rubinstein JD, Delehanty LL, Ngoh VS, Greer PA, Li S, Lee JK, Li Z, Orkin SH, Mihaylov IS, et al. Calpain 2 activation of P-TEFb drives megakaryocyte morphogenesis and is disrupted by leukemogenic GATA1 mutation. *Dev Cell.* 2013;27(6):607-20.

266. Rink J, Ghigo E, Kalaidzidis Y, and Zerial M. Rab conversion as a mechanism of progression from early to late endosomes. *Cell.* 2005;122(5):735-49.

267. Fleming RE, Ahmann JR, Migas MC, Waheed A, Koeffler HP, Kawabata H, Britton RS, Bacon BR, and Sly WS. Targeted mutagenesis of the murine transferrin receptor-2 gene produces hemochromatosis. *Proc Natl Acad Sci U S A.* 2002;99(16):10653-8.

268. Iwasawa R, Mahul-Mellier AL, Datler C, Pazarentzos E, and Grimm S. Fis1 and Bap31 bridge the mitochondria-ER interface to establish a platform for apoptosis induction. *EMBO J.* 2011;30(3):556-68.

269. Abok K, Hirth T, Ericsson JL, and Brunk U. Effect of iron on the stability of macrophage lysosomes. *Virchows Arch B Cell Pathol Incl Mol Pathol.* 1983;43(2):85-101.

270. Chen B, Zheng B, DeRan M, Jarugumilli GK, Fu J, Brooks YS, and Wu X. ZDHHC7-mediated S-palmitoylation of Scribble regulates cell polarity. *Nat Chem Biol.* 2016;12(9):686-93.

271. Kaup M, Dassler K, Weise C, and Fuchs H. Shedding of the transferrin receptor is mediated constitutively by an integral membrane metalloprotease sensitive to

tumor necrosis factor alpha protease inhibitor-2. *J Biol Chem.* 2002;277(41):38494-502.

272. Zahn C, Kaup M, Fluhrer R, and Fuchs H. The transferrin receptor-1 membrane stub undergoes intramembrane proteolysis by signal peptide peptidase-like 2b. *FEBS J.* 2013;280(7):1653-63.

273. Pan BT, Blostein R, and Johnstone RM. Loss of the transferrin receptor during the maturation of sheep reticulocytes in vitro. An immunological approach. *Biochem J.* 1983;210(1):37-47.

274. Pan BT, and Johnstone RM. Fate of the transferrin receptor during maturation of sheep reticulocytes in vitro: selective externalization of the receptor. *Cell.* 1983;33(3):967-78.

275. Geminard C, Nault F, Johnstone RM, and Vidal M. Characteristics of the interaction between Hsc70 and the transferrin receptor in exosomes released during reticulocyte maturation. *J Biol Chem.* 2001;276(13):9910-6.

276. Hamilton AJ. MicroRNA in erythrocytes. *Biochem Soc Trans.* 2010;38(Pt 1):229-31.

277. Sangokoya C, LaMonte G, and Chi JT. Isolation and characterization of microRNAs of human mature erythrocytes. *Methods Mol Biol.* 2010;667(193-203.

278. Bergsmedh A, Szeles A, Henriksson M, Bratt A, Folkman MJ, Spetz AL, and Holmgren L. Horizontal transfer of oncogenes by uptake of apoptotic bodies. *Proc Natl Acad Sci U S A.* 2001;98(11):6407-11.

279. Holmgren L. Horizontal gene transfer: you are what you eat. *Biochem Biophys Res Commun.* 2010;396(1):147-51.